

SEA LEVEL MOMENTUM SPECTRA
OF MUONS IN THE WESTERN AZIMUTH
AT 53° N

by

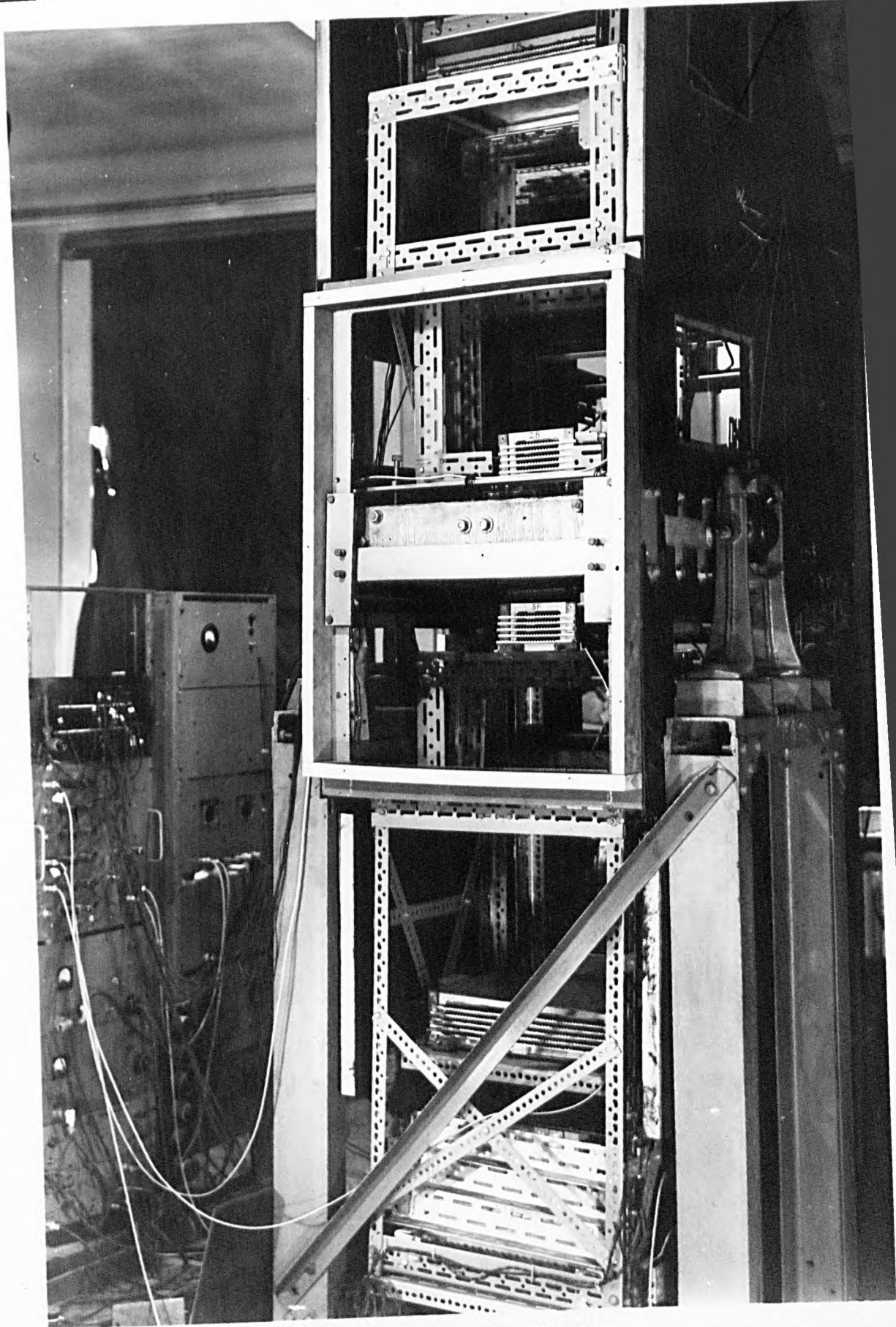
D. W. COATES, B.Sc.

Thesis submitted to the
University of Nottingham
for the degree of
Doctor of Philosophy,
February, 1961

CONTENTS

		<u>Page</u>
<u>Chapter 1.</u>	<u>General Introduction</u>	
1.1	The Origin of the Cosmic Radiation at Sea Level	1.
1.2	Outline of Previous Spectrographs	3.
1.3	Review of Previous Measurements of Inclined Spectra	6.
<u>Chapter 2.</u>	<u>Description of the Spectrograph</u>	
2.1	Introduction	9.
2.2	Description of the Spectrograph	11.
2.3	The Magnet	13.
2.4	Manufacture of Flash Tube Arrays	14.
2.5	Testing of the Tubes	17.
2.6	The Tube Trays	19.
2.7	The Electronic Circuits	21.
<u>Chapter 3.</u>	<u>A Computer Method for the Analysis of Flash Tube Data</u>	
3.1	Introduction	24.
3.2	Previous Methods	24.
3.3	Computer Method of Analysis	26.
3.4	Errors in Analysis of Flash Tube Data .	34.
3.5	The Efficiency Distribution	39.
3.6	Conclusion	41.

	<u>Page</u>
<u>Chapter 4.</u>	<u>Results and Conclusions</u>
4.1	Introduction 43.
4.2	Measurement of Errors due to Multiple Scattering 45.
4.3	Calculation of the Magnetic and Scattering Correction Factors 48.
4.4	Derivation of Comparison Spectra 50.
4.5	Discussion, and Comparison with Other Work 58.
4.6	Conclusions 61.
<u>Acknowledgements</u> 63.
<u>References</u> 64.
<u>Appendix</u>	<u>The Design of Flash Tube Arrays</u>
A.1	Introduction 68.
A.2	Design of Flash Tube Arrays 69.
A.3	Conclusions 85.



THE SPECTROGRAPH.

Chapter 1

General Introduction

1.1 The Origin of the Cosmic Radiation at Sea Level

The primary component of the cosmic radiation, which consists mainly of protons, interacts in approximately the first 100 gm./cm² of the atmosphere to produce π -mesons and a small fraction of heavy mesons and hyperons. The π -mesons are removed from the beam by the competing processes of decay into muons and interaction to produce further π -mesons which subsequently decay into muons. The heavy mesons and hyperons are removed by similar competing processes; the decay of K^+ and K_{μ}^+ mesons contributing a few muons at very high energies. The mesons travelling in tenuous regions of the atmosphere have a higher probability of decay than those of the same energy moving in denser regions; which may offset the overall relativistic effect of increasing probability of interaction with energy. As muons have the relatively long life time of 2.25×10^{-6} sec. (~ 100 times that of the π -meson), and are weakly interacting, they have a high probability of

survival to sea level. The neutral π -mesons decay rapidly into two photons, which may give rise to a photon-electron cascade. Unless the initiating photons are of very high energy this cascade is unlikely to reach sea level. Another contribution to the electronic component at sea level is made by electrons produced in muon decay, and knock-on electrons in equilibrium with the muons. The "hard" component ($p > 500 \text{ Mev}/c$) at sea level thus consists predominantly of muons with a small admixture of protons and π -mesons, and the "soft" component of electrons, photons and low energy muons.

The momentum spectrum of muons at sea level provides information on the production spectrum of π -mesons in high energy nuclear collisions. Measurements made in directions inclined to the vertical contribute information concerning π -mesons produced in collisions of progressively higher energy as the zenith angle is increased (Stern, 1960). In the horizontal direction the mean arrival energy of muons is 250 Gev., and their minimum initial energy 70 Gev. Further, π -mesons travelling in directions inclined to the vertical are travelling just after production in a tenuous region of the atmosphere, and

have therefore a relatively high probability of decay rather than interaction.

1.2 Outline of Previous Spectrographs

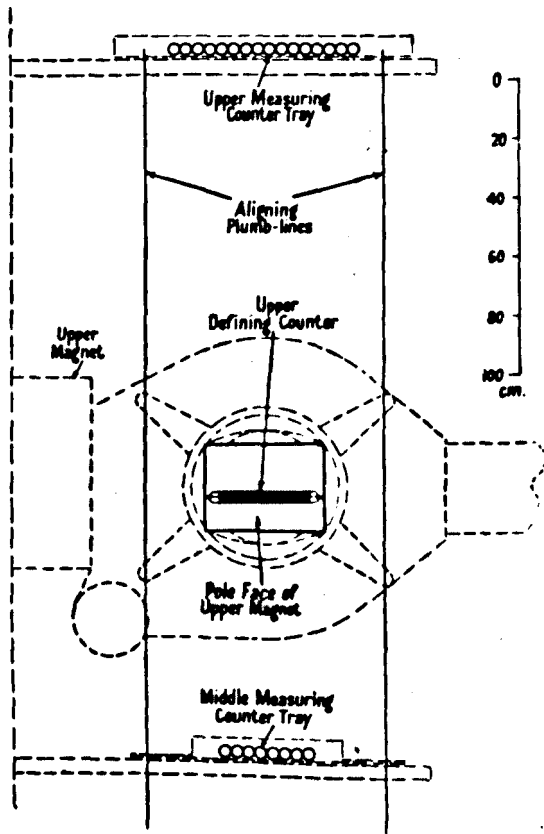
In order to compare the accuracy of measurement of various instruments it is conventional to define a "maximum detectable momentum" (m.d.m.) as the momentum at which the probable error in deflection measurement equals the magnetic deflection of a particle. Some workers have used the r.m.s. error in angular deflection in this definition, giving an m.d.m. lower by a factor 0.675.

Most of the momentum spectrum measurements have utilised the deflection of a charged particle in a magnetic field. Others have used scattering in multi-plate cloud chambers or nuclear emulsions. However, scattering methods are not reliable above $\sim 8 \text{ Gev}/c$ due to unavoidable spurious track distortion. The early magnetic field methods used a cloud chamber between the poles of an electromagnet to measure the track curvature. Again, the m.d.m. is set by track distortion, and in addition inefficient

use is made of the field. Hyams et al. (1950) estimated that only 5% of the available field volume is utilised by a magnet cloud chamber, whereas 50% is useful when advantage is taken of the line integral of the field by using geiger counter trays as detectors some metres above and below the magnet.

An instrument having this advantage was described by Owen and Wilson (1951), fig. 1.2.(i). It had two electromagnets, with hodoscoped geiger counters as detectors, and an m.d.m. of 31 Gev/c was achieved. Rodgers (1956) increased the m.d.m. to 240 Gev/c by placing flat cloud chambers at the measuring levels, a total of three being employed. Only fast particles triggered the chambers, and the point of intersection of the tracks on grids ruled on the top of the chambers was measured.

The reliability of spectrographs has been improved by replacing the cloud chambers by neon flash tube trays, which give comparable accuracy of location and a larger collecting area of particles. This has been done by Ashton et al. (1959) who describe a prototype spectrograph with an m.d.m. of 8 Gev/c, Ashton et al. (1960) who built a spectrograph of



Geometry of spectrograph. (The upper half of the instrument, which is symmetrical about the middle counter tray, only is shown.)

Fig. 1.2. (i)

The Manchester spectrograph.

expected m.d.m. 1,000 Gev/c , and Greisen et al. (private communication) who have operated a flash tube spectrograph of m.d.m. 130 Gev/c at 68° to the vertical. The advantages of neon flash tubes when used in momentum spectrographs will be further discussed in chapter 2.1.

Considerable advances have been made in the development of spark discharge counters as detectors. Allkofer (1959,1960) describes their development and successful use in a spectrograph of m.d.m. 60 Gev/c. A permanent magnet of $\int_{-\infty}^{+\infty} Hdl = 4000 \times 20$ gauss-cm. was used, and the overall height of the instrument was only 70 cms., compared with ~ 140 cms. for the instrument of m.d.m. 8 Gev/c using a magnet with $\int_{-\infty}^{+\infty} Hdl = 5000 \times 16$ gauss-cm. described by Ashton et al. (1959). It thus seems likely that the use of spark discharge counters offers good possibilities of extending the range of measurement to very high momenta, particularly if detectors of large area can be made to work reliably over long periods.

An instrument described by Apostalakis (1957) utilises fourteen layers of nuclear emulsion,

6.

separated by air gaps of 1.5 cms., accurately located between the poles of a magnet giving a field of 7,000 gauss. Trajectories may be traced through the layers with high precision, but the main disadvantage is the tedium of analysis. The m.d.m. of the instrument was 300 Gev/c.

A disadvantage of detectors such as flash tubes and spark counters is the labour of analysis, which has largely been performed manually. The time taken in analysis tends to offset the advantage gained by a high rate of collection of particles. In chapter 3 this problem is discussed further, and details presented of a fast and accurate computer method of analysis of flash tube data.

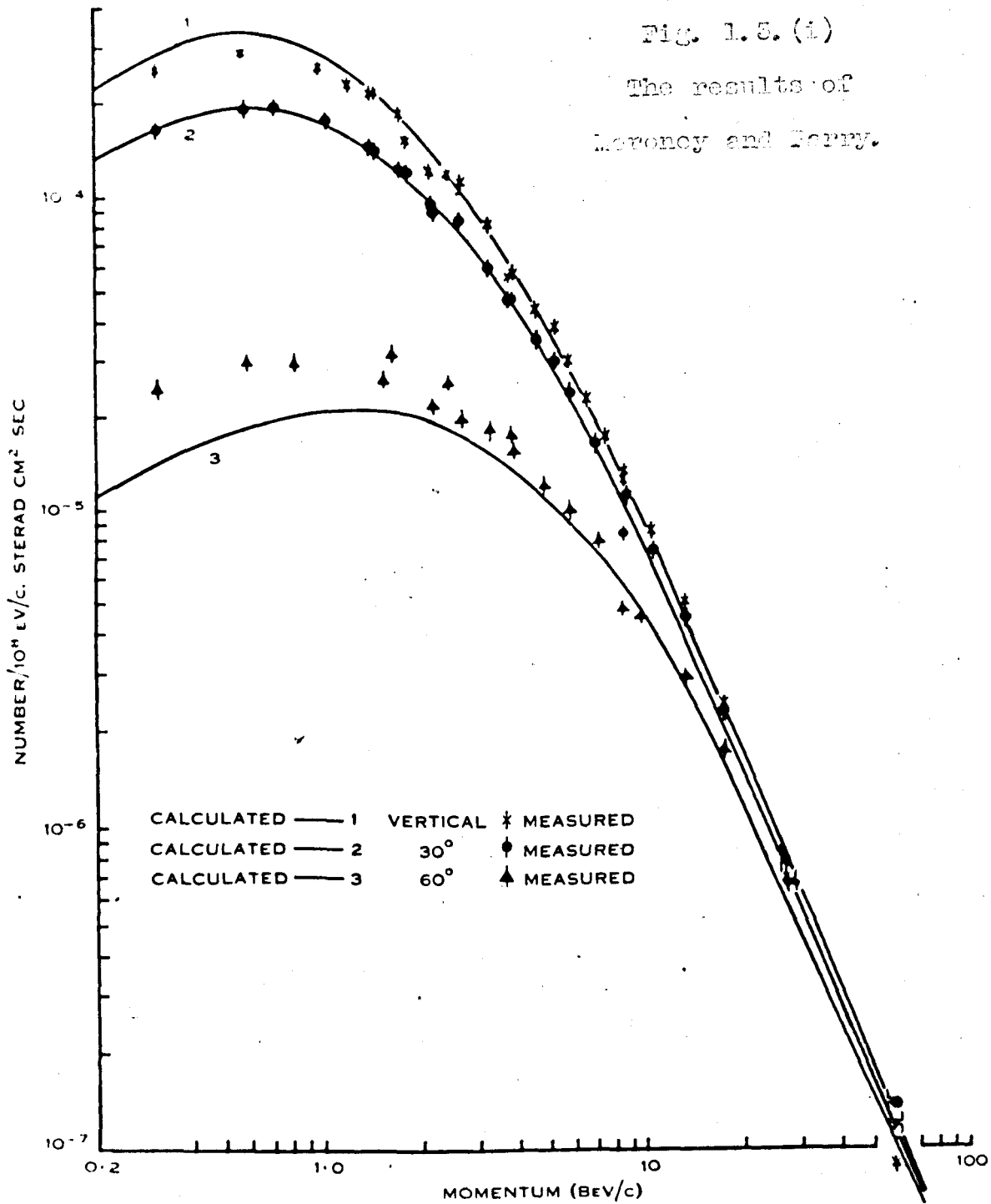
1.3 Review of Previous Measurements of

Inclined Spectra

The only previously published work on inclined spectra is that of Moroney and Parry (1954) who made measurements at zenith angles of 0° , 30° and 60° in the E - W plane, (fig. 1.3.(i)). These spectra show the expected hardening with increased zenith

Fig. 1.5. (i)

The results of
Moroney and Terry.



angle due to increased energy loss in the atmosphere. The spectrograph, which had an m.d.m. of 60 Gev/c, used hodoscoped geiger counters and a large electromagnet. Other work has been carried out by Greisen, Ozaki and Rose (private communication), who measured the spectrum at a zenith angle of 68° , using neon flash tubes in association with a geiger counter spectrograph.

Moroney and Parry carried out calculations of the form described by Janossy and Wilson (1946), and concluded that spectra at zenith angles of 0° , 30° and 60° could not be explained simultaneously in terms of a process involving production of the muons at a single level close to the top of the atmosphere. They found that their results at 0° and 30° were consistent with extended production of muons (Sands, 1950), assuming a momentum spectrum of the muons at production of the form

$$0.147 (p)^{-3.0} \exp(-r/125).$$

where p is in units of μc , r is the range in gm/cm^2 of the production level from the top of the atmosphere, and the intensity is in units of the number of muons $(10^8 \text{ ev/c})^{-1} \text{ cm}^{-2} \cdot \text{sec}^{-1}$. At 60°

the sea level spectrum calculated in this way falls below the experimental results by $\sim 50\%$ over a considerable range at low momentum. The authors indicate that calculations taking into account coulomb scattering in the atmosphere show that this effect is of the right order to account for the discrepancy. The results of Greisen et al. at 68° (fig. 1.3.(ii)), although not directly comparable with those of Moroney and Parry, appear to show fair agreement with them.

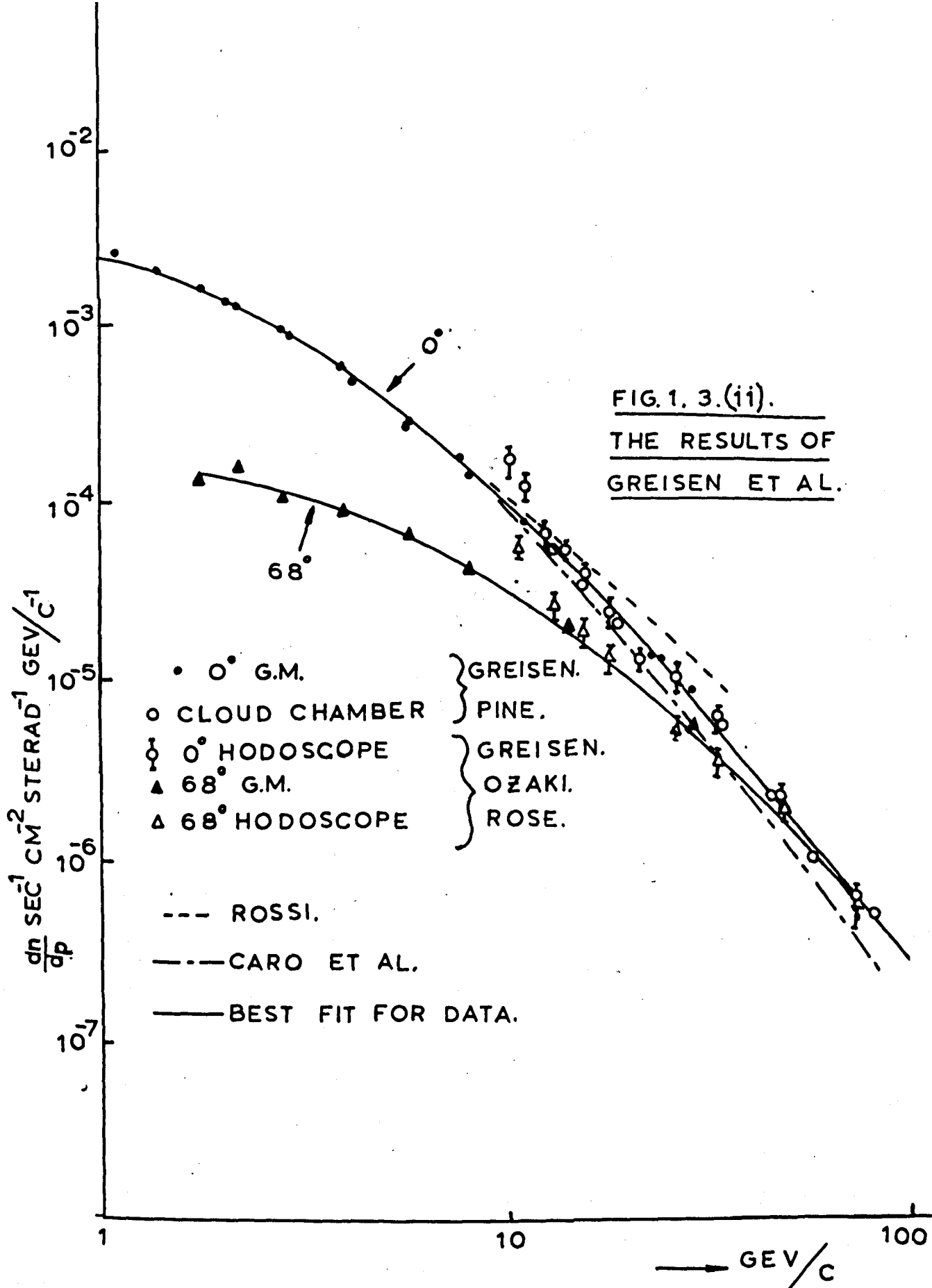


FIG. 1. 3. (ii).
THE RESULTS OF
GREISEN ET AL.

Chapter 2

Description of the Spectrograph

2.1 Introduction

The spectrograph to be described utilises trays of neon flash tubes as detectors above and below the field of a permanent magnet. The trays (fig.2.6.(i)) consist of horizontal layers of tubes separated by sheet electrodes. A few micro-seconds after the passage of a particle, a pulse of $\sim 7 \text{ K.V.cm}^{-1}$ is applied across each layer, and the tubes through which the particle passed may flash. These flashes are photographed, and the particle trajectory may be accurately determined.

Flash tube arrays have several advantages over cloud chambers when used in a momentum spectrograph:

- (i) They may be easily constructed to cover a large solid angle of acceptance of particles.
- (ii) They are stable and reliable in operation, having no moving parts.
- (iii) The error of angular measurement, σ_{ϕ} may be determined objectively and accurately (chapter 3), and does not vary with temperature or humidity.
- (iv) When used in the way to be described, no contribution to σ_{ϕ} is made by optical distortion in the recording system.

Throughout, the notation used by Gardener et al. (1957) will be used. That is, the characteristics of the pulse applied across the layers will be described in terms of the delay, T_D between the passage of the particle and the application of the pulse; its rise-time, T_R ; length, τ ; and height, E_{\max} . Also the absolute efficiency, η , of a tube is defined as the ratio of the number of times it flashes to the number of particles passing through it; and the layer efficiency of a set of tubes as the ratio of the number of flashes in a layer to the number of particles passing through it.

2.2 Description of the Spectrograph

The instrument is shown diagrammatically in fig. 2.2.(1), and consists of neon flash tube trays (O, P, Q and R), two above and two below the field of a permanent magnet (M). The flash tubes are triggered by a fourfold coincidence of the geiger counter trays (A, B, C and D) which define the solid angle of acceptance of the spectrograph. This was chosen to give a statistically high flux of particles with momentum in the range to be investigated, and to permit use only of a sensibly uniform region of the magnetic field. A layer of lead (Σ) 47.3 cm. thick between the lowest flash tube tray and the counter tray D imposes a cut-off of 0.7 Gev/c in the momentum of the particles accepted.

The flashes are recorded photographically through a mirror system which permits of two trays being photographed by one camera, making analysis easier and reducing considerably the required dimensions of the camera supports. A mechanical counter is photographed by each camera to correlate the data. The inclination of each trajectory to a chosen axis is determined, and the momentum of the particle estimated using the

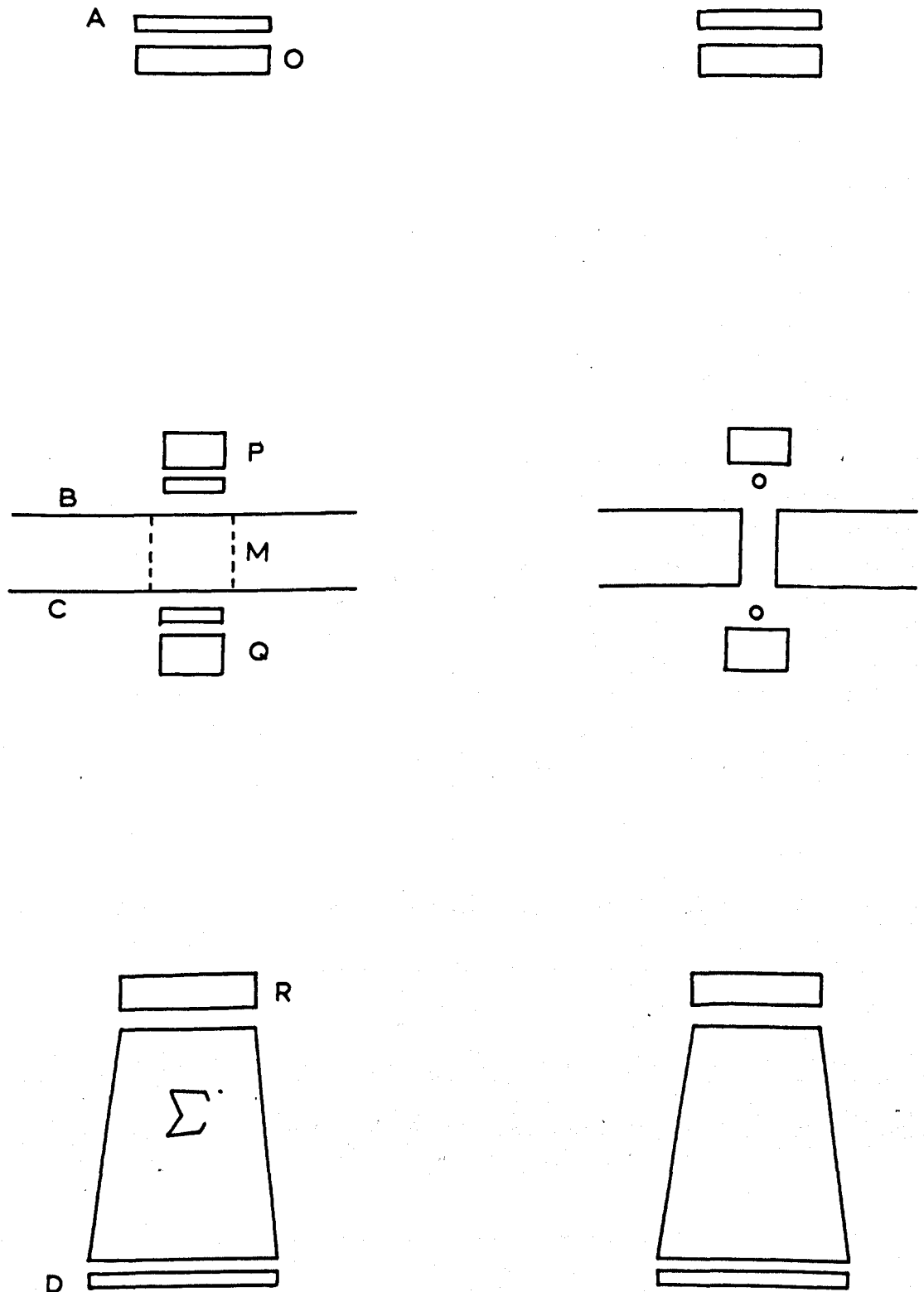


FIG. 22.(i) THE SPECTROGRAPH
 (SCALE $\frac{3}{40}$ FULL SIZE)

relation

$$pc = eH \left(\frac{ds}{d\theta} \right) \quad (2.2.1)$$

where p is the momentum of the (relativistic) particle of single electronic charge e e.s.u. moving in a plane perpendicular to a magnetic field H oersteds. $\left(\frac{ds}{d\theta} \right)$ is the radius of curvature of the path (cm.) at the point considered, ds being the arc length along the path, and θ the angle between the path and the y -axis, defined as a line passing through the centres of the tube arrays and the magnet gap. Further

$$ds = \frac{dy}{\cos\theta} \quad (2.2.2)$$

Hence, if $\int_{-\infty}^{+\infty} Hdy$ is constant over the whole of the region occupied by the trajectory of the particle, equation (2.2.1) may be written

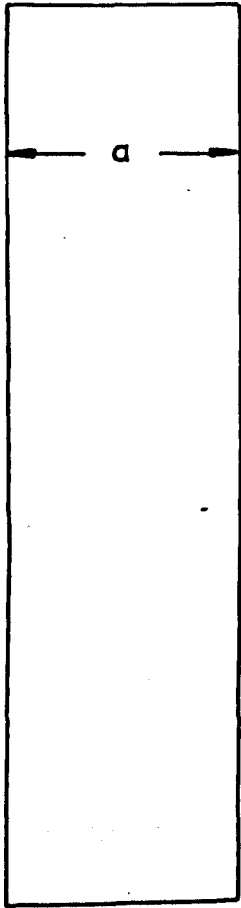
$$pc = \frac{e \int_{-\infty}^{+\infty} Hdy}{\int_{\theta_1}^{\theta_2} \cos\theta d\theta} \quad (2.2.3)$$

where θ_1, θ_2 are the angles of the track of the particle above and below the field, and $\int_{-\infty}^{+\infty} Hdy$ is the vertical line integral of the field intensity measured right through the magnetic field, including

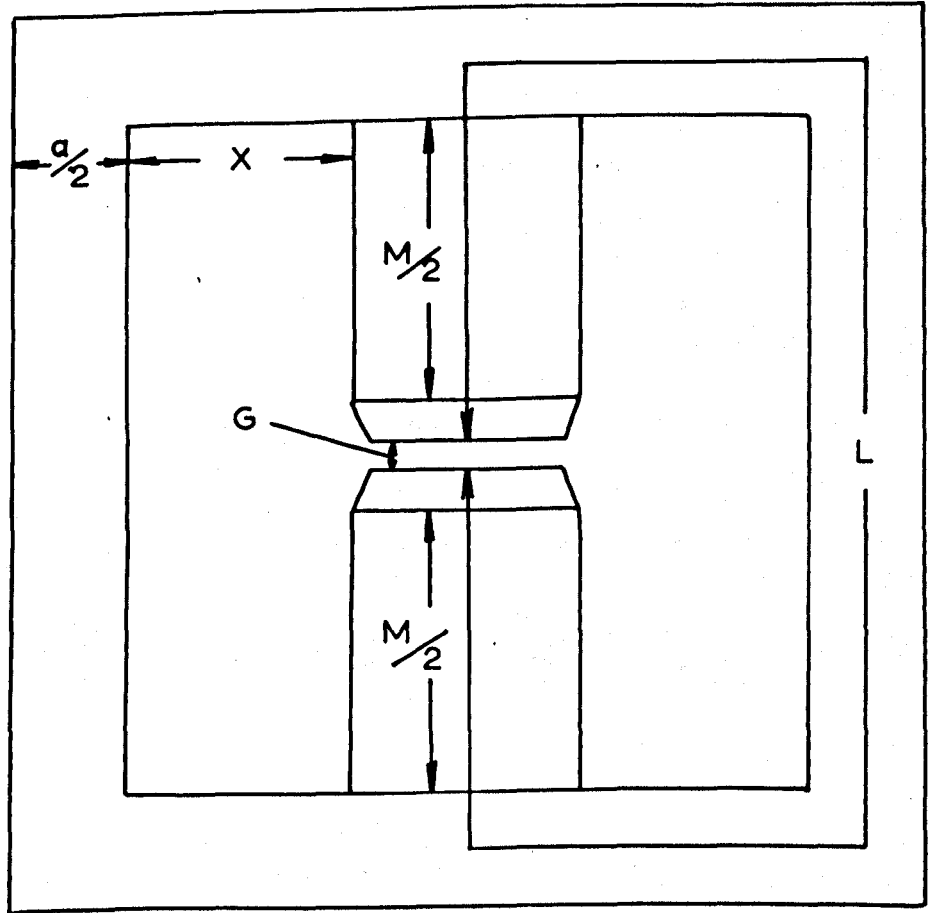
the fringing field. An accurate knowledge of the variation of the magnetic field is therefore required.

2.3 The Magnet

This is a double-yoke permanent magnet, originally designed by Cousins and Nash (1959), and illustrated in fig. 2.3.(1). It was designed to give a maximum value of $\int_{-\infty}^{+\infty} Hdy$ for a given quantity of magnetic alloy, and a given gap size. The basic data are:- (L - M), iron circuit = 49 in.; G = 1.27 in., (chosen as a compromise between a high value of $\int_{-\infty}^{+\infty} Hdy$ and a large flux of high momentum particles, the solid angle subtended by the gap being $\propto G^2$), M = 16.8 in.; volume of alcomax 687 cu.in., a = 6.6 in. The pole faces are $\frac{1}{2}$ in. thick, and of cross section 2.2 in. x 2.2 in. They are fixed to the pole pieces by brass bolts which screw into them to a depth of $\frac{1}{4}$ in., air gaps being eliminated by grinding the faces of the pole pieces which contact the yoke and pole tips. The yoke consists of four main arms and two short sections, one in each of the arms of the yoke parallel to the pole pieces, of such a size that the gap may be made a minimum of $\frac{1}{2}$ in. Bolts passing through these short sections are used to clamp the yoke at the corners.



SIDE VIEW



PLAN

FIG. 23.(i) THE MAGNET.

The magnet was energised by placing coils on the poles, and packing the air gap tightly with soft iron bars. 128,000 ampere turns were employed, and a small demagnetizing field applied after magnetization.

Measurements of the variation of the field in a plane through the centre of the gap and parallel to the pole faces were made by Cousins and Nash using a search coil of small cross sectional area, and a Pye fluxmeter; the results are shown in basic form in fig. 2.3.(ii) which is a plot of the equipotential surfaces. Fig. 2.3.(iii) shows the variation of the field along the central vertical path, which is typical of that for other vertical paths. Over a strip 12 cm. wide, the centre of the region being the vertical which passes through the centre of the magnet gap, graphical integration gives $\int_{-\infty}^{+\infty} Hdy = 109.0$ kilo-oersted cm. These measurements have been checked, and no changes of greater than 1% detected, indicating the high stability of the magnet against time variations in field.

2.4 Manufacture of Flash Tube Arrays

The specifications of the tubes used in this experiment are based on the design considerations of

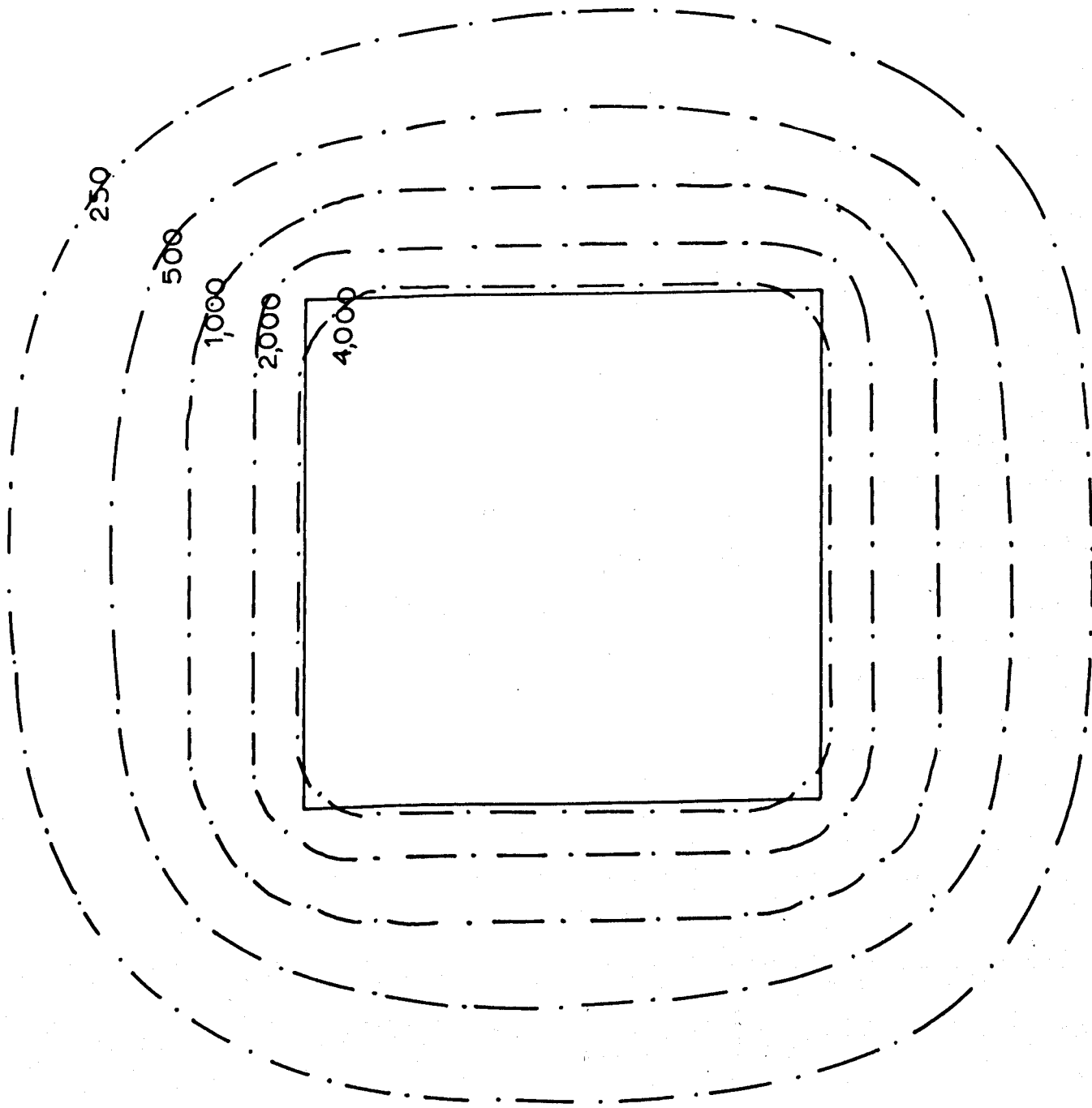


FIG 2.3.(ii)
PLOT OF
EQUIPOTENTIAL
SURFACES.

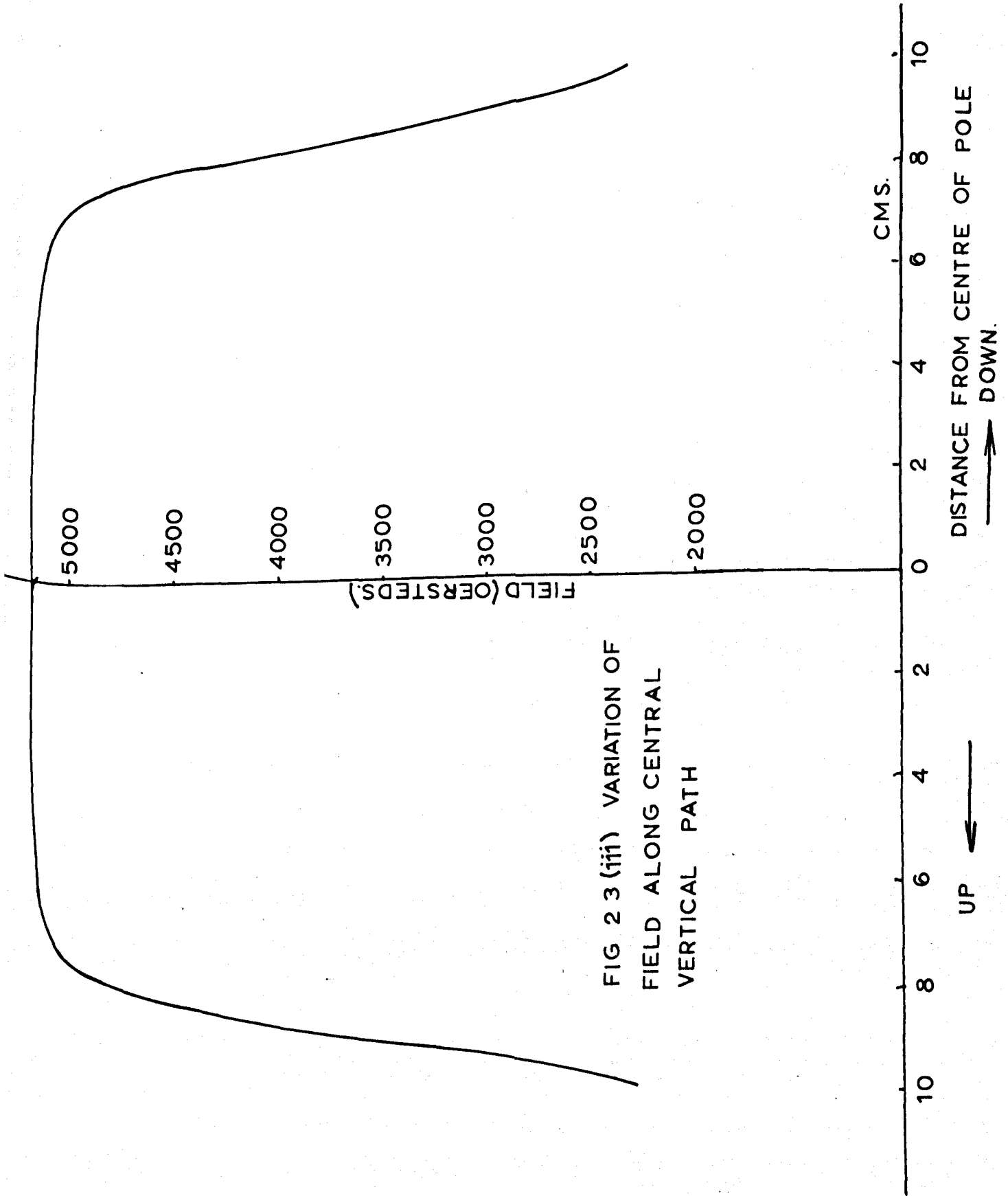


FIG 2 3 (iii) VARIATION OF
FIELD ALONG CENTRAL
VERTICAL PATH

Gardener et al. (1957), Ashton et al. (1958), and Coxell and Wolfendale (1960). The chief requirement was a high probability of flashing for a pulse applied some 5 μ sec. after the passage of the particle, since this was the delay expected in the experiment. Tubes of internal diameter 0.6 cm. and wall thickness 0.07 cm. are the smallest which can conveniently be manipulated during manufacture, and the final flash tube specifications are:-

Mean internal diameter	5.9 mm.
Mean external diameter	7.3 mm.
Residual air pressure	$\sim 10^{-5}$ mm. Hg.
Pressure of neon (commercial)	2.3 π .

The constitution of commercial neon is:-

<u>GAS</u>	<u>CONCENTRATION</u>
Ne	(98 \pm 0.2) %
He	(2 \pm 0.2) %
O	10 vol. per million
N	100-200 vol. per million

The tubes were constructed of X8 soda glass, and their characteristics are given in figs. 2.4.(i) and 2.4.(ii). The former shows the variation of absolute efficiency, η , with the field in KV cm.⁻¹, under

↑
 η
ABSOLUTE
EFFICIENCY
%

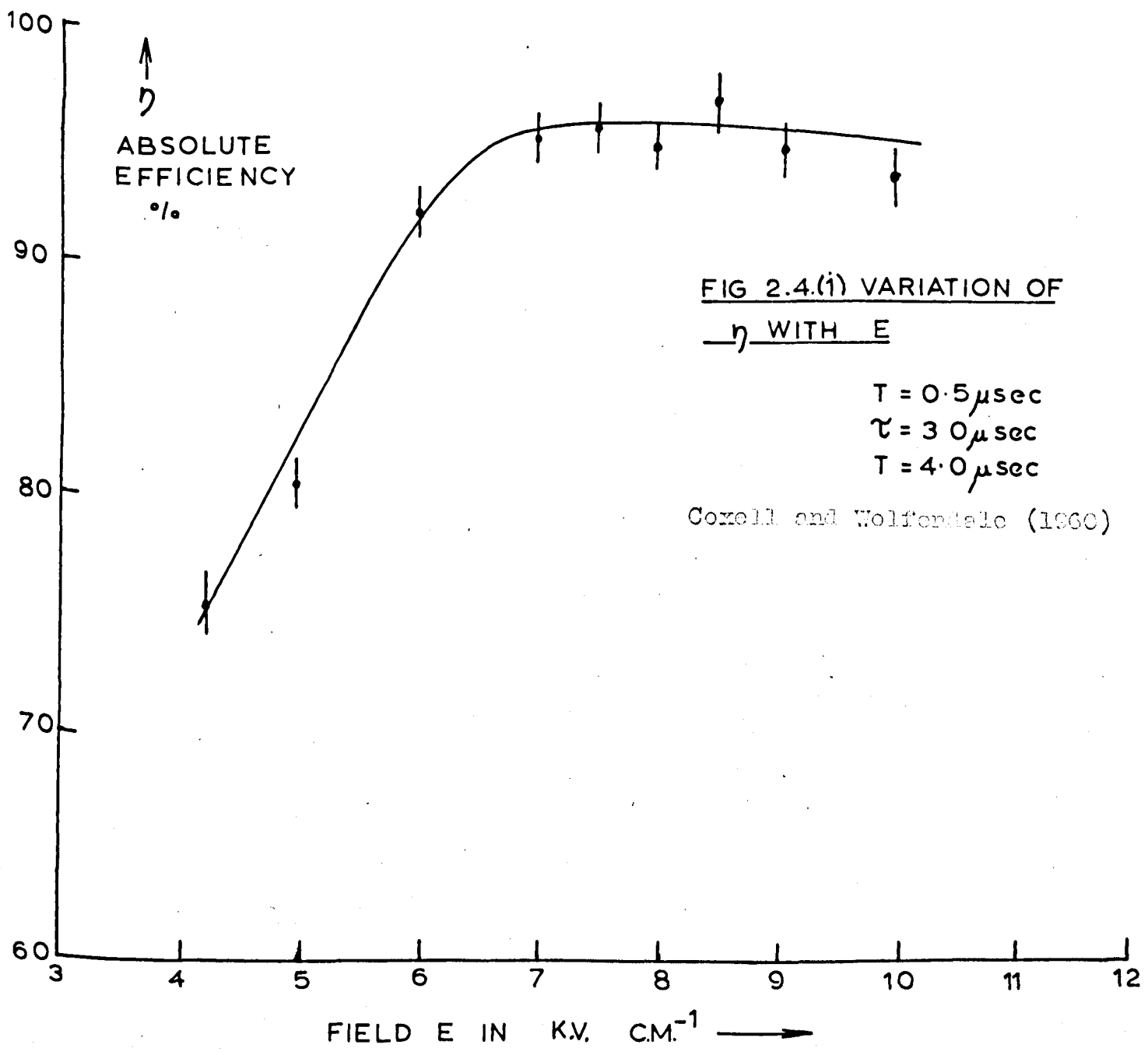
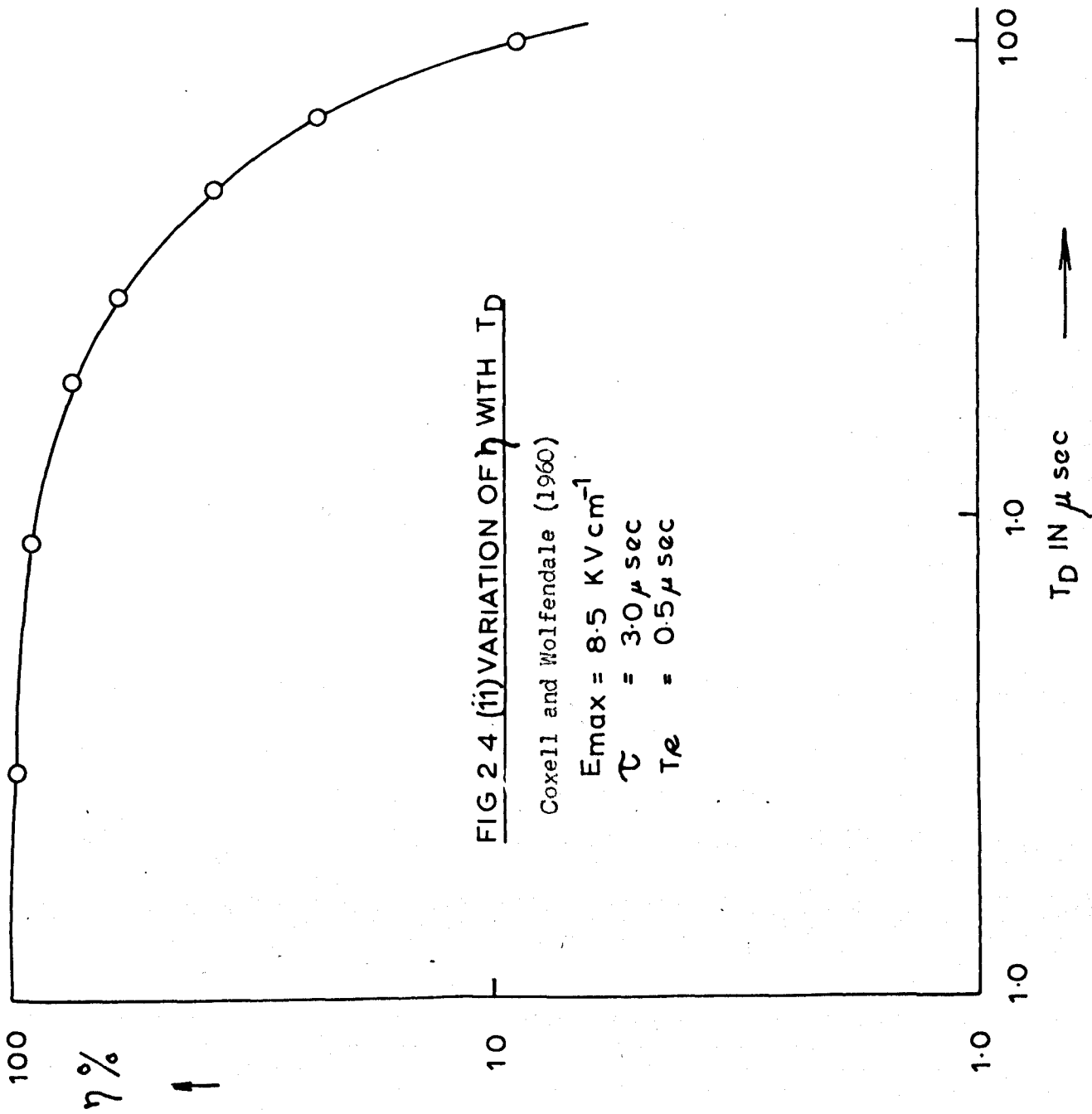


FIG 2.4.(i) VARIATION OF
 η WITH E

$T = 0.5 \mu\text{sec}$
 $\tau = 3.0 \mu\text{sec}$
 $T = 4.0 \mu\text{sec}$

Coxell and Wolfendale (1960)



conditions expected to be fulfilled in the running of the spectrograph, and the latter the variation of η with τ_D ; $E \text{ max.} = 8.5 \text{ KV cm.}^{-1}$, $TR = 0.5 \mu \text{ sec.}$, and $\tau = 3.0 \mu \text{ sec.}$

In the manufacture of the tubes, lengths of soda glass were selected so that they were straight to within 0.5 mm., and had external diameter in the range 7.0 - 7.5 mm. After cutting to the appropriate length, the glass was washed with tap water, chromic acid, and distilled water, and allowed to dry completely. A constriction of uniform wall thickness equal to that of the tube was made close to one end, and the other end sealed and carefully flattened.

The tubes were sealed on to a manifold, evacuated to a final pressure of $\sim 10^{-5}$ mm. of mercury, and filled with commercial neon to a pressure maintained at 65 cm. of mercury. After allowing one hour for complete diffusion of gas throughout the system, each tube in turn was immersed to approximately two-thirds of its length in liquid nitrogen, and temperature equilibrium established. While still in the nitrogen, it was sealed off at the constriction and allowed to return to room temperature.

The relation giving the final pressure attained is:-

$$\frac{p_i l_i}{273-195.8} + \frac{(l_0 - l_i) p_i}{273 + 20} = \frac{p_f l_0}{273+20} \quad (2.4.1)$$

l_0 is the length of tube (from flattened to constricted end); l_i is the length immersed in liquid nitrogen; p_i is the pressure of gas in the tube while immersed; and p_f is the final pressure when the tubes attain room temperature.

As the tubes are photo-sensitive, and likely to be triggered by photons from adjacent tubes, they were cleaned and painted black, allowing them to dry while hanging vertically, so that the paint was uniformly distributed on their surface. This was to prevent errors of location when they were subsequently rested on supports in the spectrograph.

2.5 Testing of the Tubes

Each batch of tubes was tested in the following way. A geiger counter telescope traced particle trajectories through a tray of tubes consisting of 5 layers, with 12 tubes in each. The characteristics of the pulse applied across the tubes were those

expected in the running of the spectrograph,

$$E_{\max} = 8.5 \text{ KV cm.}^{-1}, \text{ TR} = 0.5 \mu \text{ sec.},$$

$\tau = 3.0 \mu \text{ sec.}$, and $\text{TD} = 3.5 \mu \text{ sec.}$ The flashes were recorded photographically, approximately 100 particles being observed for each batch. Typical events are shown in fig. 2.5.(i). To find the mean efficiency, the results of events involving single particles only were analysed, neglecting obvious knock-on and shower particles. The results are shown in table 2.5.(a), and a typical histogram of the number of events involving 0, 1, 2, flashes is shown in fig. 2.5.(ii).

Table 2.5.(a)

Batch	1	2	3	4	5	6	7	8	9	10
Mean(%) layer effi- ciency	70 \pm 2	67 \pm 2	69 \pm 2	66 \pm 2	68 \pm 2	65 \pm 2	68 \pm 2	68 \pm 2	65 \pm 2	66 \pm 2
Mean absolute effi- ciency	92 \pm 2%									

For each batch, with the film in the same position, the tubes were triggered until all were expected to have flashed at least 20 times. Any "dead" tubes were rejected, as were any which flashed spuriously, i.e. had continually produced a flash inconsistent with the trajectory indicated.

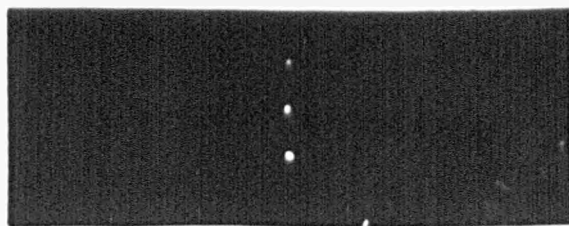
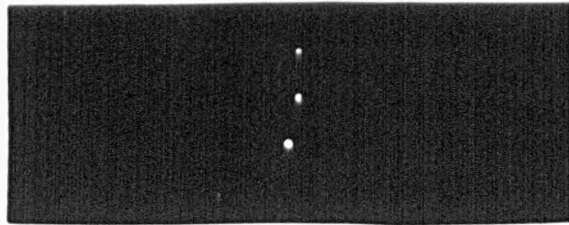
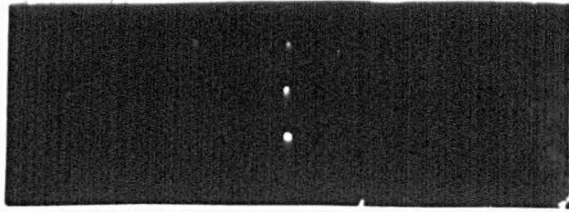


FIG 2.5(i)
TYPICAL TEST EVENTS

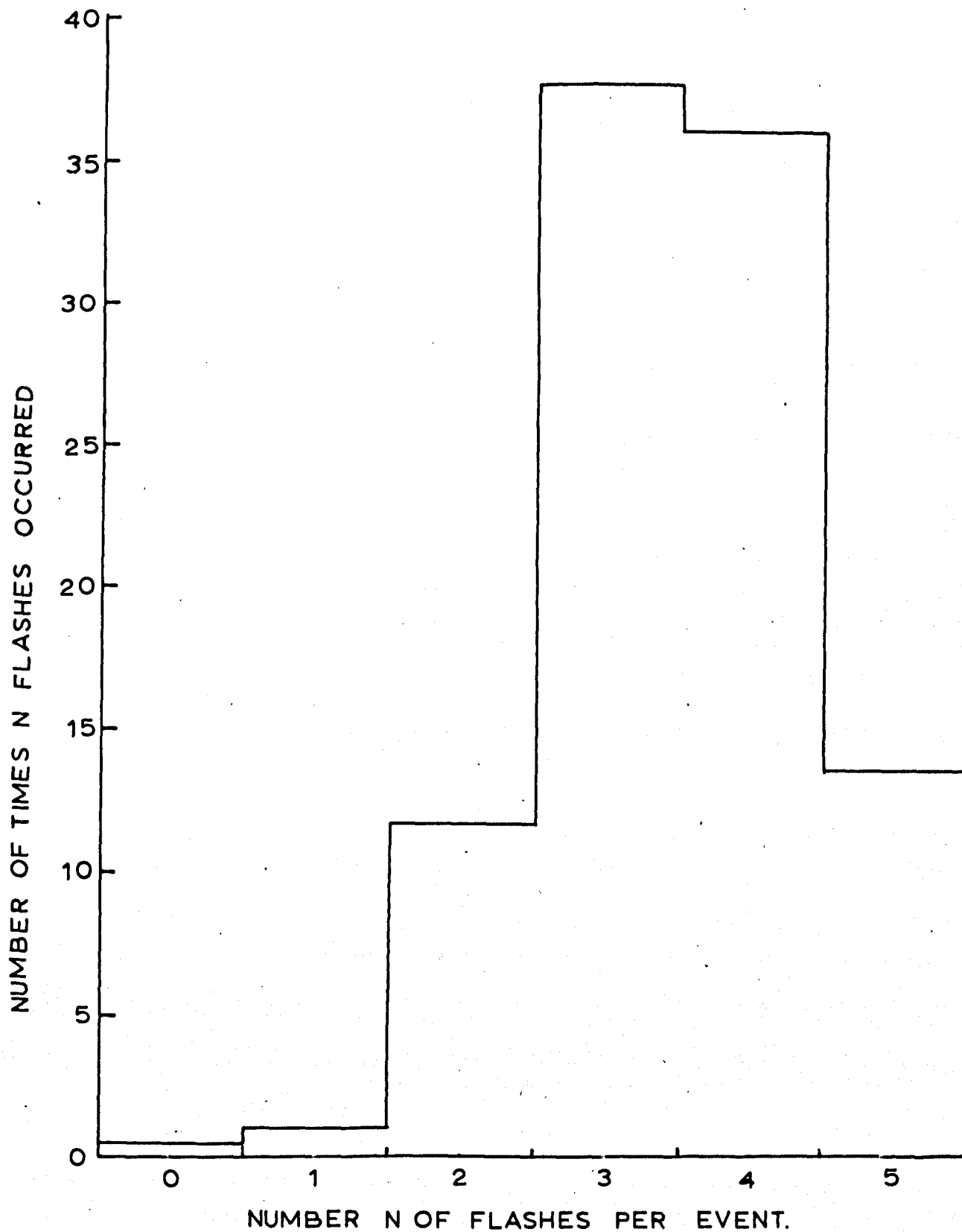


FIG. 2.5.(11) DATA FROM TYPICAL BATCH TEST.

2.6 The Tube Trays

The requirements were that the tubes should be mounted rigidly parallel to one another with their centres accurately located. They are mounted on slotted strips in trays consisting of angle and sheet dural, $3/16$ in. and $1/4$ in. thick respectively, see fig. 2.6(1). Wherever possible, the sides were machined together, and the completed trays are square to $\pm 1/500$ in. The slots were cut 0.800 ± 0.0025 cm. apart in dural of cross-section $1/8$ in. x $3/8$ in., which is sufficiently rigid to prevent sag when under load. The strips were mounted 1.470 cm. apart in slots cut in $1/4$ in. brass strip, so that they could easily be moved laterally, and clamped in any desired position. The tubes were held in position by foam rubber strip, which served this purpose without distorting the supports.

The electrodes consisted of aluminium foil of thickness $1/1000$ in. stretched on a tufnol "picture-frame". In this way, scattering in the spectrograph is reduced to a minimum, and the uniformity of the field applied to the tubes is comparable with that attainable using thicker and more rigid plates.

The relation giving the final pressure attained is:-

$$\frac{p_i l_i}{273-195.8} + \frac{(l_0 - l_i) p_i}{273 + 20} = \frac{p_f l_0}{273 + 20} . \quad (2.4.1)$$

l_0 is the length of tube (from flattened to constricted end); l_i is the length immersed in liquid nitrogen; p_i is the pressure of gas in the tube while immersed; and p_f is the final pressure when the tubes attain room temperature.

As the tubes are photo-sensitive, and likely to be triggered by photons from adjacent tubes, they were cleaned and painted black, allowing them to dry while hanging vertically, so that the paint was uniformly distributed on their surface. This was to prevent errors of location when they were subsequently rested on supports in the spectrograph.

2.5 Testing of the Tubes

Each batch of tubes was tested in the following way. A geiger counter telescope traced particle trajectories through a tray of tubes consisting of 5 layers, with 12 tubes in each. The characteristics of the pulse applied across the tubes were those

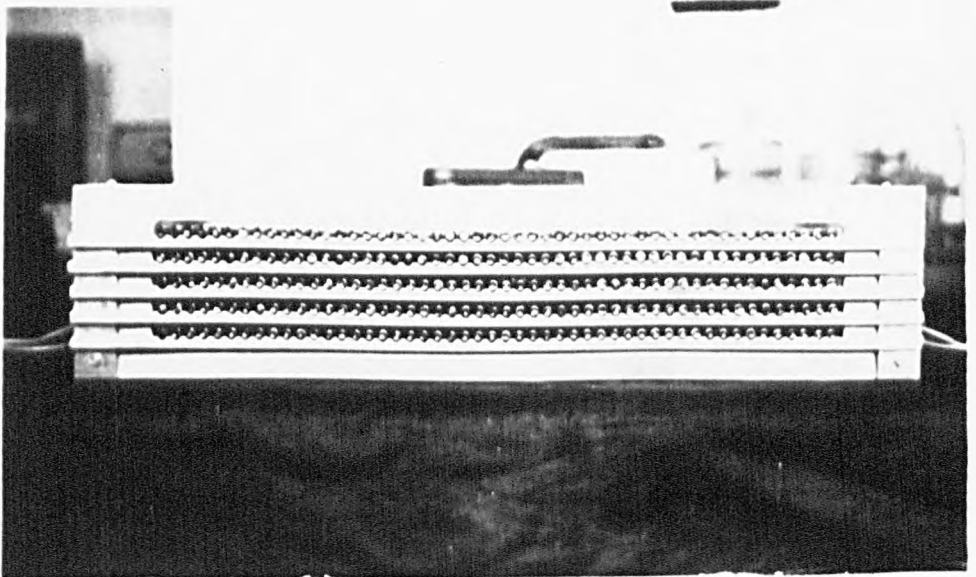
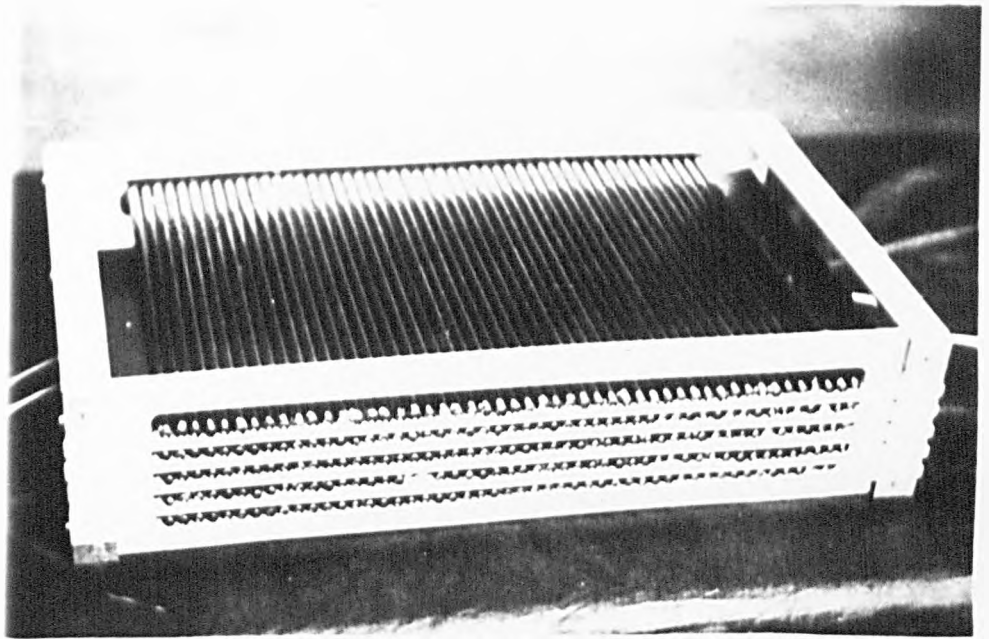


FIG 2.6.(1)

TUBE TRAY

Electrical contact with the electrodes is made through copper foil held firmly in contact with them.

It is important that the tubes at each of the recording levels in the spectrograph be accurately parallel to one another. A rectangle, two of the sides of which were accurately parallel to the tubes, was scribed on the top of the trays (fig. 2.6.(ii)). The co-ordinates of the corners of the rectangle were accurately known with respect to the centre of each tube. Circles of known radius were drawn with these corners as centre, the points of intersection of these circles being G_1 and G_2 , whose co-ordinates are again accurately known with respect to the tube centres and the grids g_1 and g_2 which consist of lines scribed 1/100 in. apart. Holes of diameter 2 mm. were drilled with G_1 and G_2 as centre. Two plumb lines, forming a vertical plane with respect to the defining counters, could be hung through the holes, and by moving each framework until the plumb lines had the same co-ordinates with respect to g_1 and g_2 at each level, the tubes could be made parallel to one another to $\pm 4/1000$ in. The trays could also be moved in a vertical plane to any desired position, and thus the tube centres form an accurately known co-ordinate system within the spectro-

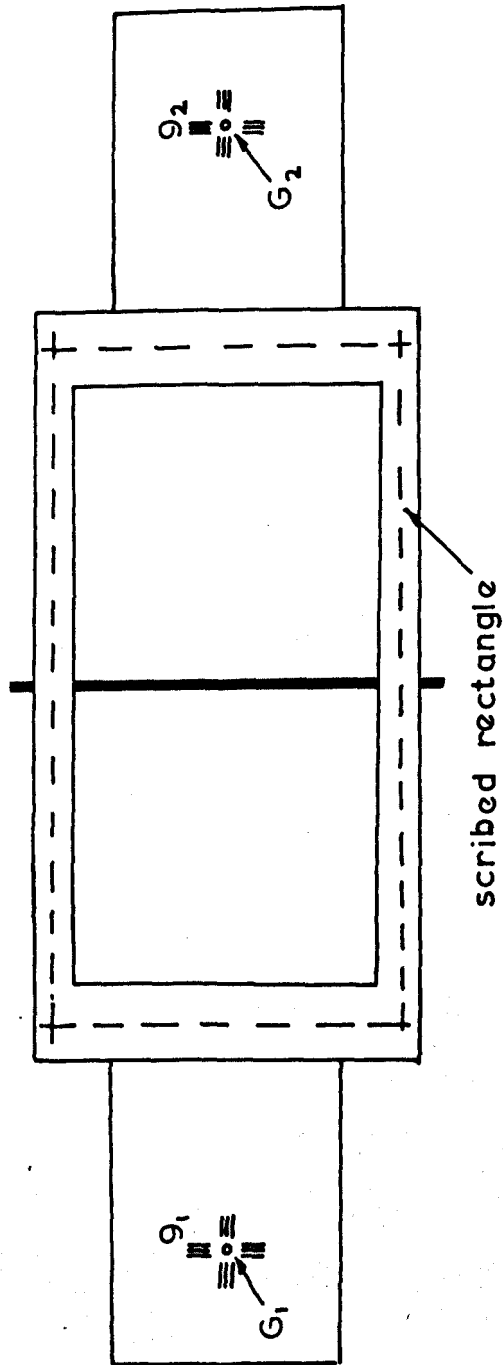


FIG 2 6(ii)

LOCATION OF THE TUBE ARRAYS

graph. This is important, since the spectrograph was to be operated at various zenith angles, and the use of plumb lines for reference in analysis would have been impracticable.

2.7 The Electronic Circuits

The electronic circuits associated with the spectrograph are shown in block diagram form in fig. 2.7.(i). The coincidence circuit is of the Rossi type, and the coincidence pulse is fed to the high voltage pulse generator shown in detail in fig. 2.7.(ii). In this a positive pulse of height 7 K.V., rise-time 0.4μ sec. and length 3μ sec. is produced by discharging a capacitance of 0.012μ F through a hydrogen filled thyatron and the primary of a pulse transformer, and fed to the trigger electrodes of three trigatrons (CV 85). The $100 \text{ K}\Omega$ resistor serves to prevent quenching of the trigger voltage across the trigger gaps. A capacitance of 0.08μ F is discharged through each trigatron and the primary of a pulse transformer, the resulting pulse of height 11 K.V., rise-time 0.5μ sec. and length 4μ sec. being fed to the electrodes of the tube trays from a tapping point on a resistor chain, R.

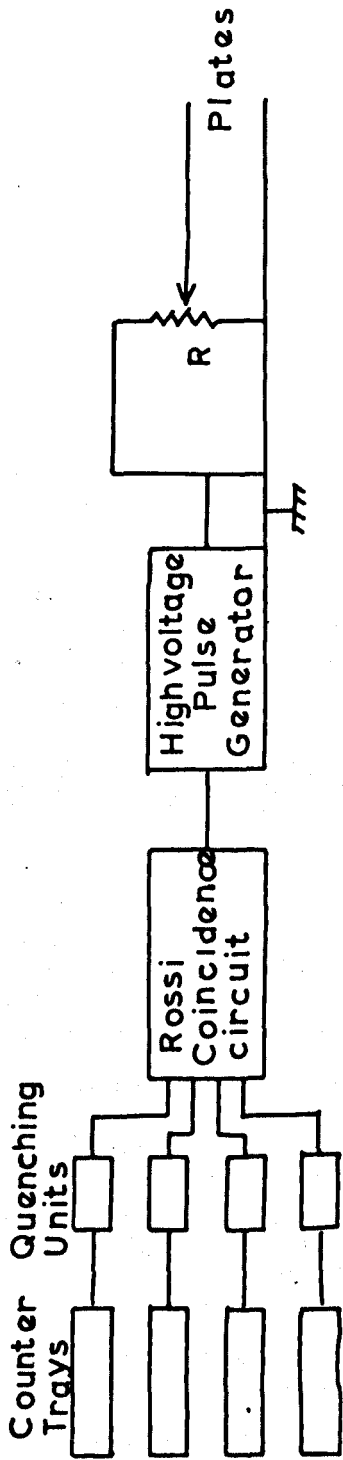


FIG 2 7 (i) ELECTRONIC ARRANGEMENT

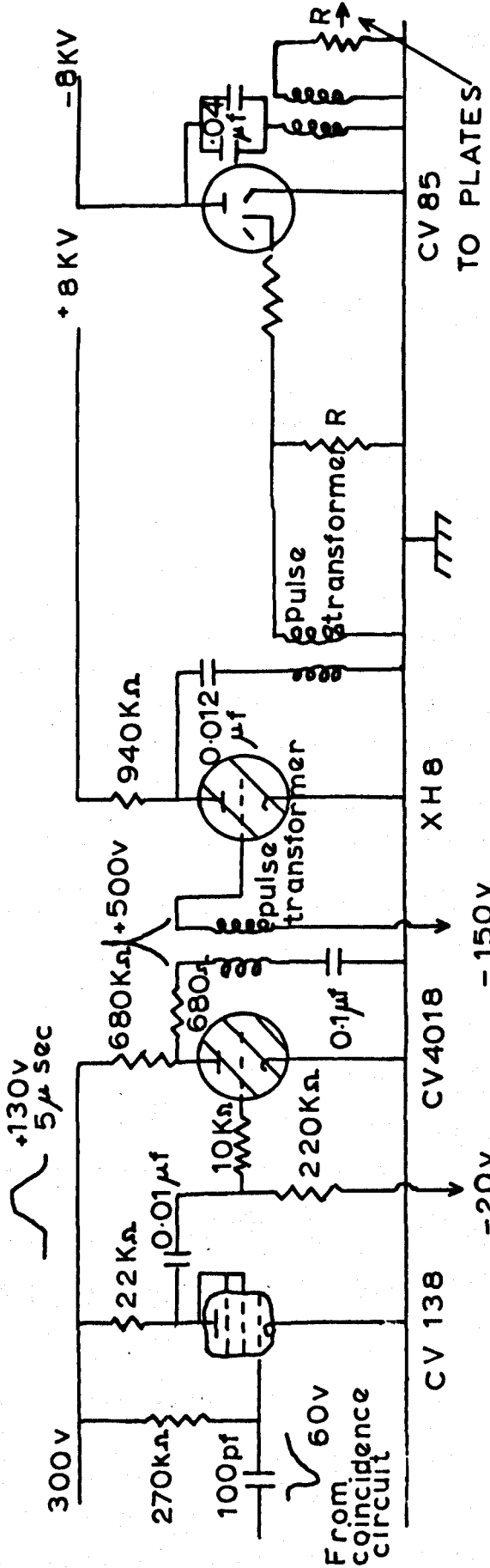


FIG 2 7 (ii) HIGH VOLTAGE PULSE GENERATOR

GENERATOR

The tube efficiency does not depend critically on the value of this load. A further stage after the XH8 is required to charge as rapidly as is practicable the capacity (1000 pf) of the large tube trays. These are fed by two separate trigatrons, the two small trays from a third. The overall time-delay from the passage of the particle through the counter telescope and the application of the high voltage pulse is 3.5μ sec.

A cycling unit (fig. 2.7.(iii)), whose operation is initiated by the coincidence pulse, performs the following operations:-

1. The negative input pulse momentarily cuts off the anode current of the valve.
2. The relay R1 flies open, closing contacts R1A and R1B. Because R1A is closed, R1 is held off.
3. Closure of R1B starts the cycling unit motor (C.U.). Micro-switch (M.S.) (b) is closed.
4. The starting of C.U. shuts relay R2 (normally open). This closes contact R2A, shorting to earth further coincidence pulses, thus paralysing the apparatus.
5. A cam on C.U. opens M.S.(a), resetting R1,

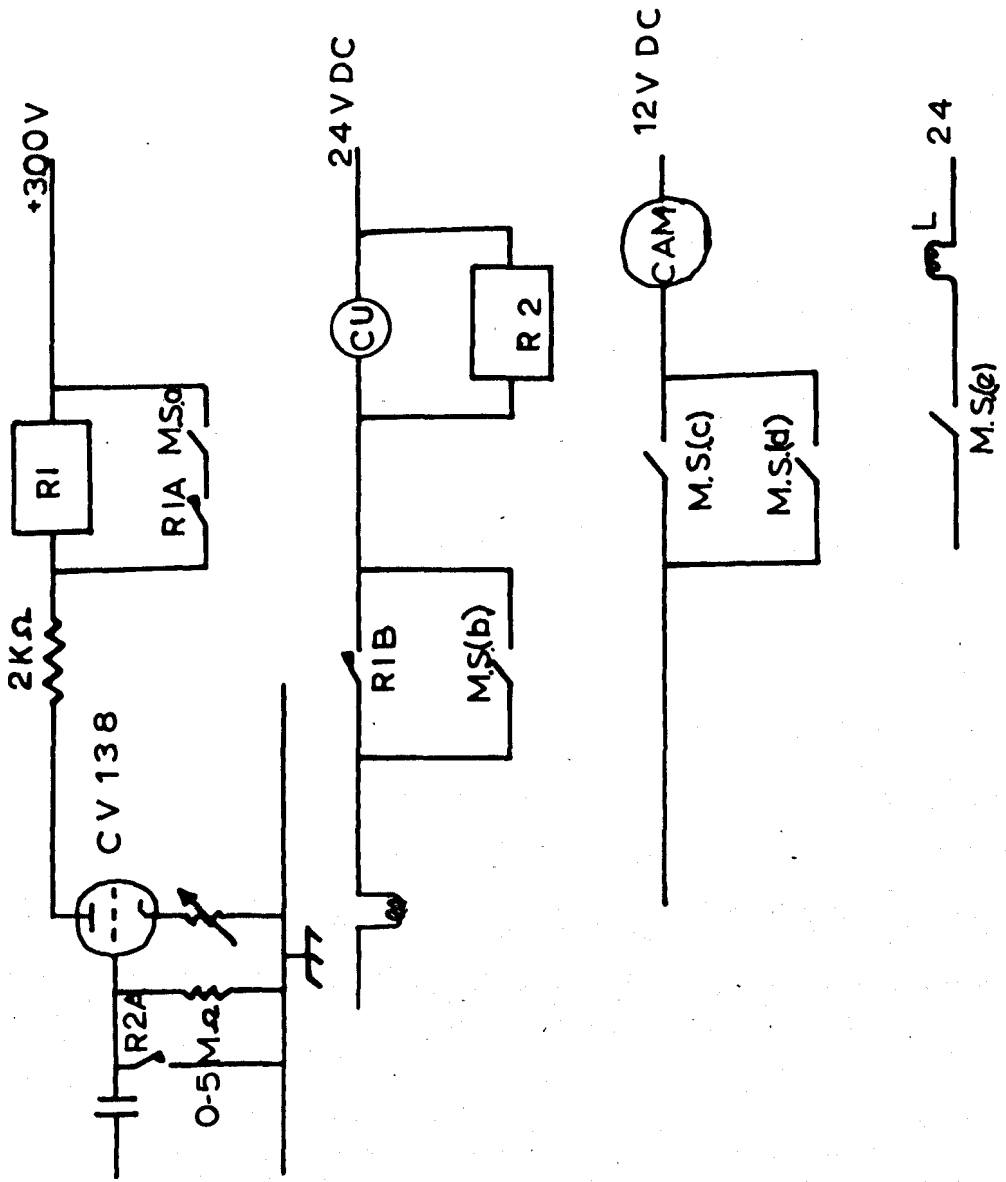


FIG. 2. 7. (iii)
THE CYCLING UNIT

opening R1A and R1B. C.U. continues to run, the cam reclosing M.S.(a).

6. M.S.(e) is closed for 9 secs. by the cam on C.U., illuminating the reference counters.

7. The cam on C.U. closes M.S.(c), starting the camera motor (C.M.).

8. A cam on C.M. closes M.S.(d) and the cam on C.U. opens M.S.(c).

9. The cam on C.M. opens M.S.(d), and it stops.

10. The cam on C.U. re-opens M.S.(b), stopping itself and re-sensitising the apparatus by opening R2A.

Chapter 3

A Computer Method for the Analysis of Flash

Tube Data

3.1 Introduction

The analysis of data from flash tube spectrographs is difficult and laborious when maximum resolution is required. In this chapter is described a method of analysis using a digital computer, which is faster, more accurate, and more reliable than previous methods.

The computer has been programmed primarily to analyse the results obtained with the flash tube momentum spectrograph at Nottingham, but the principle is probably applicable to other projects employing flash tubes, in particular those investigating extensive showers.

The speed of the computer analysis has facilitated a close study of the design considerations of flash tube arrays. These considerations are found in the Appendix.

3.2 Previous Methods

Methods of analysis previously contemplated have involved either the computation of the best line through the centres of tubes which flashed, or the adjustment of a thread over a scale diagram or

reprojection of the array to give the best estimate of track direction. Whilst the former method is objective it has not found practical use since the accuracy is impaired by the inability to utilise knowledge of the tube dimensions and those layers in which a tube did not flash. The latter method is potentially more accurate since it is capable of using this information, but it is subjective, slow, and laborious.

In order to use a knowledge of the tube dimensions it is necessary to assume a distribution function $P(\theta)$ for the probability of flashing, when a particle traverses a tube a distance θ from its centre. A method which assumes that $P(\theta)$ is unity for all θ within the tube and zero outside was described by Ashton et al. (1958), but difficulties are encountered because events frequently occur which are inconsistent with this assumption. Ashton (1959) described a method for which the criterion of the best line is that it should have maximum path length in the flashed tubes. This effectively assumes a $P(\theta)$ for the flashed tubes which is consistent with that measured by Ashton et al. (1958) for low pressure tubes. However

the treatment of layers in which a tube did not flash is not clear, nor is it apparent how this criterion was applied in practice.

A recent method mentioned by Ashton et al. (1960) assumes that for high pressure tubes $P(\theta)$ is unity for $0 \leq \theta \leq \lambda$ where λ is smaller than the tube radius, and that it falls in an undefined manner to zero at the tube edge.

The analysis to be described extends these methods by using, in an objective way, the measured $P(\theta)$ for both flashed and unflashed tubes. The measured $P(\theta)$ automatically accounts for the effects of random variations in tube diameter.

3.3 Computer method of analysis

The type of array considered is typical of those used in momentum spectrographs and is illustrated in fig. 3.3.(i). It consists of two trays separated by a distance D, each consisting of N layers of tubes separated by a distance S. The internal diameter of the tubes is Δ and the horizontal separation between their centres Γ .

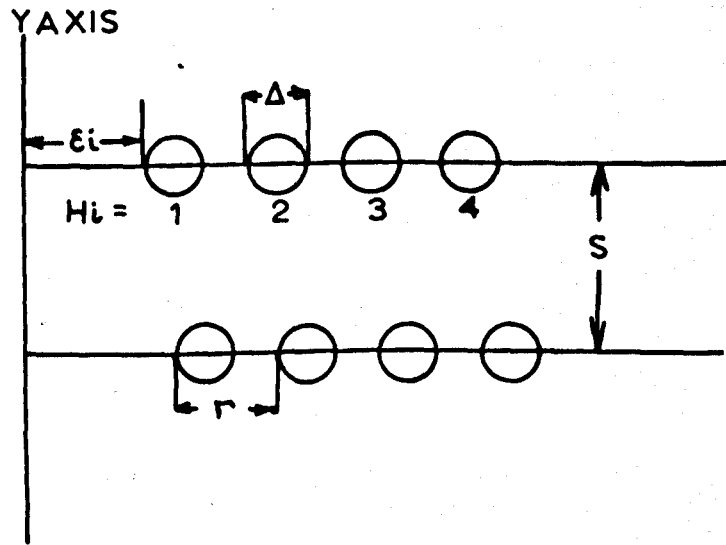
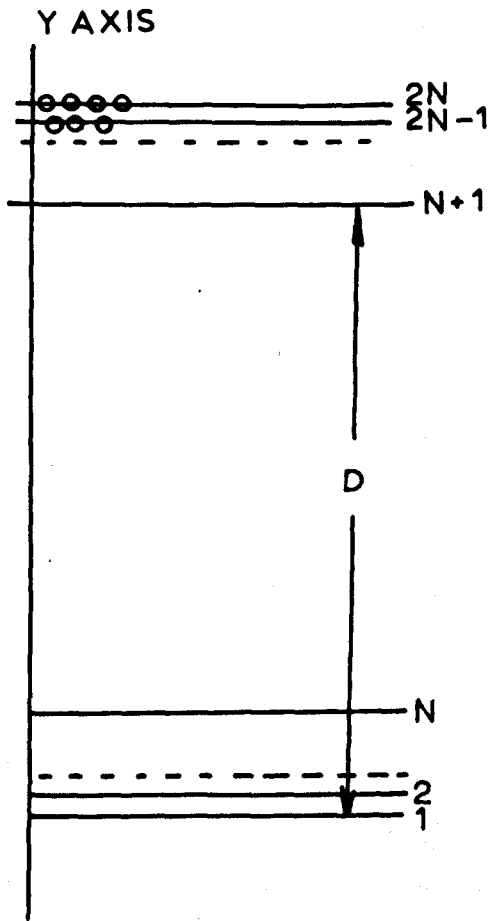


FIG. 3.3. (i).
TYPICAL SPECTROGRAPH
ARRAY.

Cartesian coordinate axes are constructed, the x-axis horizontal and perpendicular to the length of the tubes. The layers and tubes are numbered as in fig. 3.3.(i), the edge of the i^{th} layer being a distance E_i from the y-axis. The number of the tube which flashed in the i^{th} layer is designated H_i . Failure of a tube to flash in the i^{th} layer is indicated by setting $H_i = 0$.

If k is the number of the highest layer in which a tube flashed (i.e. $H_k \neq 0$; and $H_r = 0$ for all layers for which $r > k$), and similarly j is the number of the lowest layer in which a tube flashed (i.e. $H_j \neq 0$ and $H_r = 0$ for $r < j$), the gradient (A_0) and intercept on the y-axis (A_r) of the trajectory may be represented by the equations:

$$\frac{1}{A_0} = \frac{(H_k - H_j) + (E_k - E_j) + (\alpha - \beta)}{\gamma_k - \gamma_j}$$

and

$$A_r = \gamma_j - [(H_j - 1)\Gamma + E_j + \beta]A_0.$$

where α and β are unknown fractional distances across the H_k^{th} and H_j^{th} tube respectively.

The probability of a tube flashing in the i^{th} layer is a function of the intercept Φ_i on that layer. If Φ_i is measured in units of Γ ,

the integral part determines the unit which the trajectory crossed, and the fractional part the probability of the tube flashing. The variation of probability of flashing across the tube diameter can be determined experimentally (section 3), and for an assumed α and β , Φ_i is calculated:

$$\Phi_i = \frac{\gamma_i - A_r}{A_o \Gamma}$$

and the probability of obtaining the observed value of H_i computed. This can be repeated at each of the $2N$ levels, the product of such probabilities being an estimate of the merit of the assumed line as a representation of the actual trajectory. A number of such trial lines may be tested in this way, and the values of α and β selected which correspond to the line which gives the greatest probability of flashing the observed group of tubes. This line is referred to as the 'most probable trajectory' or m.p.t.

Each combination of α and β defines a line with an associated probability p of producing the observed group of H_i values. This is illustrated by an α, β diagram (fig. 3.3.(ii)), the contours of which are the loci of lines having an equal probability of representing the actual trajectory.

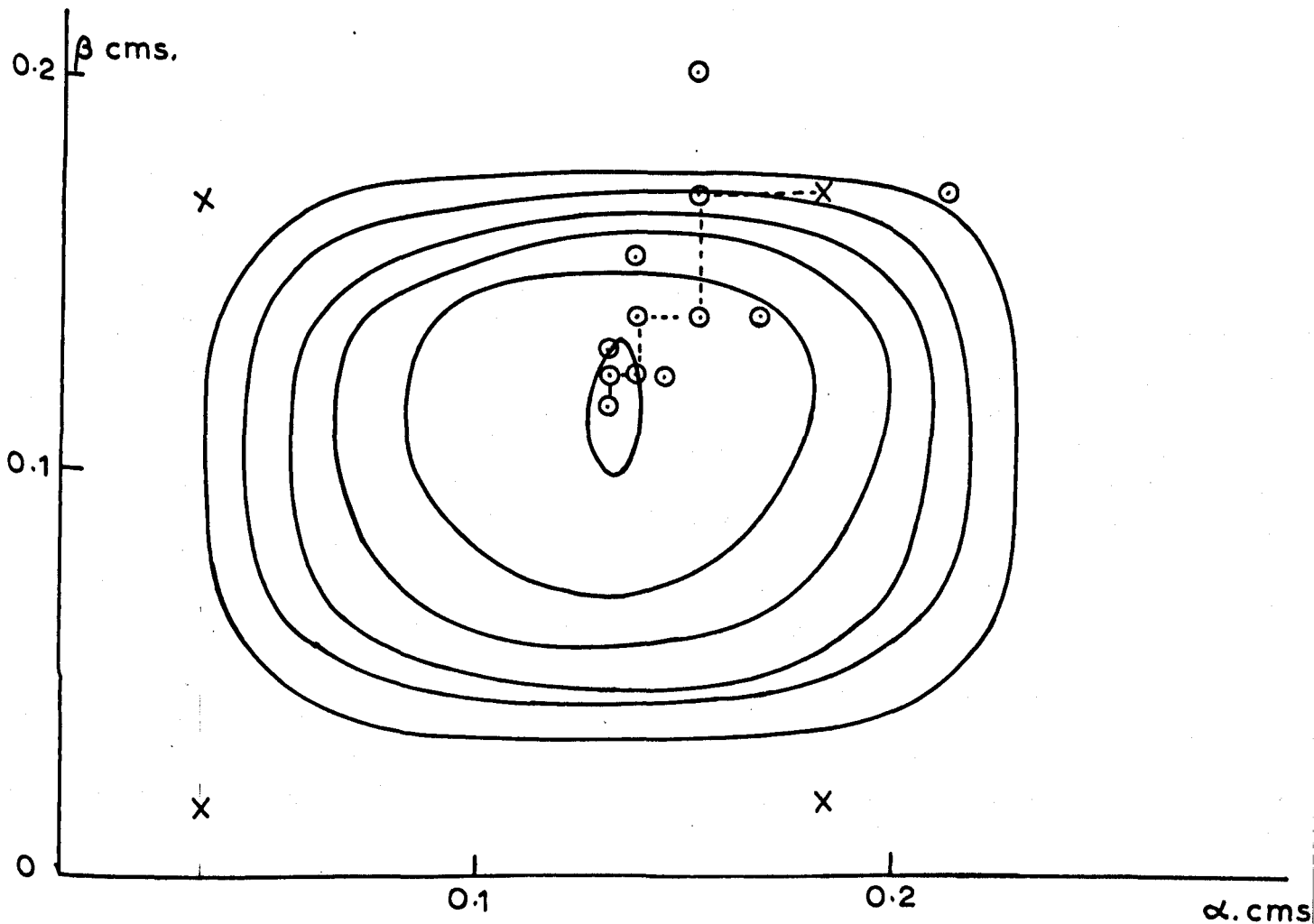


FIG. 3.3.(ii) α, β DIAGRAM
ILLUSTRATING "JUMP" ANALYSIS

- X INITIAL TRIAL LINES
 - LINES TRIED DURING JUMP ANALYSIS
 - COURSE TAKEN IN "JUMP" ANALYSIS
 - CONTOUR LINES OF EQUAL PROBABILITY.
- THERE IS A CONSTANT PROBABILITY DIFFERENCE BETWEEN EACH CONTOUR.

Figure 3.3.(iii) is a cross-section of this diagram showing the variation of the probability as a function of α , maintaining β constant. Several of these diagrams have been constructed and it is apparent that all are uni-modal, smooth, and approximately symmetrical curves. A direct result of this behaviour is that it has enabled a quicker and equally accurate 'jump' method to be developed.

Initially a small number of lines (α, β) are tried, and that with the greatest probability of occurrence selected, say α', β' . Keeping $\beta = \beta'$ (Constant), two new lines are tried, for which $\alpha = \alpha' + \delta$, and $\alpha = \alpha' - \delta$. The probability of each line is computed, and the value of α adjusted such that

$$\left. \begin{aligned} \alpha'' &= \alpha' + \delta \\ \alpha'' &= \alpha' \\ \alpha'' &= \alpha' - \delta \end{aligned} \right\} \begin{array}{l} \text{According to which} \\ \text{gives rise to the} \\ \text{greatest probability} \end{array}$$

This is repeated keeping $\alpha = \alpha''$ (constant), so as to arrive at a new value of β'' . The cycle is now repeated several times with decreasing values of δ . In fig. 3.3.(ii) the crosses represent the initial trial lines, the circles the various lines tried during the 'jump stages', and the dotted lines

indicate the path followed during these stages. The necessary number of trial lines, jump stages and their magnitude will be discussed in section 3.4 where specific consideration is given to errors.

The method has been applied in particular to data from the Nottingham spectrograph. In this apparatus there are two identical arrays of the type discussed, symmetrically situated about the common x-axis at the centre of an air gap magnet. The dimensions of the apparatus are summarised in Table 3.3.(i).

Number of layers per tray,	$N = 5$
Separation of trays,	$D = 95.38 \text{ cm.}$
Internal tube diameter,	$\Delta = 0.59 \text{ cm.}$
Horizontal separation of tube centres,	$\Gamma = 0.800 \text{ cm.}$
Vertical separation of tube centres,	$S = 1.47 \text{ cm.}$
Vertical length over which field may be assumed constant,	$l = 16.5 \text{ cm.}$

TABLE 3.3.(i)

Each particle trajectory is independently analysed above and below the field and the angular deflection assumed to occur at the x-axis may be deduced. The integral part of ϕ_i may be used as a check on the initial data. If the m.p.t. does not intersect the tube indicated, the computer prints the number of the layer at which the discrepancy occurred. This is useful because errors in interpreting the photographic records occur occasionally and knock-on electrons are not infrequent. The computer also detects occurrences when the m.p.t. does not satisfy the acceptance conditions imposed upon it. Again a characteristic fault number is recorded.

In this way the computer has successfully analysed results from the Nottingham spectrograph. The accuracy achieved surpasses that for any previous method of analysis and will be discussed fully in section 3.4. Approximately 100 complete events may be analysed in 12 minutes.

Wolfendale (private communication) has pointed out that a further restriction may be applied to a trajectory in the particular case of a momentum spectrograph; as a consequence of the association of the initial and final trajectories.

If this condition is enforced, an increase in accuracy of the analysis might be expected. For high momentum particles it is reasonable to assume that multiple scattering is negligible and that the angular deflection is small. For low momentum particles, neither of these assumptions is justified and the treatment is more complicated. However, since these particles are analysed with sufficient accuracy without using this further criterion, we may consider only those particles showing small angular deflections in the preliminary analysis. It may be shown that the initial and final trajectories will coincide at

$$y_c = \frac{l}{2} \tan \psi/2 \tan (i - \psi/2).$$

where l is the vertical length over which the field may be assumed constant, and ψ is the angular deflection. The angle of incidence, i , is restricted by the acceptance conditions imposed on the apparatus and is usually small (e.g. ~ 0.1 radians in the Nottingham spectrograph). y_c is very small and will be approximately zero for high momentum particles.

If the preliminary 'jump analysis' indicates a small angular deflection, the particle is subjected to further analysis treating its two trajectories as dependent and intersecting at the x-axis. If the most probable initial and final trajectories are given by

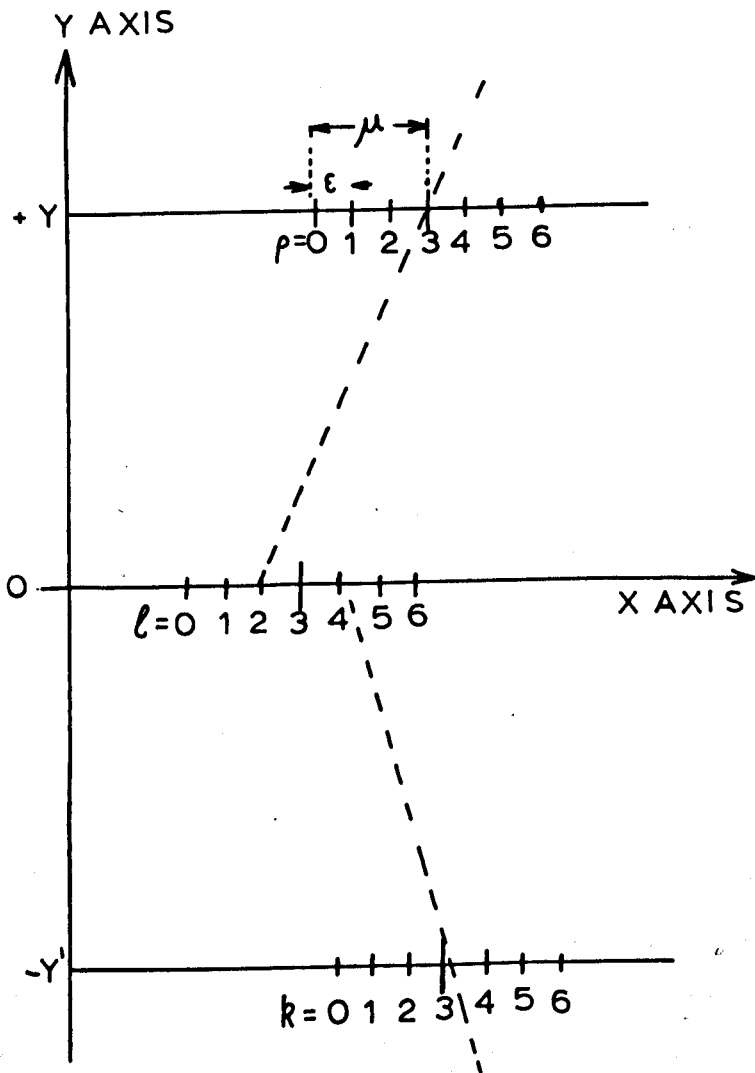
$$y = a_i x + b_i \quad \text{and} \quad y = a_f x + b_f.$$

then points are defined on two arbitrary levels ($\pm y^1$) at

$$\begin{aligned} x_1' &= (y' - b_i)/a_i - \mu + pE, \\ \text{and } x_2' &= (-y' - b_f)/a_f - \mu + kE. \quad (\text{Fig. 3.3. (iv)}) \end{aligned}$$

Similarly points are defined at $y = 0$, $x_3' = \frac{1}{2} (b_i/a_i + b_f/a_f) - \mu + lE$, in which p , k , and l take integral values from 0 to n , E is a constant and $\mu = \frac{nE}{2}$. A complete trial trajectory is now defined by its p, k, l values, and the associated probability W_{pkl} . If the angular deflection measured in the preliminary analysis is ψ_J then the angular deflection of any trial line is given by

$$\psi_{pkl} = \psi_J + \frac{E}{y'} (4x + p + k - 2l).$$



--- PRELIMINARY ESTIMATE
OF TRAJECTORY.

FIG. 3.3. (i v)

ILLUSTRATING
ENFORCEMENT OF
ASSOCIATION OF TWO
HALVES OF A
TRAJECTORY

and the mean angular deflection may be defined as

$$\bar{\psi} = \frac{\sum \psi_{pkl} w_{pkl}}{\sum w_{pkl}}$$

where the summation is over all values of p, k and l. This may be regarded as the best estimate of the angular deflection of the trajectory.

The magnitude of E is such that the limiting values of ψ_{pkl} considered have negligible probability of occurrence (fig. 3.3. (v)). Since $(n+1)^3$ trajectories are tested for any particle, the size of n is solely determined by the time taken in analysis.

3.4 Errors in Analysis of Flash Tube Data

The errors arising in the analysis of flash tube data may be considered in four categories:

- (1) that in obtaining the best estimate of the actual trajectory;
- (2) that introduced as a result of the best estimate not coinciding with the actual trajectory;
- (3) that introduced by unavoidable defects of the apparatus.

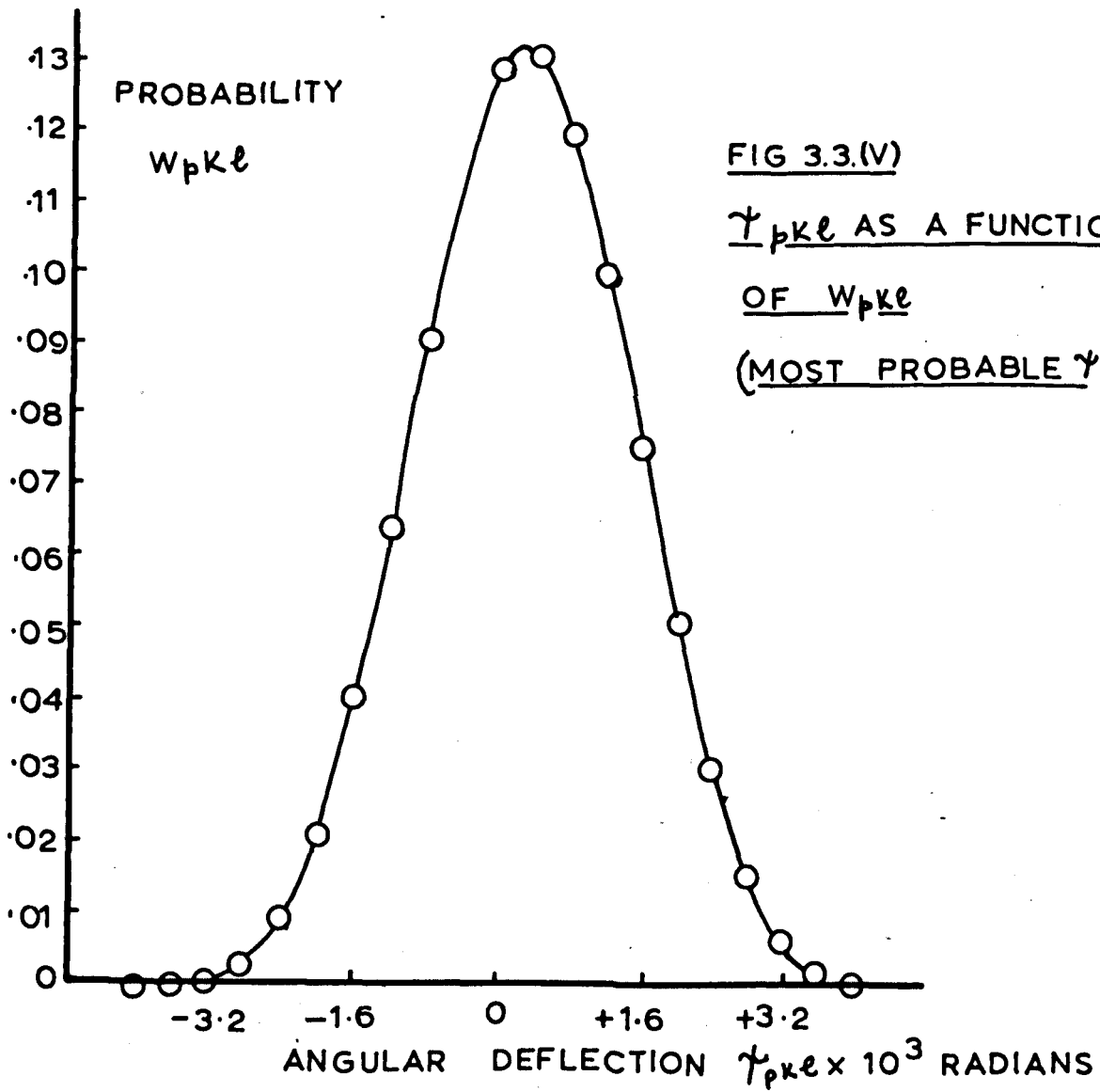


FIG 3.3.(V)

$\gamma_{pk\ell}$ AS A FUNCTION

OF $W_{pk\ell}$

(MOST PROBABLE $\gamma_{pk\ell} = 0$)

(4) that introduced by errors in $P(\theta)$.

(3) and (4) will be considered in the Appendix.

Before considering the first two categories, it is necessary to establish a reasonable criterion for the 'best estimate'. It is assured that the salient parameter is the angle ϕ which a trajectory makes with some reference direction. On the α, β diagram a straight line inclined at 45° to the axes and passing through a point (α, β) (fig. 3.4.(1)) is the locus of points representing trajectories each with the same angle as the particular trajectory (α, β) . The error in angle $\delta\phi_i$ made if the point (α_i, β_i) with an associated probability P_i represents the actual trajectory is

$$\delta\phi_i = t_i / (y_k - y_j) = \frac{(\alpha_i - \beta_i) + (\beta_0 - \alpha_0)}{y_k - y_j}$$

where (α_0, β_0) represents any estimate of the trajectory. The probability of occurrence of such an error is proportional to P_i , and we define the quantity

$$\mu_\phi = \frac{\sum P_i \delta\phi_i}{\sum P_i}$$

for many points (α_i, β_i) . The 'best estimate' of the direction of the trajectory is defined such that

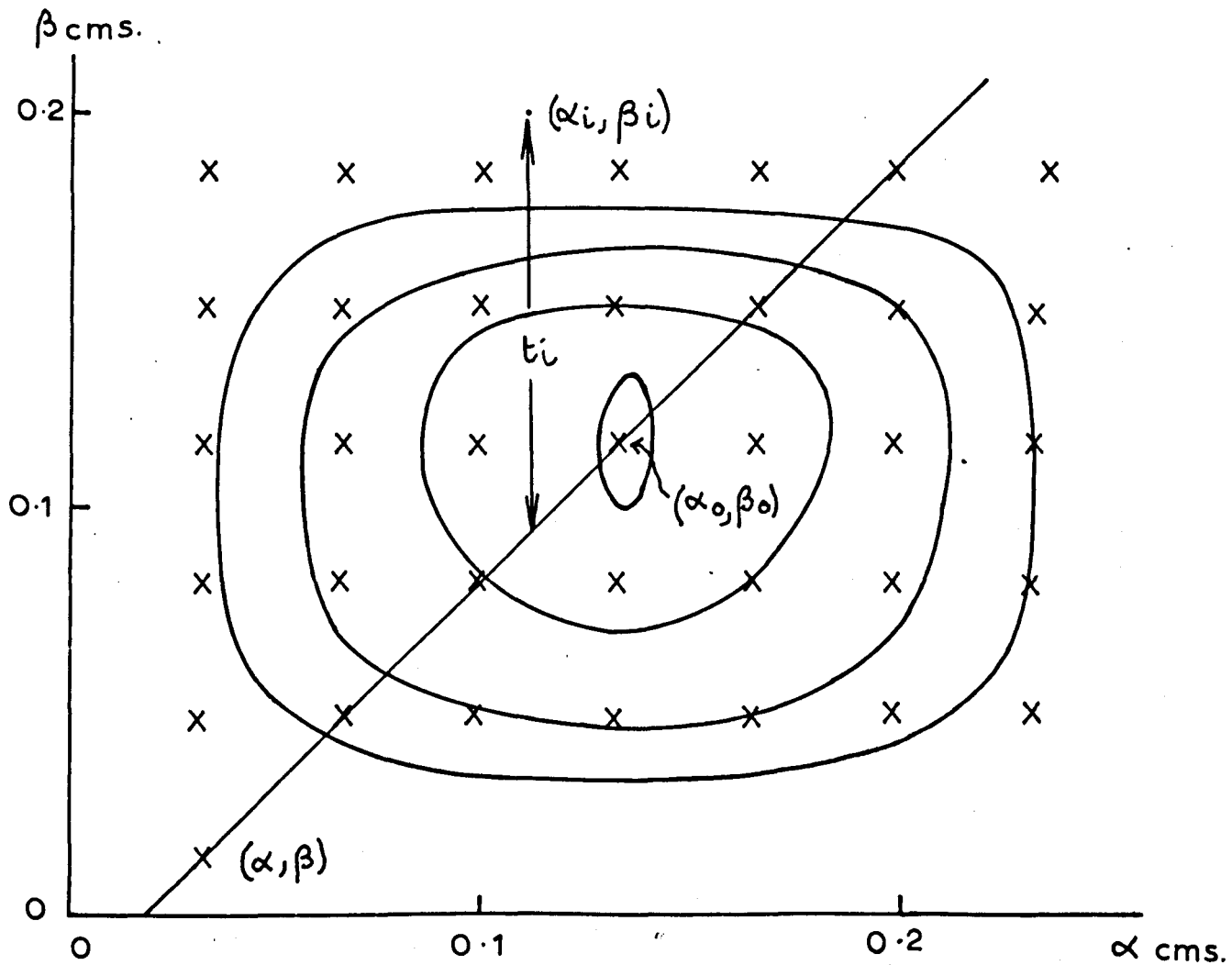


FIG. 3.4. (i). ILLUSTRATING DERIVATION OF
ANGULAR ERROR μ_ϕ

X TYPICAL POINTS (α_i, β_i) USED IN THE
 DERIVATION.

$\mu\phi = 0$; that is, it is assumed to be the weighted mean of all possible directions. The computer is used to derive $\mu\phi$ based on an assumed direction (α_0, β_0) , and the 'best estimate' computed as:

$$\phi_b = \phi_0 + \mu\phi$$

(1) Errors in deriving ϕ_b

It is time consuming and unnecessary to derive the actual 'best estimate', and in practice the m.p.t. is used as an approximation to it. Errors are introduced in this way, and also because the true m.p.t. may not be found. The latter is dependent on the number and sizes of jump steps and the number of initial trial lines used in the analysis. This was investigated by analysing several trajectories using various values of these parameters. By comparing the probability of occurrence of each of the m.p.t.'s it was found that, for a five-layer array, a reasonable compromise between time of analysis and accuracy was obtained when 16 trial lines and 3 jump stages were used. The magnitude of the successive jump steps was approximately in the ratio 2 : 1 with the first equal to half the distance between two trial lines (fig. 3.3.(ii)).

(2) Errors as a Result of the Non-coincidence of the Actual and the 'Best Estimate of the Trajectory

These errors are inherent in all flash tube arrays, independent of the method of analysis. From the preceding discussion, a reasonable measure of this error is the mean square value of $\delta\phi$, thus

$$\sigma_{\phi}^2 = \frac{\sum P_i (\delta\phi)^2}{\sum P_i} - (\mu_{\phi_0})^2$$

When the m.p.t. is used as the estimate of the trajectory the errors due to (1) and (2) may be combined to give

$$\sigma_t^2 = \frac{\sum P_i (\delta\phi)^2}{\sum P_i}$$

Using information from a ten layer array (table 3.3.(i)), about 30 particles were analysed, and mean values of

$$\sigma_{\phi} = (7.6 \pm 0.2) \times 10^{-4} \text{ c} \quad \text{and} \quad \sigma_t = (8.3 \pm 0.3) \times 10^{-4} \text{ c}$$

were deduced. The small difference indicates the effect introduced by the mode of analysis as discussed in (1).

A more direct measurement of the total error involved in analysis was obtained by simulating the passage through an array of a particle of known

trajectory, and comparing directly the known and the measured angle. Whilst being more direct, it cannot distinguish between inherent and analysis error, and furthermore is less precise. It provides, nevertheless, a reasonable check on the results of the previous method. Using 100 particles, a mean value of

$\sigma_{\epsilon} = (9.3 \pm 0.9) \times 10^{-4} \text{ } ^{\circ}$ was deduced for the same ten layer array.

In the particular case of momentum spectrographs, the intercept method described in section 3.3 is of some interest. The inherent error of this method is determined by the spread of such probability versus angular deflection curves as shown in fig. 3.3. (v). This may be measured in terms of an r.m.s. error such that

$$\sigma_{\gamma}^2 = \frac{\sum (\gamma_{pk\ell})^2 w_{pk\ell}}{\sum w_{pk\ell}} - (\bar{\gamma})^2$$

and has been computed for 12 particles traversing the Nottingham spectrograph giving $\sigma_{\gamma} = 0.00093$. This may be compared with the inherent error for the same particles when analysed not using this refinement. These figures are obtained using an effective $P(\theta)$ for the spectrograph (section 3.5).

3.5 The Efficiency Distribution

The method of analysis described utilises the experimentally derived function $P(\theta)$. The nature of the distribution has been investigated by Ashton et al. (1958) in the case of tubes filled with neon at a pressure of 0.8 atmospheres. Using a similar procedure the distribution has been determined for the high pressure (2.4 atmospheres) tubes used in the Nottingham spectrograph.

The magnet was removed from the spectrograph, and the trajectories were defined by ten layers of tubes, viz. two or three layers in each of the four arrays. The intercepts on the remaining group of ten layers were obtained, and since it was known whether the appropriate tube flashed, the function $P(\theta)$ could be derived. To increase the statistical precision, the events were re-analysed using the second group of ten layers to define the trajectory. In order to reduce errors due to scattering, trajectories were selected which had previously shown an angular deflection of less than 0.0005° . The experimental points obtained from 580 layer traversals are shown in fig. 3.5(i).

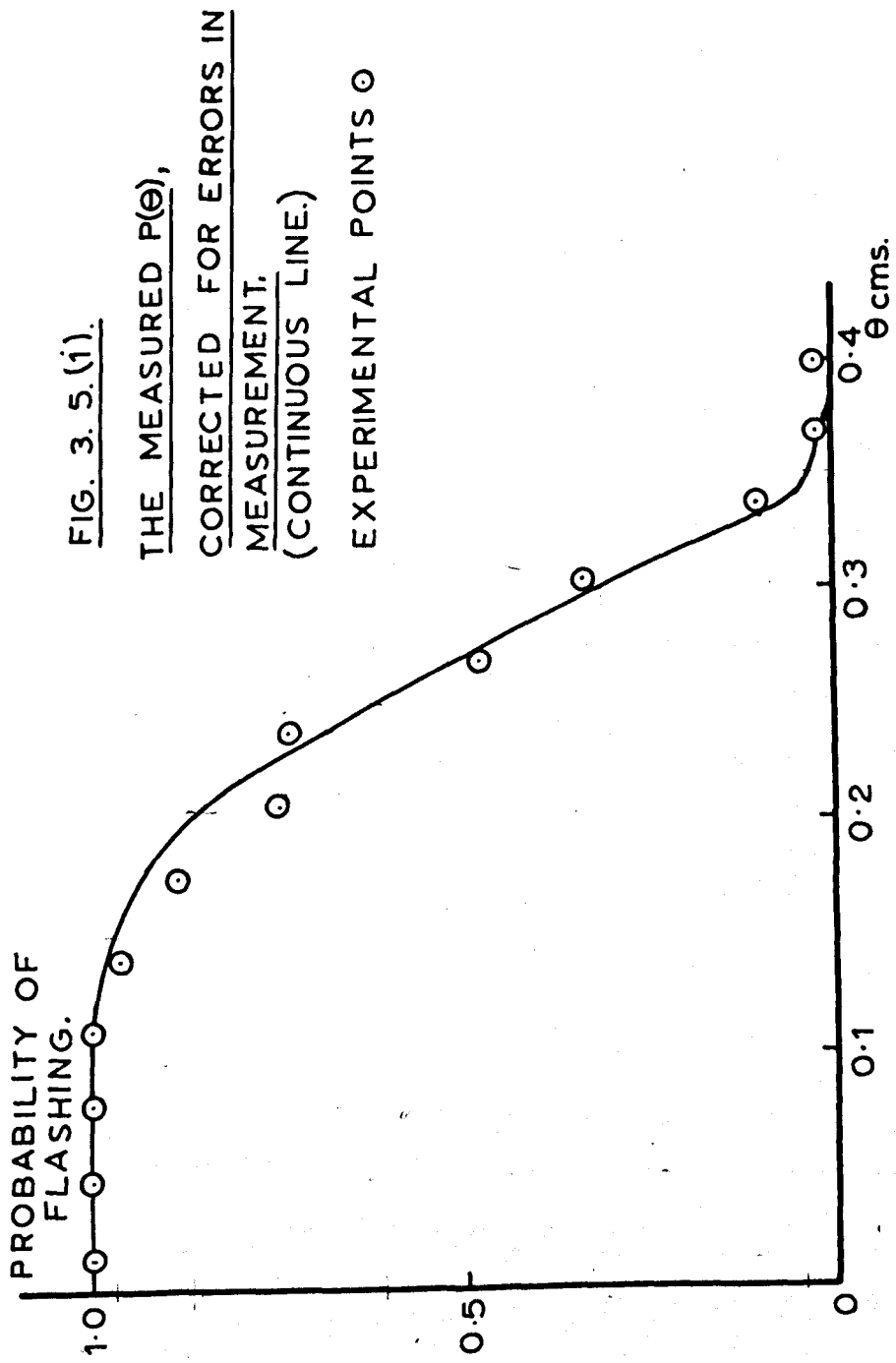


FIG. 3. 5. (1).
THE MEASURED $P(\theta)$,
CORRECTED FOR ERRORS IN
MEASUREMENT,
(CONTINUOUS LINE.)
EXPERIMENTAL POINTS \circ

The measured distribution is broadened by several factors, the most important being:

- (1) Variations in tube diameters and random errors in locating the tubes.
- (2) Knock-on electrons.
- (3) Errors in locating the trays.
- (4) Errors in determining θ .

However, for the purpose of analysis of spectrograph data, only the effective probability distribution is required and this is obtained from the measured distribution corrected only for errors introduced by (4). By a series of successive approximations, using a knowledge of the r.m.s. error (0.032 ± 0.003 cm) in measurements of θ , the small correction for (4) was computed, and $P(\theta)$ determined (fig. 3.5.(i)). It is not necessary to correct for (1), (2), and (3) because these will inevitably be present in any measurements made by the array, and actually contribute to the effective distribution.

3.6 Conclusion

The computer method has several advantages, the most important of which are the following:-

(i) The trajectory (m.p.t.) of a particle may be computed in 0.06 minute. In a spectrograph very high momentum particles may be automatically reanalysed using the intercept method with a consequent 20% gain in accuracy.

(ii) The method objectively uses all the information available, and its accuracy surpasses that of previous methods even if the m.p.t. is used as an estimate. At the expense of a further 0.25 minute a trajectory can be analysed with negligibly small errors due to the mode of analysis. Furthermore it is possible to determine the angular error with considerable accuracy.

(iii) The method is extremely flexible, enabling any stage of the calculation to be recorded (e.g. the intercept of a trajectory at each level as in the measurement of $P(\theta)$) and minor amendments and additions to the programme may be made with ease.

The speed, accuracy, and flexibility of the method may be used to particular advantage in array design (Appendix). These advantages are also expected

Chapter 4

Results and Conclusions

4.1 Introduction

In this chapter an investigation will be described to determine whether the sea level spectra of muons at zenith angles of 0° , $30^\circ W$ and $45^\circ W$ in the range 0.7 - 30 Gev/c can be explained simultaneously by processes involving an inverse power law momentum distribution at production, which is assumed to occur at a single level in the atmosphere, and the retention by the muons of the direction of the parent π -mesons.

The data were recorded by re-projecting the photographic records on to a scale diagram of the flash tube arrays, and noting the co-ordinates of the tubes which had flashed. If ambiguity occurred because of the flashing of more than one tube in a layer, the event was rejected. However, many of the events in which two adjacent tubes had flashed could be interpreted unambiguously, and were accepted. As the probability of knock-on electron or shower production is not momentum sensitive in the range under investigation (Fowler and Wolfendale, (1958)), no bias is introduced by this arbitrary acceptance condition. The results were analysed using the

method described in chapter 3, trajectories showing an intercept difference of > 10 mm. at the x-axis being regarded as unassociated, and in all 1052, 1010 and 1033 particles were accepted at $45^\circ W$, $30^\circ W$ and 0° respectively. The overall evaluation of the muon production spectrum is thus based on the observation of 3095 particles, which consist of at least 99.5% muons, this being ensured by the 47.3 cm. of lead above the lower tray of geiger counters.

4.2 Measurement of Errors due to Multiple Scattering

The magnetic deflection, θ_M , of a particle of momentum p traversing the spectrograph is given by

$$\theta_M = \frac{300 \int_{-\infty}^{+\infty} H dl}{p} \quad (1)$$

and its r.m.s. projected angle of scattering $\langle \theta_s \rangle$ is

$$\langle \theta_s \rangle = \frac{1}{\sqrt{2}} \sum \frac{K t^{1/2}}{p \beta} \quad (2)$$

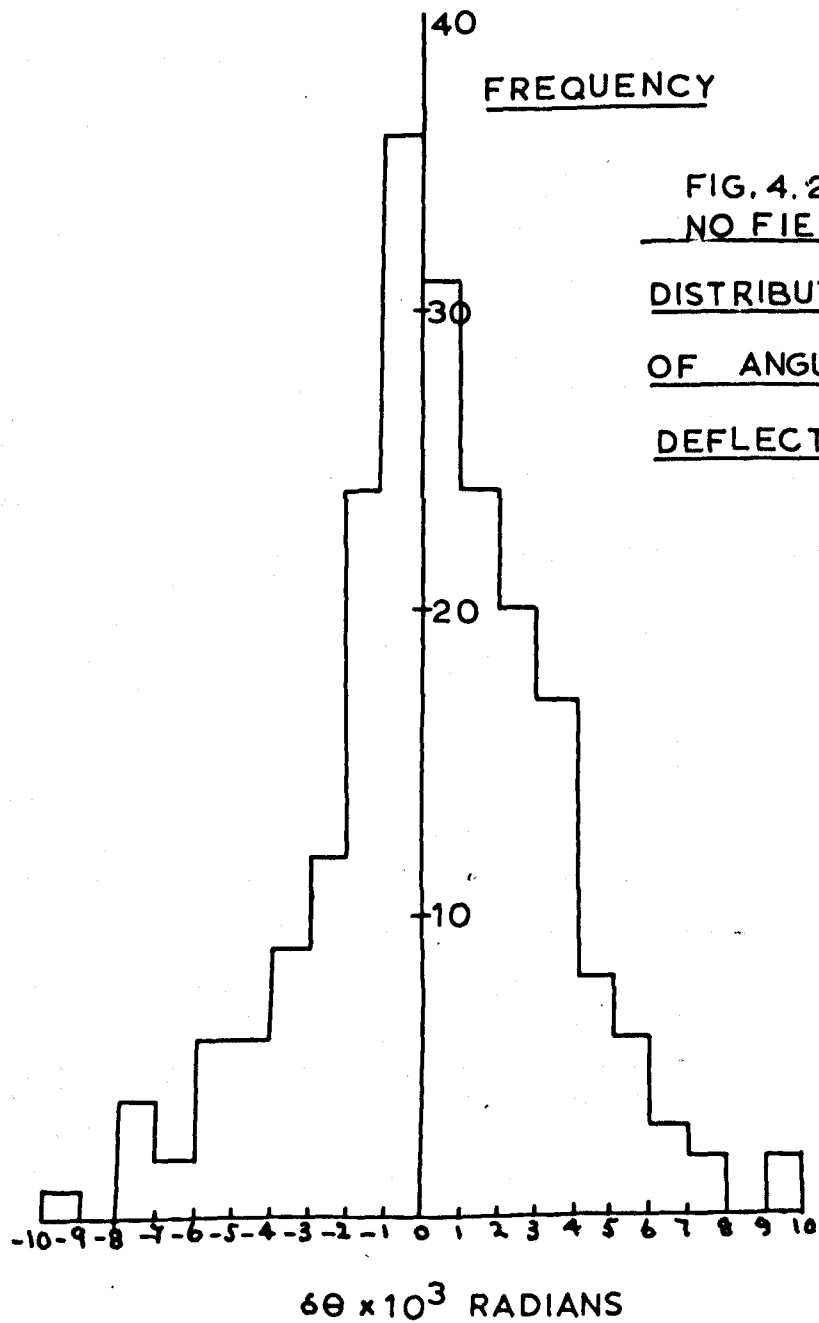
where $K = 22$ Mev., and t is the thickness in radiation lengths of material traversed. The sum is taken over the material in the trays P, Q and the geiger counters B, C, which contributes to $\langle \theta_s \rangle$. Thus the ratio $\langle \theta_s \rangle / \theta_M$ is

$$\frac{\langle \theta_s \rangle}{\theta_M} = \frac{1}{\sqrt{2}} \frac{\sum K t^{1/2}}{300 \int_{-\infty}^{+\infty} H dl} \cdot \frac{1}{\beta} \quad (3)$$

which for $\beta \rightarrow 1$, i.e. $p > 0.5 \text{ Gev}/c$, is a constant, independent of momentum.

The value of $\langle \theta_s \rangle$ for the spectrograph was calculated by integrating (2) over the range $0.76 \omega/c - \infty$ for the sea level momentum spectrum corrected for scattering in and out of the instrument (see 4.3). The value obtained is $\langle \theta_s \rangle = 2.97 \times 10^{-3}$ radians. Combining this with the error in deflection measurement, $\sigma_\psi = 1.15 \times 10^{-3}$ radians (chapter 3) gives a value $\sigma = 3.18 \times 10^{-3}$ radians to be expected for the "no field" distribution in angular deflection, ψ . The measured distribution, based on 214 events, is shown in figure 4.2.(1). It is seen to be approximately normal, and has a standard deviation, $\sigma = (3.21 \pm 0.27) \times 10^{-3}$ radians. The good agreement with the value predicted is taken to indicate an accurate assessment of the thickness, t , of scattering material contributing to $\langle \theta_s \rangle$.

Assuming this value of t , a value of $\langle \theta_s \rangle / \theta_M = 0.177$ was calculated using equation (3). This value, and that of σ_ψ , was checked using the method of Ashton (1959). The "no field" distribution in intercept differences on the x-axis of the two halves of a trajectory (figure 4.2.(ii)) is again seen to be approximately normal, justifying the following procedure.



FREQUENCY

FIG. 4.2(i).
NO FIELD
DISTRIBUTION
OF ANGULAR
DEFLECTIONS

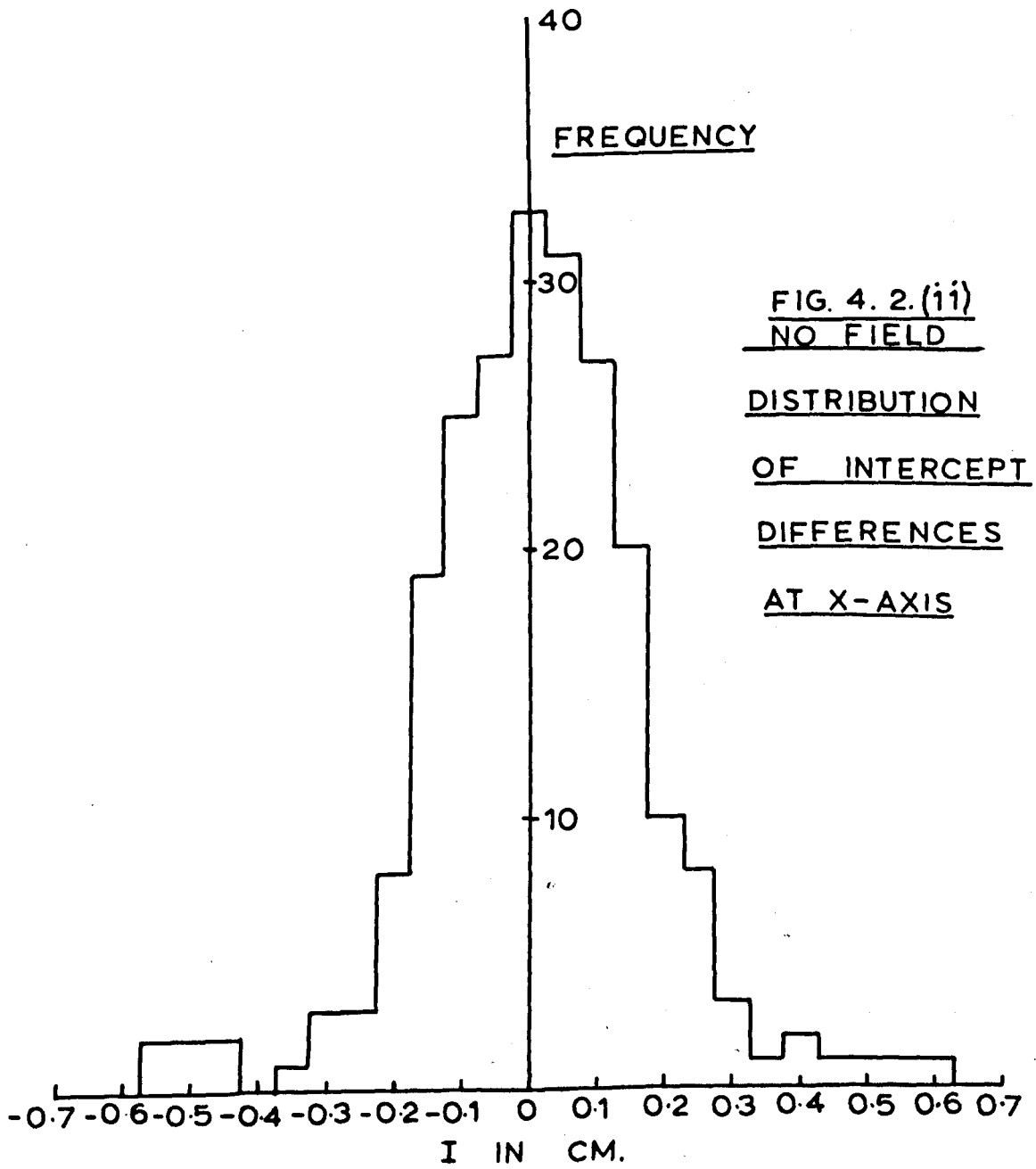


FIG. 4. 2. (ii)
NO FIELD
DISTRIBUTION
OF INTERCEPT
DIFFERENCES
AT X-AXIS

At any momentum:

$$\sigma_I^2 = 2 D^2 \langle \theta^2 \rangle + \sigma_0^2$$

where σ_I is the r.m.s. value of the intercept difference, I (figure 4.2.(iii)) due to errors of deflection measurement and scattering, $\langle \theta \rangle$ is the r.m.s. projected scattering angle in one half of the spectrograph, D is the distance between the x-axis and the centre of gravity of the scattering material (20 cms.), and σ_0 is the r.m.s. value of I due only to errors in deflection measurement.

From equation (3):

$$\frac{\langle \theta_s \rangle}{\theta_M} = K_1 \quad \text{where} \quad \langle \theta_s \rangle = \sqrt{2} \langle \theta \rangle.$$

$$\text{i.e.} \quad \sigma_I^2 = K_1^2 D^2 \theta_M^2 + \sigma_0^2$$

A graph of σ_I^2 versus θ_M^2 is shown in figure 4.2.(iv). The gradient gives $K_1 = 0.19 \pm 0.02$, and the intercept $\sigma_0^2 = (1.34 \pm 0.20) \times 10^{-2} \text{ cm}^2$, giving

$$\sigma_\gamma = \sqrt{2} \frac{\sigma_0}{H} = (1.25 \pm 0.10) \times 10^{-3} \text{ radians.}$$

The agreement with theoretical calculations is good,

and the values $\langle \theta_s \rangle / \theta_M = 0.177$ and σ_γ

= 1.15×10^{-3} radians have been employed

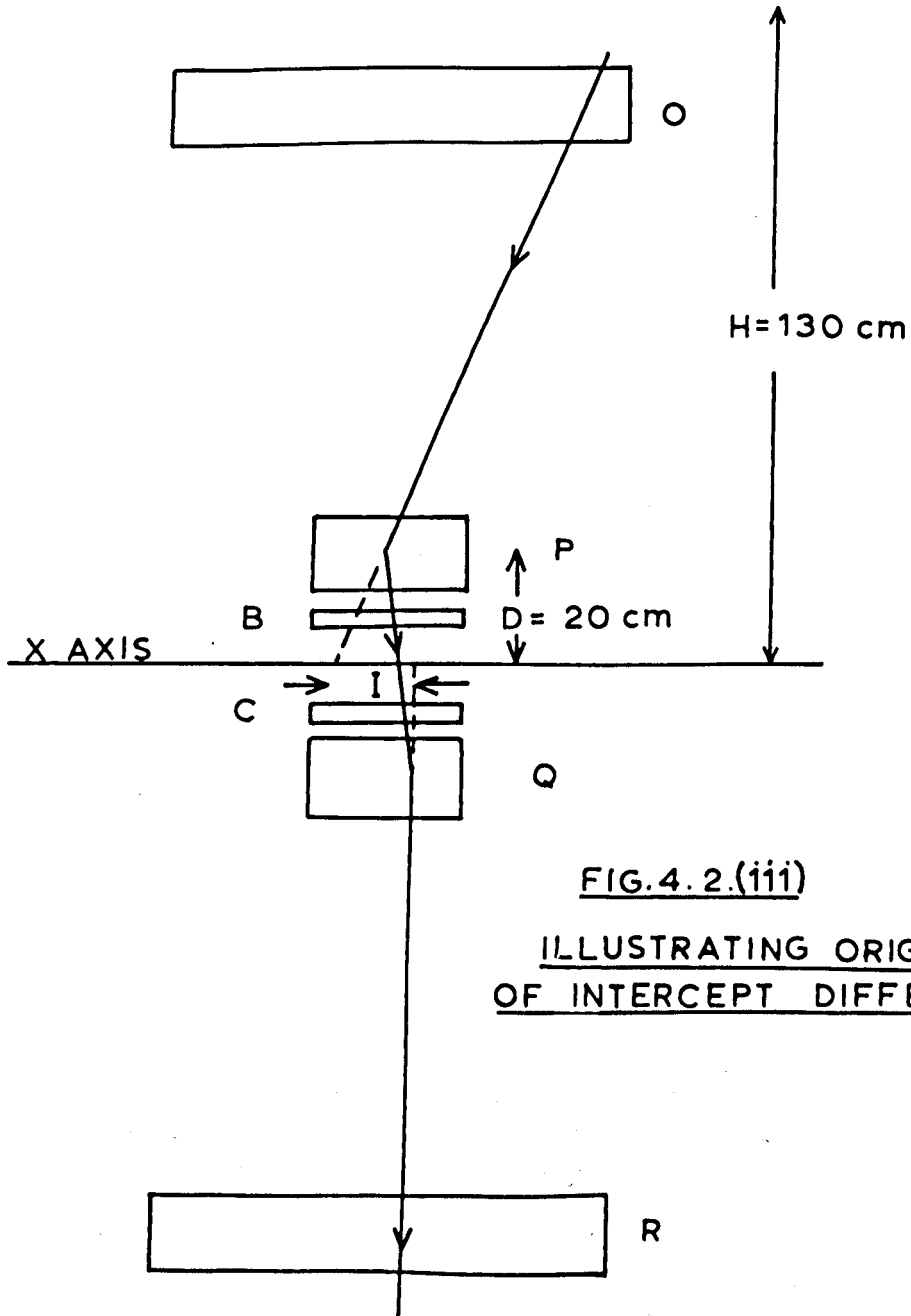


FIG. 4.2.(iii)
ILLUSTRATING ORIGIN
OF INTERCEPT DIFFERENCE.

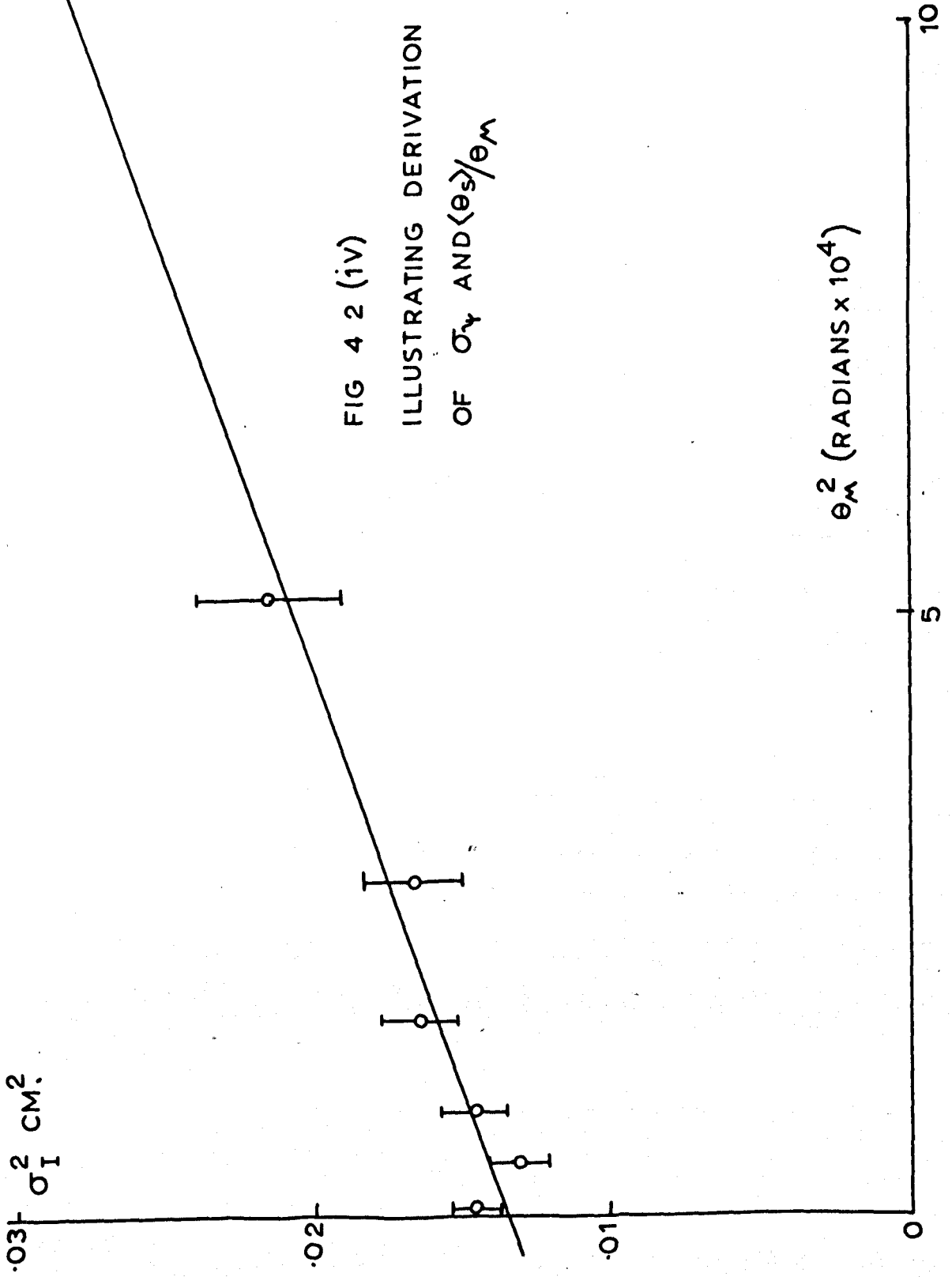


FIG 4 2 (iv)

ILLUSTRATING DERIVATION
OF σ_V AND $\langle \theta_s \rangle / \theta_M$

θ_M^2 (RADIAN x 10⁴)

throughout. Using the r.m.s. error in deflection measurement, the m.d.m. (chapter 1) of the spectrograph is 28.5 Gev/c.

4.3 Calculation of the Magnetic and Scattering Correction Factors

As with all spectrographs of the type used, there is a finite probability of loss of particles from the solid angle of the instrument due to multiple scattering and magnetic deflection. The basic geometry of the spectrograph is shown in figure 4.3.(i), the solid angle being defined by the lengths indicated. Any particles falling outside these limits were rejected in analysis. The problem is to find the probability of acceptance of a particle of momentum p , compared with that for a particle of $p = \infty$. Treating the scattering deflections in the front and back planes as independent, which is justified for the small angles considered, four causes of loss of particles may occur:

- by (1) Magnetic deflection in the front plane beyond the central 36 cm. of D
- (2) Scattering in the front plane beyond the total

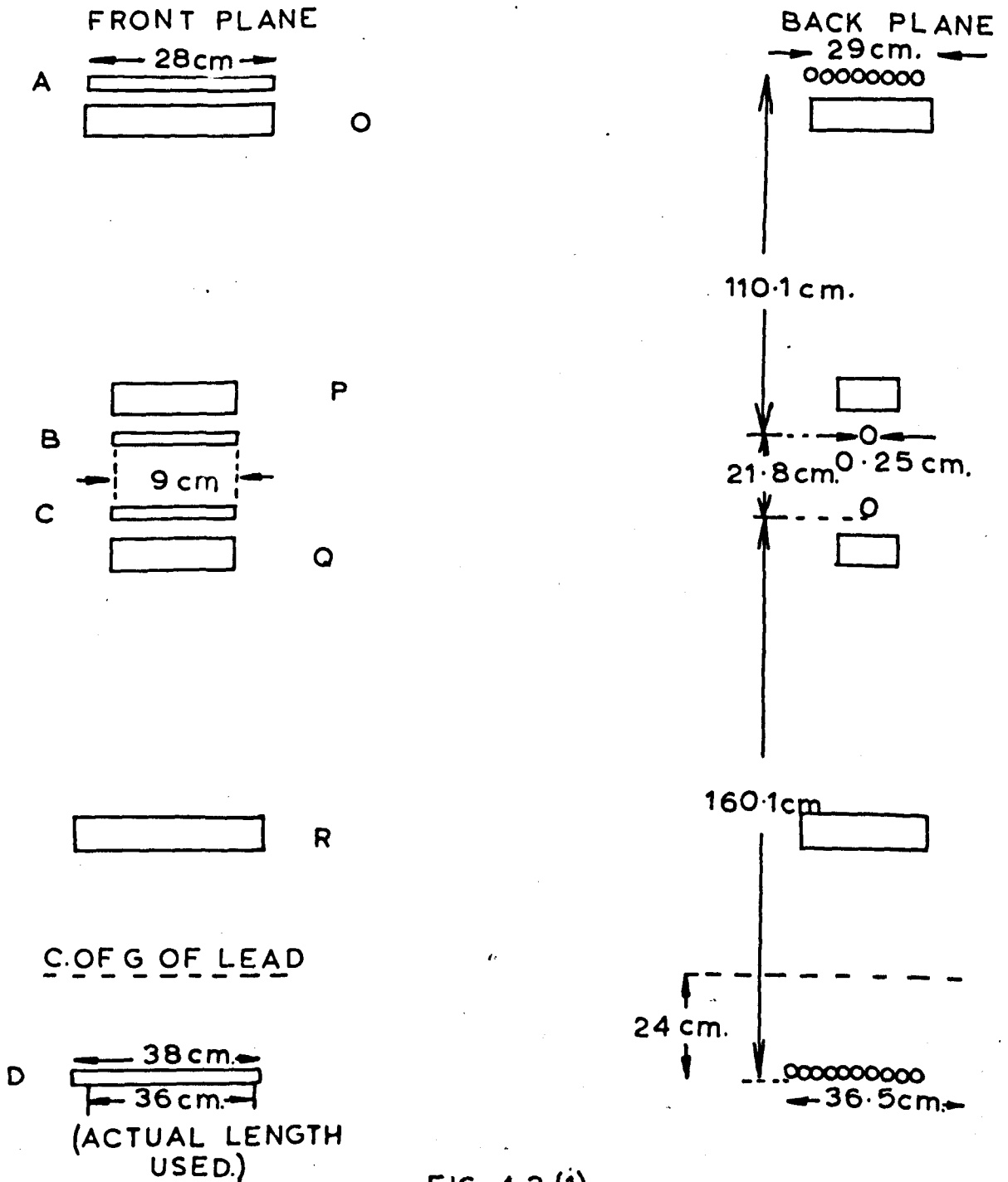


FIG.4.3.(i)

BASIC GEOMETRY OF
SPECTROGRAPHY
 (NOT TO SCALE)

length of D by the lead and tray R, assumed to be concentrated at a horizontal line through the centre of gravity of the lead; resulting in non-registration of the particle by the coincidence circuit.

(3) Scattering in the front plane beyond the central 36 cm. of D by all the material except the lead, (i.e. A, B, C, O, P, Q) assumed to be concentrated at the central line of the magnetic field.

(4) Scattering in the back plane beyond the limits of D by all the material.

Particles may also be deflected into the solid angle by processes like (1), (3) and (4).

The probability of acceptance as a function of momentum was determined by computer programmes. For the purposes of computation, lines representing the counters B and C were divided into 50 equal parts in the front plane, and 25 in the back plane. Then the lines joining each combination represent particles with $p = \infty$. In calculating the probability, P_0 , of scattering out, only trajectories falling inside the solid angle were considered, and assuming a $\cos^2 \theta$

variation of intensity with inclination to the vertical, P_0 was determined using the ogive to the normal curve. To calculate the probability, P_I of scattering in, only those trajectories falling outside the solid angle were considered, and P_I determined in the same way. The magnetic correction factor was calculated by a similar process to that described above, and the scattering, magnetic, and resultant correction factors are shown as a function of momentum in figures 4.3.(i), (ii) and (iii) respectively. Any theoretical spectrum must be multiplied by the resultant correction factor before comparison with the experimental results.

4.4. Derivation of Comparison Spectra

Following the method of Moroney and Parry (1954), theoretical deflection spectra were calculated for muons arriving at zenith angles of 30° and 45° . The survival probability,

$$W(x_0, p_0, \theta) = \exp \left\{ -\frac{1}{\tau c} \int_0^{x_0} \frac{dx}{f(x)} \right\} \quad (1)$$

represents the probability that a muon will survive to sea level with a momentum P_0 at a zenith angle θ

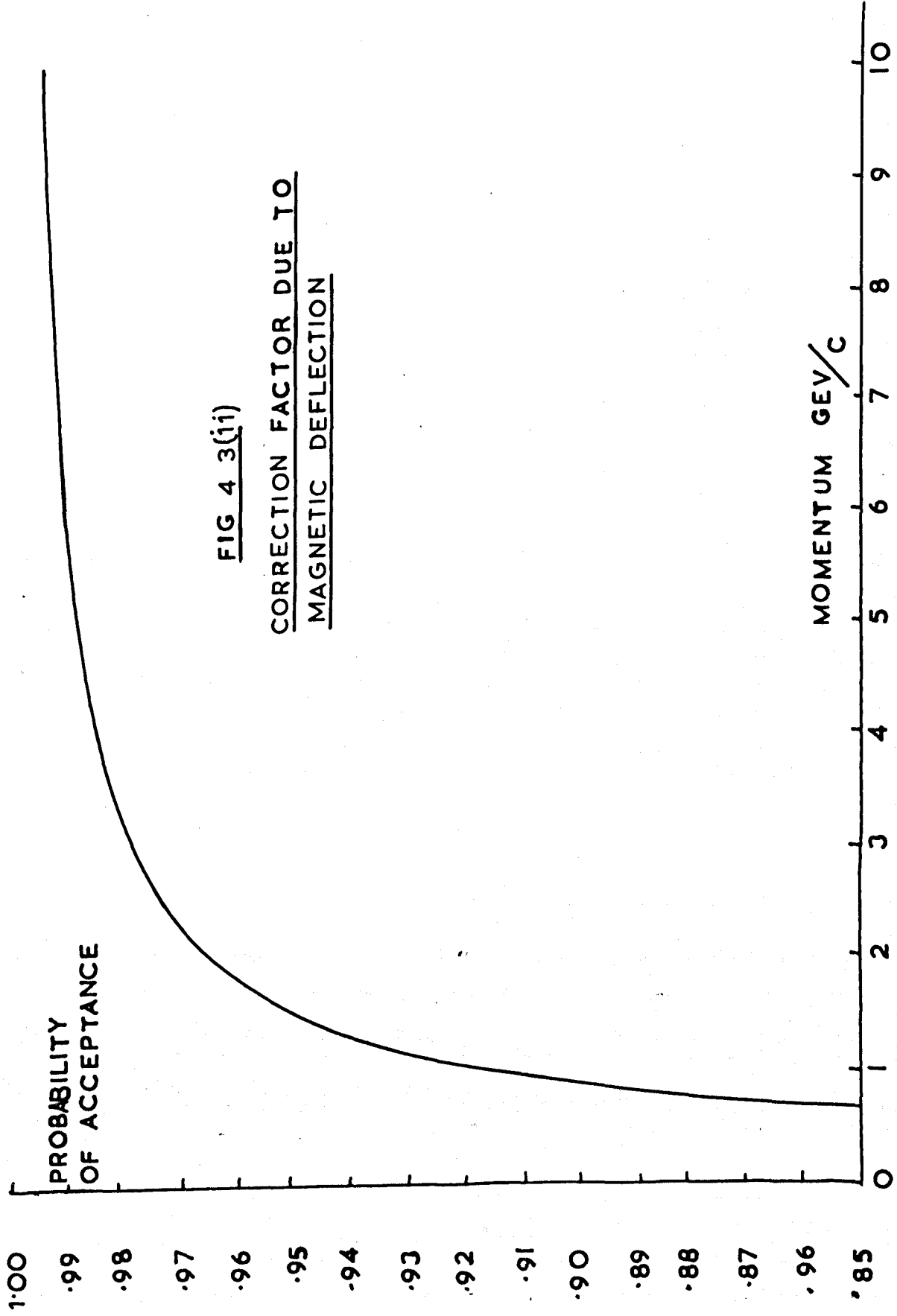


FIG 4 3(i1)

CORRECTION FACTOR DUE TO
MAGNETIC DEFLECTION

PROBABILITY OF
ACCEPTANCE

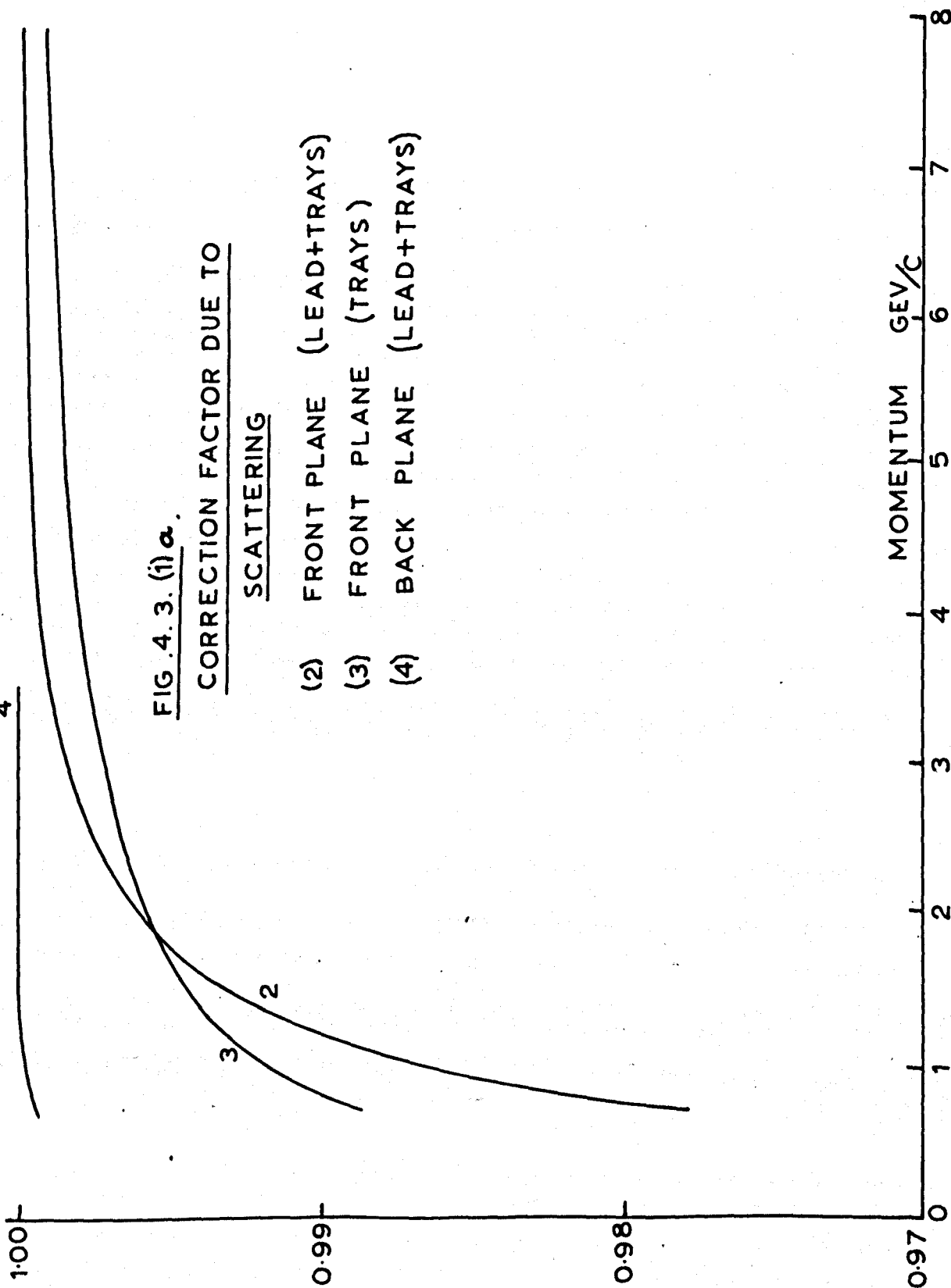


FIG. 4. 3. (1) α .

CORRECTION FACTOR DUE TO
SCATTERING

- (2) FRONT PLANE (LEAD+TRAYS)
- (3) FRONT PLANE (TRAYS)
- (4) BACK PLANE (LEAD+TRAYS)

MOMENTUM GEV/C

PROBABILITY
OF ACCEPTANCE

FIG 4.3. (iii)
OVERALL CORRECTION FACTOR
TO BE APPLIED TO
COMPARISON SPECTRUM

.99
.98
.97
.96
.95
.94
.93
.92
.91
.90
.89
.88
.87
.86

8

7

.6

5

4

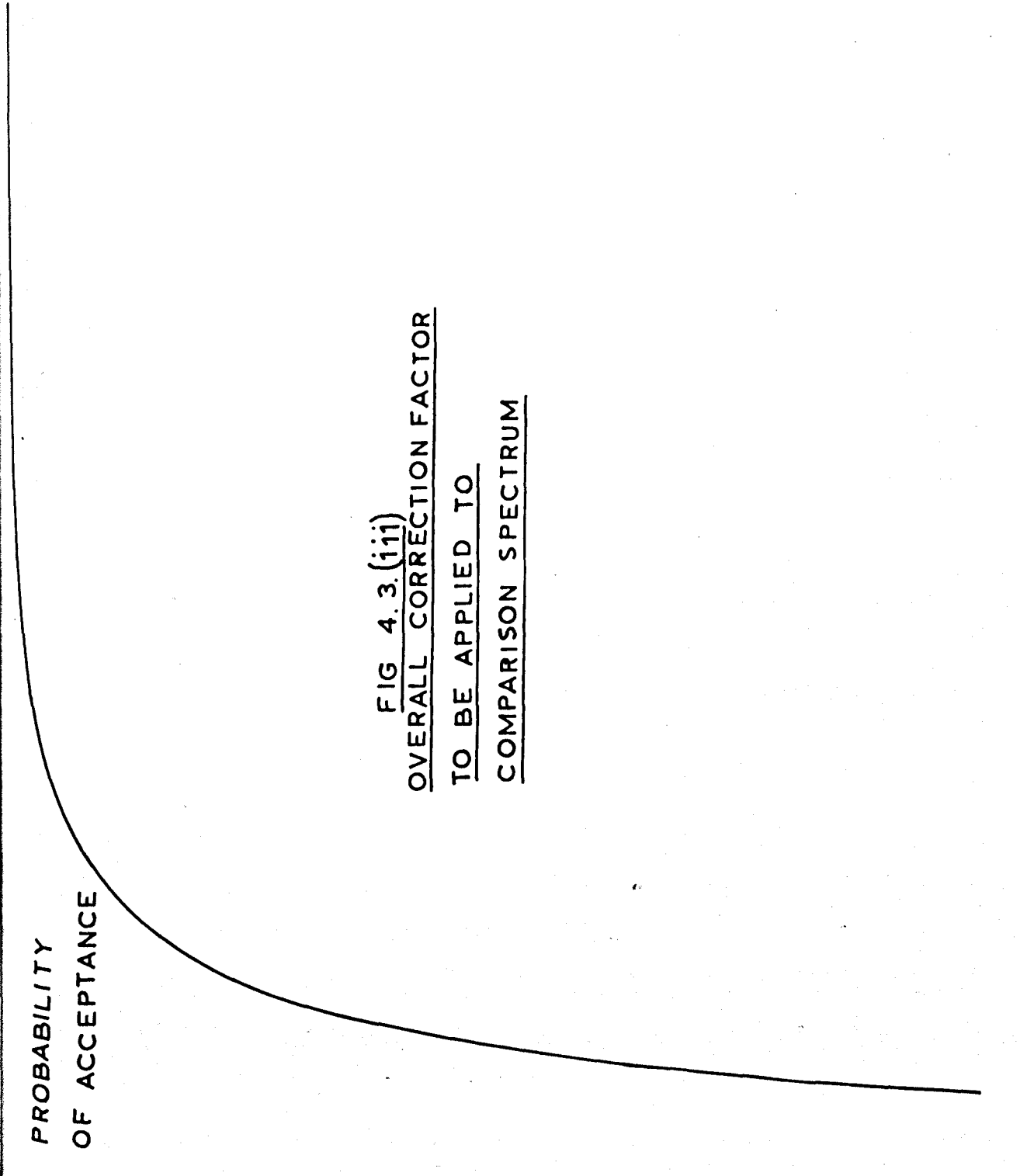
3

2

1

0

MOMENTUM GEV/C



after production at a distance x_0 cm. from sea level, measured along its path. $p(x)$ represents the momentum in μc a distance x cm. along the path,

τ is the proper mean life of the muon (2.25×10^{-6} sec.) and μ its rest mass (207 electron masses).

In the evaluation of the survival probabilities, the variation of pressure with height was assumed to be that for the International Standard Atmosphere (Admiralty Weather Manual, 1953, P.145), additional high altitude data being taken from Spencer and Dow (1954). The rate of energy loss in the atmosphere was assumed to be 2.2 Mev per gm/cm^2 , which is a good approximation in the range 3 - 40 Gev/c, and the integral (1) was evaluated graphically for 7 values of p_0 between 0.7 and 40 Gev/c. In this way a set of curves representing the variation of survival probability with production depth was constructed.

As a first approximation, the muon momentum distribution at production given by Moroney and Parry was assumed, i.e.:

$$N(p) dp = K p^{-3} \exp(-r/125).$$

where K is a constant, and r is the depth in gm. cm^{-2} .

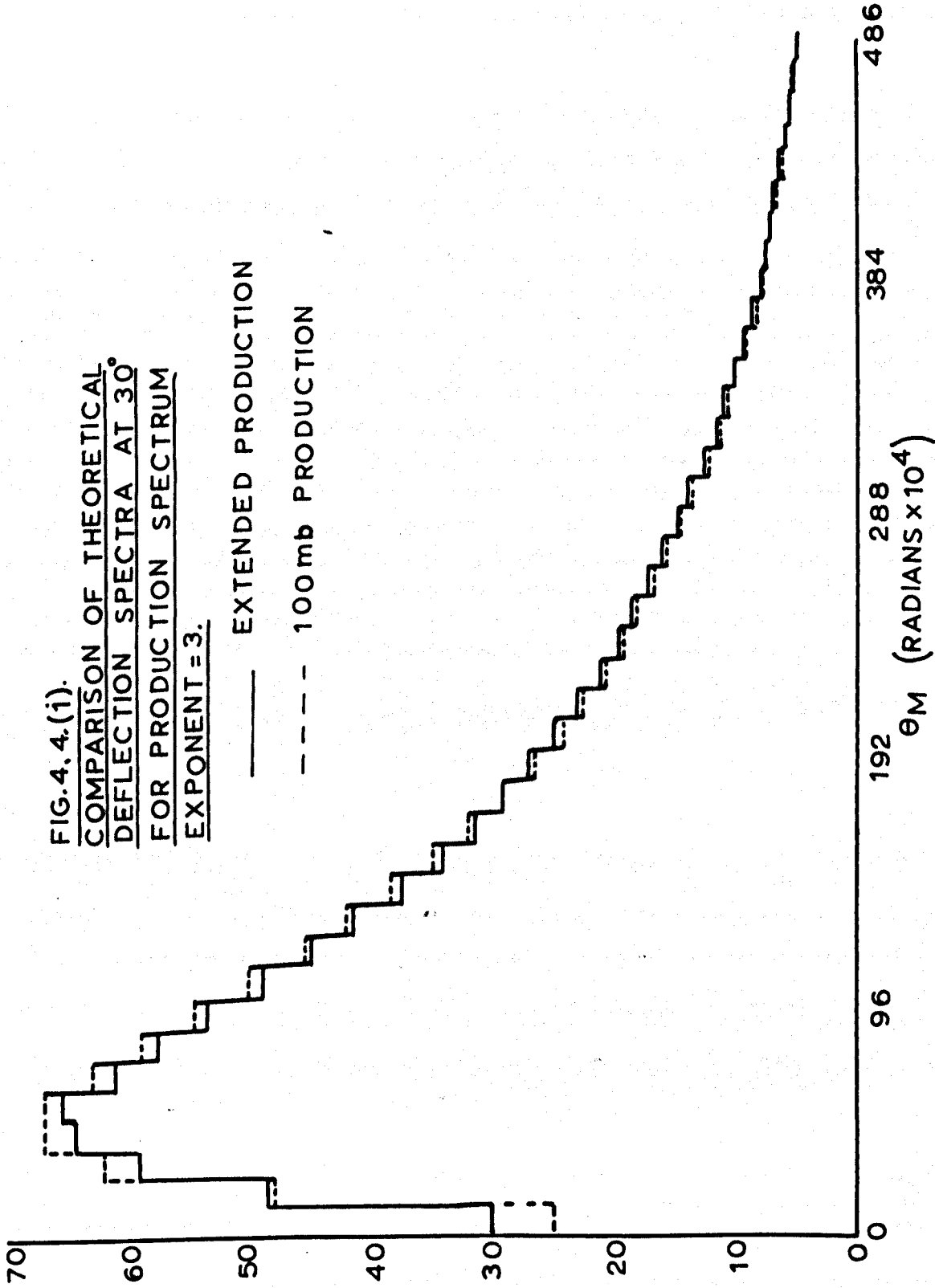
from the top of the atmosphere measured along the path. This assumes that muon production varies with depth in a similar way to the absorption of the primary protons. Then the sea level spectra were evaluated by integrating numerically through the atmosphere the product of survival probability and production spectrum. The resulting spectra were converted into deflection distributions, and normalised to a total of 1,000 particles in the range 0.7 Gev/c - ∞ .

To determine whether there is a significant difference between the above process of extended muon production, and a simpler process involving production at $\tau = 100 \text{ gm. cm}^{-2}$., sea level spectra were evaluated on the second assumption, using a momentum distribution at production of the form:

$$N(p) dp = K p^{-3}$$

These spectra were normalised as before, and the sea level deflection distributions at zenith angles of 30° and 45° are compared in figures 4.4.(i) and 4.4.(ii). It is apparent that there is good agreement between the distributions calculated assuming either

NUMBER OF PARTICLES
PER 0.0012° INTERVAL



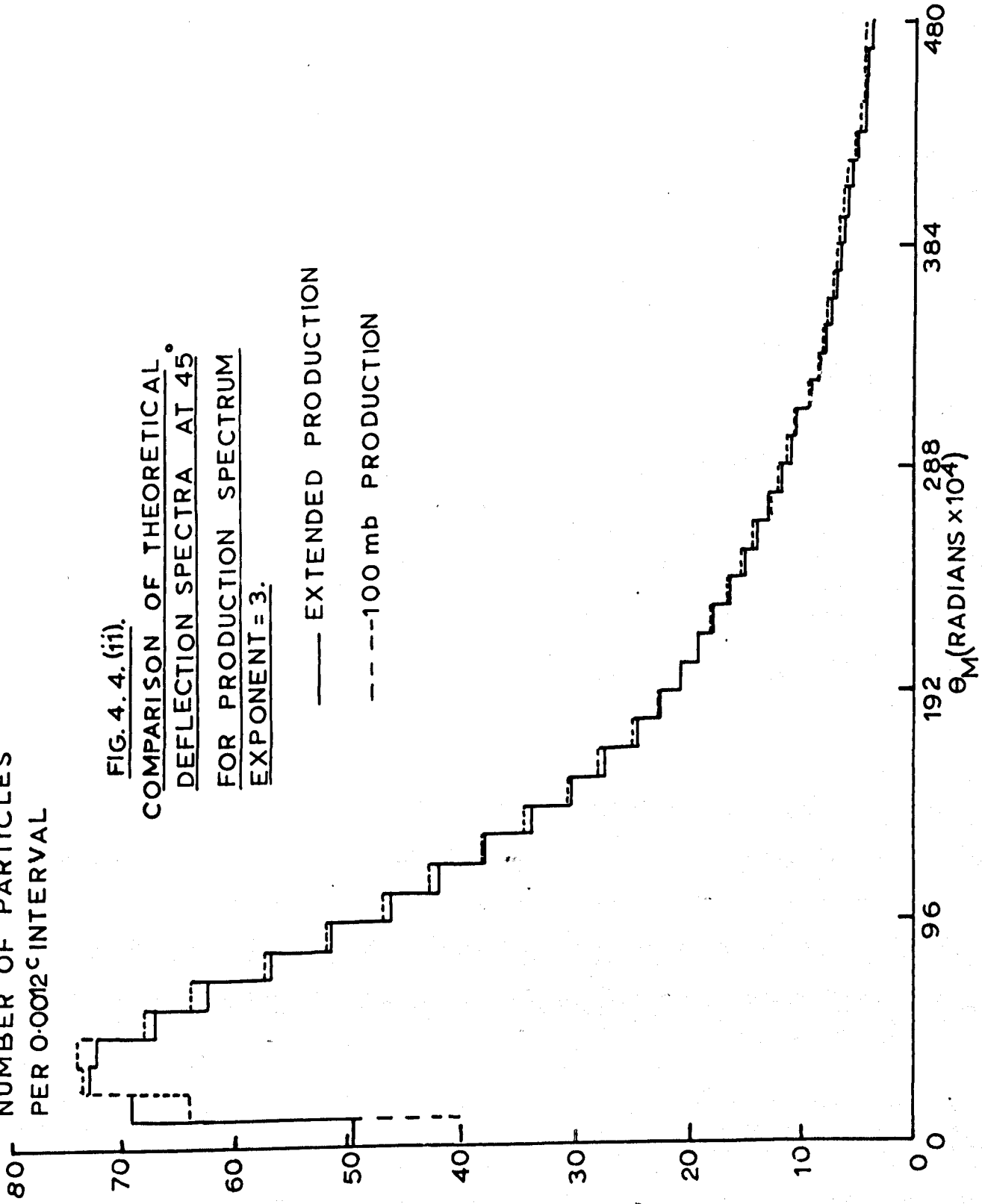
NUMBER OF PARTICLES
PER 0.0012° INTERVAL

FIG. 4. 4. (ii).

COMPARISON OF THEORETICAL
DEFLECTION SPECTRA AT 45°
FOR PRODUCTION SPECTRUM
EXPONENT = 3.

— EXTENDED PRODUCTION

-- --100 mb PRODUCTION



production process. It is also known that the distribution for muons arriving vertically is adequately explained by production at a single level in the momentum range considered (Janossy and Wilson (1946)), and as the assumption of this process considerably simplifies the calculation of theoretical deflection distributions for comparison with experimental results, it was employed throughout the following work.

Deflection distributions at zenith angles of 0° , 30° and 45° were calculated for muon production spectrum exponents, γ , in range 2.5 - 3.3. These were multiplied by the overall correction factor (fig. 4.3.(iii)); broadened in the usual way for the known errors in deflection measurement, including those due to scattering, and compared with the experimental measurements using the χ^2 test (fig. 4.5.(i)). In tables 4.4.(i), (ii) and (iii) the theoretical and experimental results are compared, for the relevant "best-fit" value of χ^2 . In addition, at 0° , the experimental results are compared with those of Owen and Wilson (1955), which are now regarded as standard in the range 1 - 20 Gev/c. The associated value of χ^2 would be

$$0^\circ, \gamma = 2.88$$

Deflection Interval (Radians $\times 10^4$)	Momentum Interval (Gev/c.)	Ob- served	Expected	
			Owen and Wilson	γ = 2.88
0 - 12	27.25 - ∞	44.57	43.47	40.55
12 - 48	6.81 - 27.25	207.6	228.0	226.3
48 - 84	3.89 - 6.81	159.3	158.8	158.9
84 - 120	2.725 - 3.89	129.1	125.9	113.1
120 - 156	2.1 - 2.725	101.0	99.72	105.1
156 - 204	1.6 - 2.1	101.7	104.0	98.29
204 - 288	1.14 - 1.6	115.1	125.5	118.9
288 - 432	0.76 - 1.14	97.22	105.37	96.01

Table 4.4.(i)

* 30° , $\gamma = 3.03$

Deflection Interval (Radians $\times 10^4$)	Momentum Interval (Gev/c.)	Observed	Expected
0 - 12	27.25 - ∞	34.73	32.01
12 - 48	6.81 - 27.25	252.0	246.0
48 - 96	3.41 - 6.81	222.0	225.6
96 - 132	2.48 - 3.41	73.6	79.81
132 - 168	1.95 - 2.48	91.66	94.31
168 - 204	1.60 - 1.95	61.91	69.34
204 - 276	1.18 - 1.60	95.61	87.90
324 - 468	0.70 - 1.01	79.33	73.16

Table 4.4.(ii)

* It will be noted that in the evaluation of χ^2 for the 30° spectrum, a deflection group making an abnormal contribution to χ^2 has not been considered. This is statistically justified by the procedure adopted by Davis and Nelson (1937), and Wilson (1952).

$$45^\circ, \gamma = 2.75$$

Deflection Interval (Radians x 10^4)	Momentum Interval (Gev/c.)	Observed	Expected
0 - 12	27.25 - ∞	49.41	60.32
12 - 48	6.81 - 27.25	238.9	263.2
48 - 84	3.89 - 6.81	198.6	183.7
84 - 120	2.725 - 3.89	140.1	136.4
120 - 156	2.1 - 2.725	119.5	124.6
156 - 204	1.6 - 2.1	75.93	85.93
204 - 288	1.14 - 1.6	68.09	71.97
288 - 432	0.76 - 1.14	81.73	89.16

Table 4.4. (iii)

exceeded for 54% of random samples of 1,000 events drawn from the Owen and Wilson distribution. This is taken to indicate good agreement between the present results and the standard vertical spectrum.

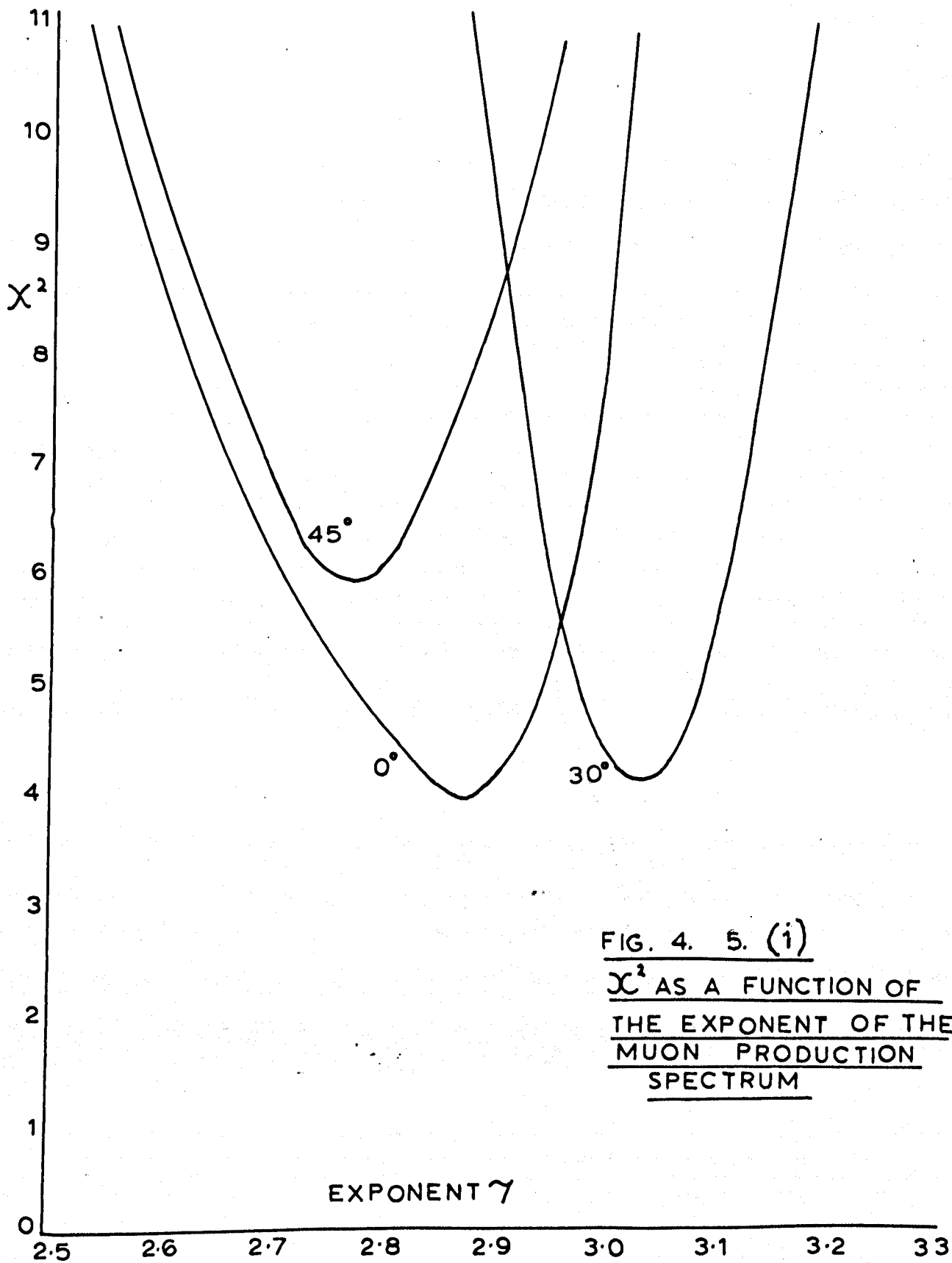


FIG. 4. 5. (i)
 χ^2 AS A FUNCTION OF
THE EXPONENT OF THE
MUON PRODUCTION
SPECTRUM

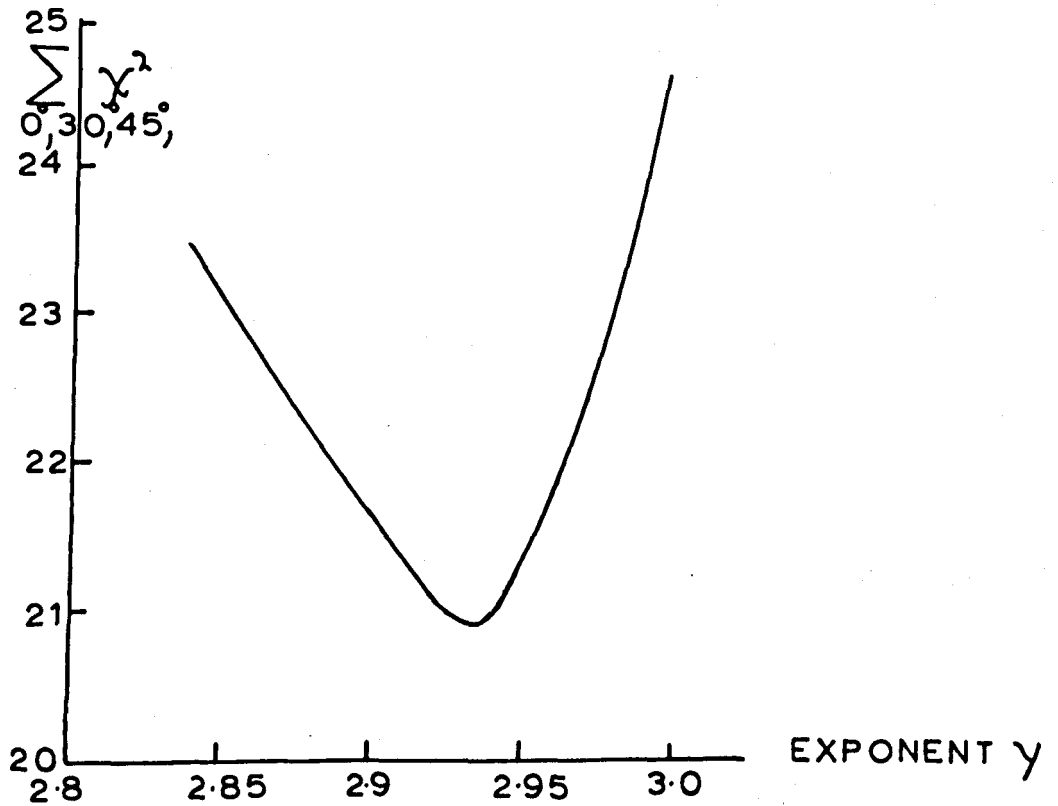


FIG 4.5. (ii)

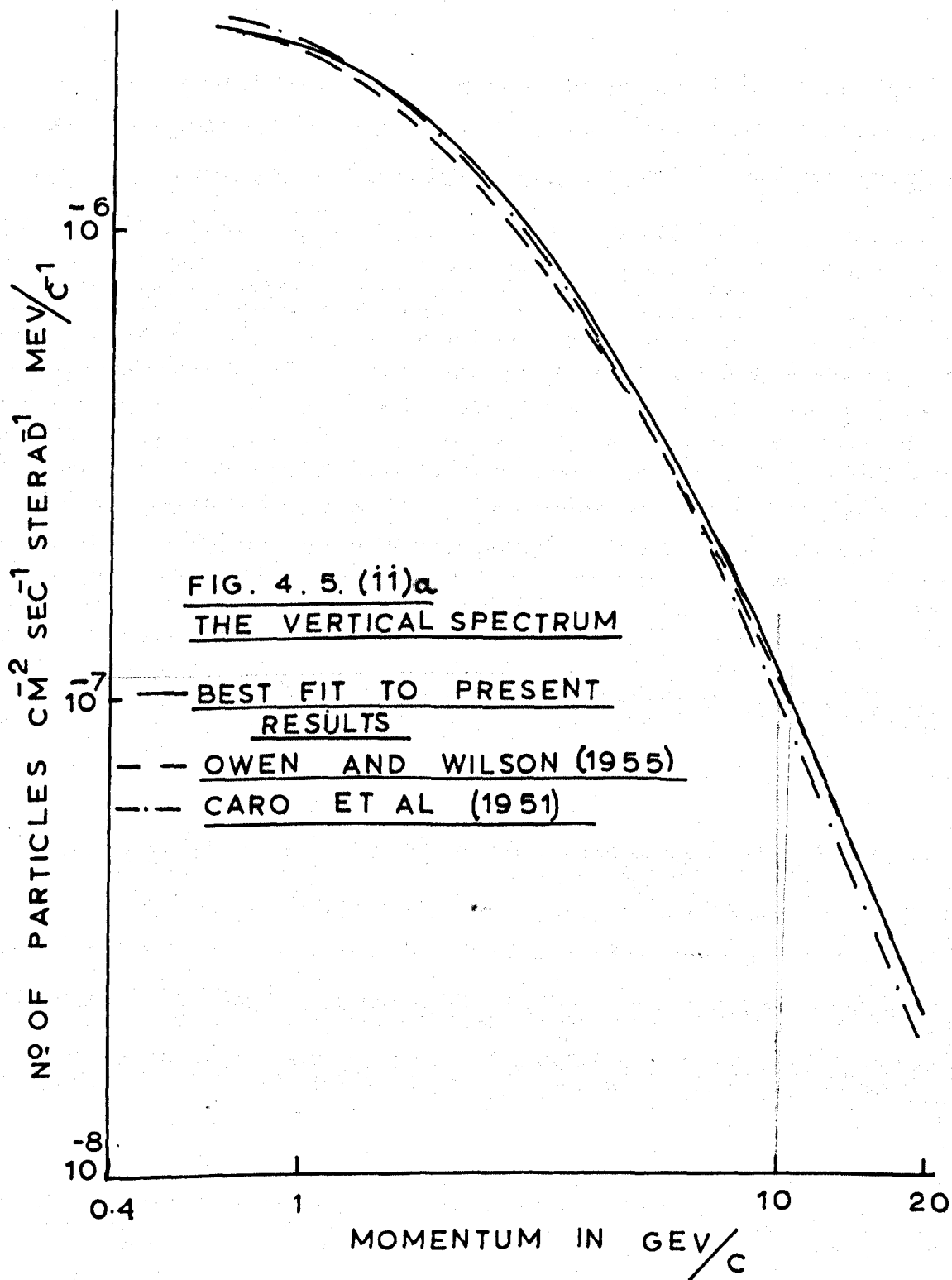
$\sum \chi^2$ AS A FUNCTION OF
0,30,45.

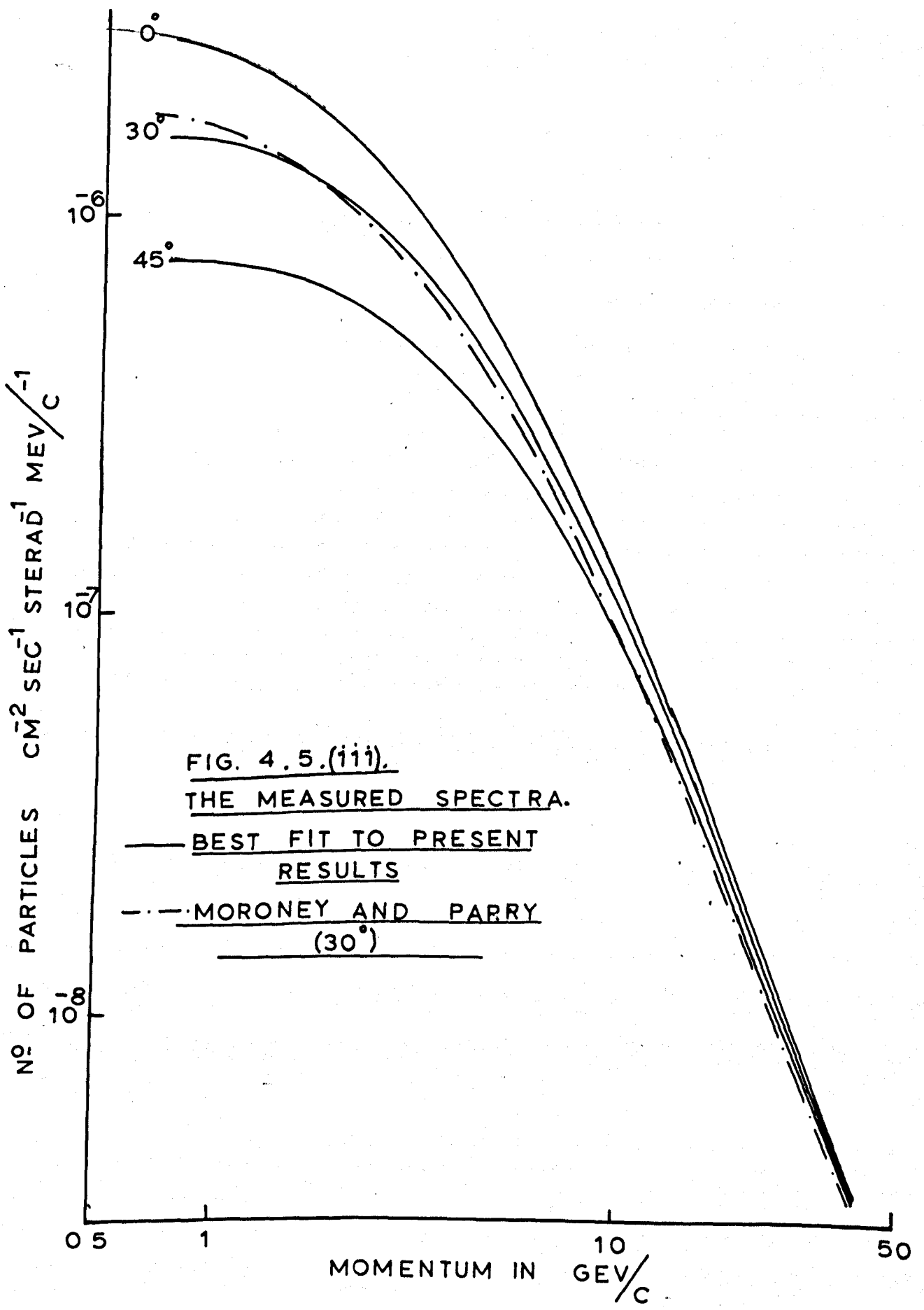
THE EXPONENT OF THE

MUON PRODUCTION SPECTRUM

4.5 Discussion, and Comparison with
Other Work

The "best fit" momentum spectrum of muons at sea level in the vertical direction is given in fig. 4.5.(ii)a where it is compared with that of Owen and Wilson and Caro et al., and in fig. 4.5.(iii). the vertical and inclined spectra are given; the 30° spectrum being compared with that of Moroney and Parry obtained using the same spectrograph as Caro et al. It is seen that the divergences between the present results and those of Moroney and Parry are similar to those between the Owen and Wilson spectrum and that of Caro et al., which is too high at low momenta, and low at momenta above approximately 6 Gev/c. Doubt has been expressed, in particular by Pine et al. (1960), on the accuracy of the Caro et al. spectrum, and it is not unreasonable to expect that the spectra at various zenith angles are also liable to error. A possible cause of this error lies in the corrections applied for magnetic cut-off and scattering out at low momenta. It may be noted that the most frequently used normalisation point at 1 Gev/c lies in the region where errors in the corrections would be important, and where statistical





accuracy is relatively poor. These effects are more important when the best line is drawn through a set of points than when the significance of the agreement between theoretical and experimental distributions is tested statistically.

No significant tendency has been found for an increased intensity at low momenta at 30° and 45° due to multiple scattering in the atmosphere (tables 4.4.(i), (ii) and (iii)). This effect would be expected on the theoretical predictions of Maeda (1960). It should be noted that Moroney and Parry, assuming a muon production spectrum of exponent - 3.0, indicated that scattering would provide the 50% correction necessary to account for their results at 60° , whereas Maeda also finds agreement using Sands' production spectrum of exponent - 3.58. Sands' spectrum predicts sea level intensities at 30° and 60° some 25% and 40% lower respectively than those predicted at 1 Gev/c by that of exponent - 3.0.

Values of "n" have been calculated from the "best fit" spectra assuming the relation

$$I_{\theta p} = I_{0p} \cos^n \theta$$

given by Budini and Molière (1952), where I_{o_p} is the intensity of muons with momentum p in the vertical direction, and I_{θ_p} is the intensity at a zenith angle θ . The theoretical curve of Budini and Molière is compared with the experimental results of Moroney and Parry and those of the present work in fig. 4.5.(iii)a. The good agreement justifies the assumption by Cousins et al. (1957) of the validity of the theoretical curve in their calculation of the variation of "n" with momentum for muons underground.

The overall ratio of positive to negative particles at the various zenith angles are given in table 4.5.(i), where they are compared with the values obtained by Owen and Wilson and Moroney and Parry in the range 0.7 - 30 Gev/c

	Present results	Moroney and Parry	Owen and Wilson
0°	1.33 ± 0.10	1.29 ± 0.04	1.32 ± 0.01
30°	1.16 ± 0.11	1.36 ± 0.05	
45°	1.29 ± 0.10		

Table 4.5.(i)

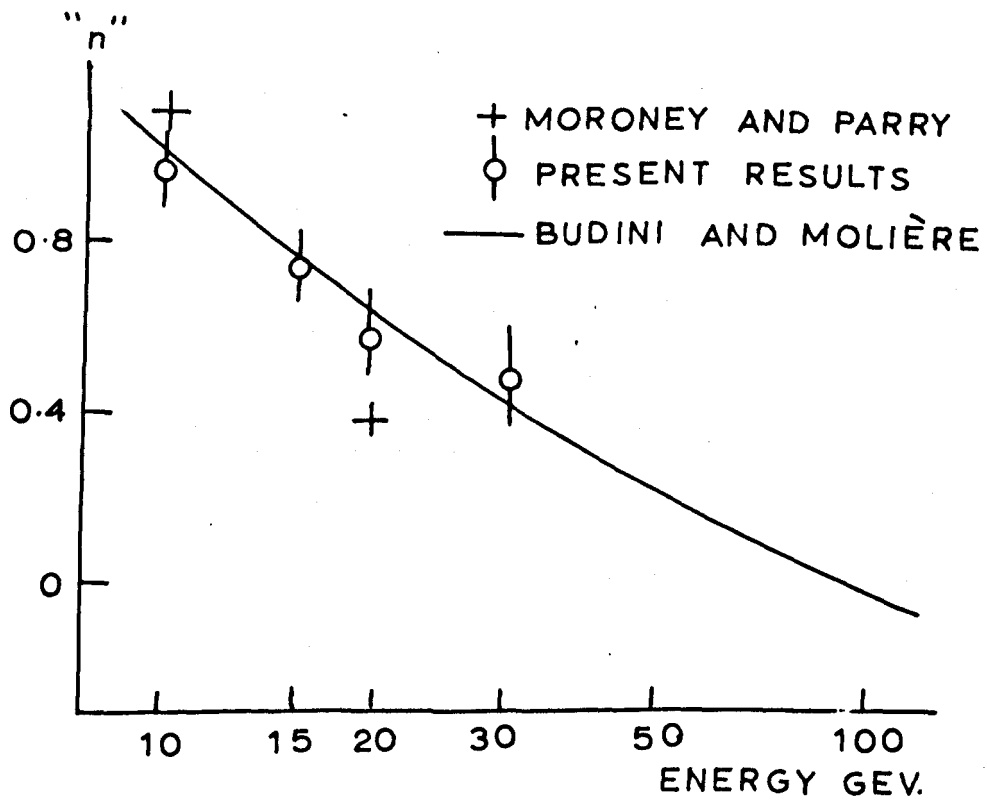


FIG. 4. 5. (iii). a.
"n" AS A FUNCTION OF ENERGY
FOR MUONS AT SEA LEVEL.

The errors quoted in the present results are root mean square values, and the agreement with other work is seen to be reasonable taking into account the limited statistical precision of the present results.

4.6 Conclusions

The conclusions of this investigation may be summarised as follows:

- (1) The measured momentum spectrum of muons in the vertical direction agrees with that of Owen and Wilson, and disagrees with that of Caro et al.
- (2) The same form of discrepancy as in (1) occurs between the measured spectrum at 30° W and that of Moroney and Parry.
- (3) Good agreement with the theoretical curve for the variation of "n" with momentum is obtained using the present results.
- (4) The sea level spectra at 0° , 30° , 45° may be simultaneously accounted for by assuming either single level or extended production of the muons, with a power law distribution in momentum at production of exponent - 2.94.

(5) No evidence has been found for an increase in intensity at low momenta due to multiple scattering in the atmosphere. Some doubt must be cast therefore on the calculations by Maeda of the effect of the scattering of muons in traversing the atmosphere.

Further evidence is required regarding (4) and (5); and this would be provided by spectrum measurements of high statistical precision at zenith angles of greater than 60° , and in particular in the horizontal direction.

Acknowledgements

The author must thank Professor L.F. Bates, F.R.S., for the facilities of his laboratories. He would also like to acknowledge the assistance of his supervisor, Dr. W.F. Nash, and to thank his colleague, Mr. R.M. Bull, for many stimulating and helpful discussions.

The tubes were constructed at the Science Laboratories of the University of Durham; and the author is grateful to Professor G.D. Rochester, F.R.S., and Dr. A. W. Wolfendale for their help and cooperation.

He would also like to thank Mr. K.M. Wright for his enthusiastic and accurate assistance in the analysis of the photographic records, and the staff of the Autocode Computing Service at the University of Manchester for their hospitality during the punching and computing of the spectra data.

He is indebted to the Department of Scientific and Industrial Research for the provision of a Research Studentship which enabled part of the work to be carried out.

REFERENCES

- Admiralty Weather Manual, H.M.S.O., 1953, P.145.
- Allkofer, O.C., 1959, Atomkernenergie, H.10. and
1960, Z. Phys., 158, No. 3, P.274.
- Apostalakis, A.J., and Macpherson I., 1957, Proc.
Phys. Soc., A 70, P.146 and 154.
- Ashton, F., Kisdnasamy, S., and Wolfendale, A.W.,
1958, Nuovo Cim., 10, P. 615.
- Ashton, F., Nash, W.F., and Wolfendale, A.W., 1959,
Proc. Roy. Soc., 253 A, P.163.
- Ashton, F., 1959, Ph.D. Thesis, Univ. of Durham.
- Ashton, F., Brooke, G., Gardener, M., Hayman, P.J.,
Jones, D.G., Kisdnasamy, S., Lloyd, J.L.,
Taylor, F.E., West, R.H., and Wolfendale, A.W.,
1960, Nature, 185 No. 3710, P.364.
- Budini and Molière, G., 1952, "New Research
Techniques in Physics", P.59

Caro, D.E., Parry, J.K., and Rathgeber, H., 1951,
Aust. J. Sci. Res., A4, P.16.

Cousins, J.E., Nash, W.F., and Pointon, A.J., 1957,
Nuovo Cim., 10, P.1113.

Cousins, J.E., and Nash, W.F., 1959, Brit. Journ. of
App. Phys., 10, P.471.

Coxell, H., and Wolfendale, A.W., 1960, Proc. Phys.
Soc., 75, P.378.

Davis, H.T., and Nelson, W.F.C., 1937 "Elements of
Statistics", Denton Printing Co., Colorado
Springs, Colorado, P.205.

Fowler, G.N., and Wolfendale, A.W., 1958, Prog. in
Elementary Particle and Cosmic Ray Physics,
4, P.107.

Gardener, M., Kisdnasamy, S., Rössle, E., and
Wolfendale, A.W., 1957, Proc. Phys. Soc.,
70B, P.687.

Hyams, B.D., Myhoi, M.G., Owen, B.G., and Wilson, J.G.,
1950, Proc. Phys. Soc., 63A, P.1053

Janossy, L., and Wilson, J.G., 1946, Nature, 158,
P.450.

Lloyd, J.L., 1960, Proc. Phys. Soc., 75, P.387.

Maeda, K., 1960, Journ. Atm. and Terr. Phys., 19,
P.184.

Moroney, J.R., and Parry, J.K., 1954, Aust. Journ.
Phys., 7, P.423.

Owen, B.G., and Wilson, J.G., 1951, Proc. Phys. Soc.,
64A, P.417, and 1955, Proc. Phys. Soc.,
68A, P.409.

Pine, J., Davisson, R.J., and Greisen, K., 1959,
Nuovo Cim., 14, P.1181.

Rodgers, A.L., 1956, Ph.D. Thesis, Univ. of Manchester.

Rossi, B., 1948, Rev. Mod. Phys., 20, P.537.

Sands, M., 1950, Phys. Rev., 77, P.180.

Spencer, N.W., and Dow, W.G., 1954, "Rocket Exploration
of the Upper Atmosphere", Pergamon Press Ltd.,
P.82.

Stern, D., 1960, Nuovo Cim., 18, 1.

Wilson, Bright E., Jr., 1952, "An Introduction to
Scientific Research", McGraw-Hill Book Co.,
Inc., P.202.

Appendix

The Design of Flash Tube Arrays

A.1. Introduction

The computer method of analysis has made possible a more complete investigation than previously contemplated of the design consideration of flash tube arrays for use in location of particle trajectories. In this Appendix results will be presented giving the effects of various parameters (e.g. gas pressure, tube size and separation, and errors in tube location) on the error in angular measurement.

In the investigation, two arrays (table A.1.(1)) were used, each of the parameters of which could be varied independently. A computer programme simulated the passage of a particle of accurately known trajectory through the arrays, providing data (i.e. flashes and blanks) which would have been obtained in practice for any combination of these parameters. The data was then analysed using the method of analysis described in chapter 3. This method is similarly flexible, in that it may use any combination of the parameters. A check on the computer analysis was provided by using a simple approximation to $P(\theta)$. This gives a quick and convenient means of obtaining the error in angular measurement. Absolute values obtained in this way

are liable to some systematic error, but relative values are more accurate.

The notation used throughout is as for chapter 3.

Spacing between layers (S)	=	0.63	cms.
Distance between the 'centre of gravity' of the trays (D)	=	84.3	cms.
Tube Diameter (Δ)	=	0.59	cms.
Distance between tube centres (Γ)	=	0.843	cms.
Number of Layers (N)	=	5	

P(θ) assumed for high pressure tubes of 0.59 cms. diameter, unaffected by variations in tube diameter and location.

Table A.1.(i) Parameters of Random Arrays

A.2 Design of Flash Tube Arrays

(1) Note on Scaling

When comparing σ_{ϕ_1} and σ_{ϕ_2} for two arrays A_1 and A_2 of different dimensions, the following procedure has been used throughout. The value of

σ_{ϕ_1} comparable with σ_{ϕ_2} is:

$$\sigma_{\phi_1}' = \frac{\sigma_{\phi_1}}{D_2} \cdot f \cdot D_1$$

where

$$f = \Gamma_2 / \Gamma_1$$

This is only true for $\Delta_1 = \Delta_2$, or constant Δ/r for 100% efficient tubes.

(2) High and Low Pressure Tubes

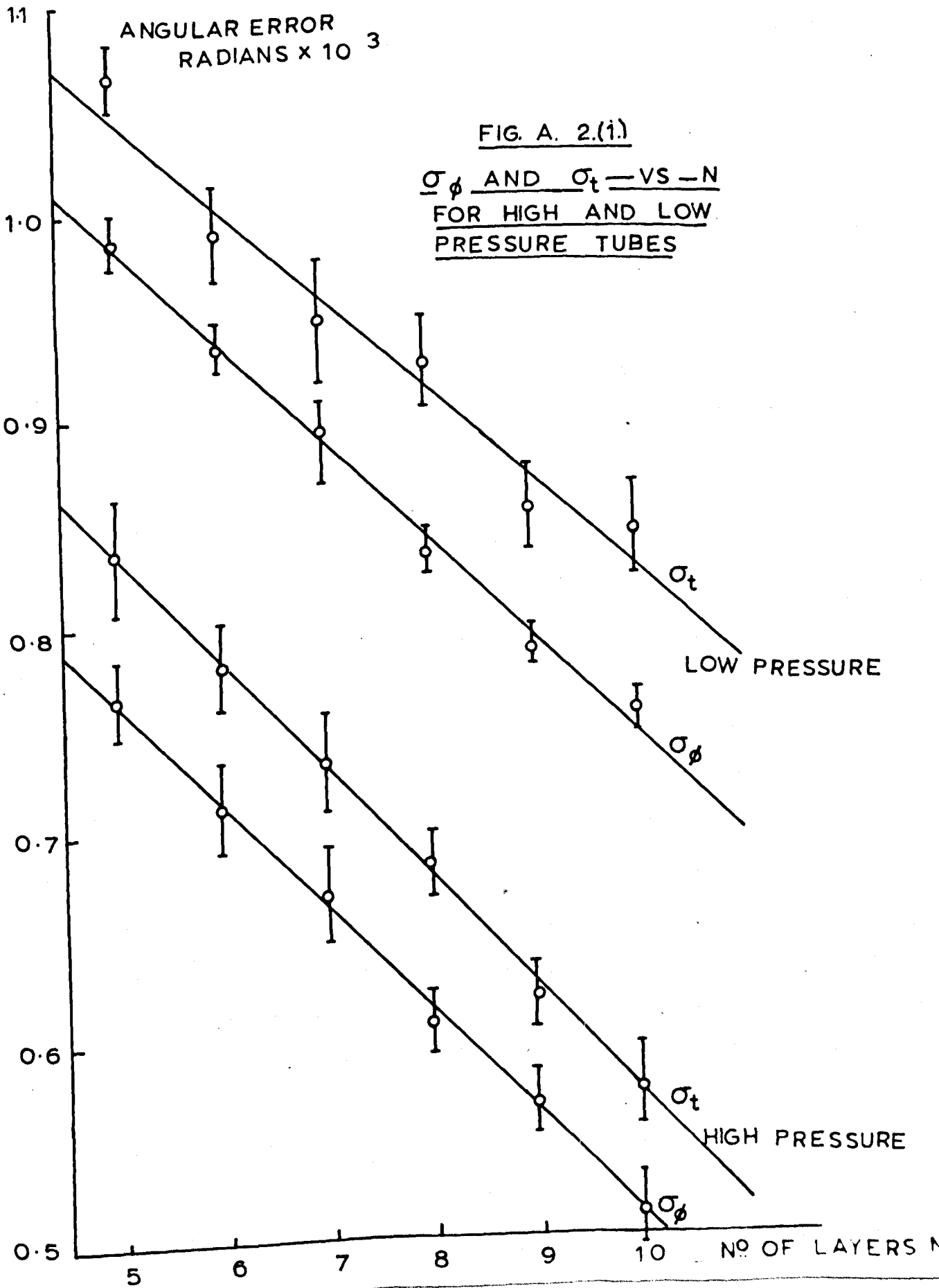
The 100% internal efficiency condition considerably simplified previous methods of analysis and consequently high pressure tubes are used at present. However, the computer uses the actual distribution $P(\theta)$ and the possibility of utilising the more easily manufactured low pressure tubes still exists. An investigation of both types of tubes was made for $N = 5$ to $N = 10$; the results are plotted in Figure A.2.(1). Unfortunately, it is apparent that low pressure tubes are at a disadvantage.

(3) Spacing between Layers (S)

The effect of varying the spacing between layers has been investigated with the negative results indicated in the Table A.2.(1) .

S cm.	0.63	1.26	1.90
σ_ϕ (radians $\times 10^4$)	7.8 ± 0.3	7.8 ± 0.3	8.0 ± 0.3

Table A.2.(1)



(4) Number of Layers (N)

Figure A.2.(1) shows the measured variation of σ_ϕ and σ_t with N. Although the theoretical derivation of this dependence has not been rigorously performed, approximate calculations based on a 100% tube efficiency and the assumption that $\Delta/\Gamma = \frac{1}{2}$, suggest that σ_ϕ is more strongly dependent on N than the experimental results indicate. An independent check of these results was therefore sought especially as it would contribute a convincing verification of the computer method of analysis.

If a 100% tube efficiency may be assumed, and since σ_ϕ is independent of the spacing between layers within a tray, we may consider the tube edges as if they existed only at a single level. Since the direction of the trajectory is approximately defined using both trays, the tube edges within either tray form a repetitive pattern of width Γ , each containing N pairs of tube edges. The distance between any adjacent tube edges is termed a 'corridor'. The information provided by the flashed and unflashed tubes will indicate the corridor through which the particle passed, and the width of the corridor the

uncertainty of location of the particle at that level. A spectrum of corridor widths, $F(\mu)$ for all allowable positions and angles of incidence exists, and this may be determined empirically. Since the probability of a particle traversing a corridor is proportional to μ , a value for the weighted mean corridor width $\bar{\mu}$ can be computed. On the assumption that the mean uncertainty occurs at both the measuring levels, an expression for the r.m.s. angular error can be obtained, and is plotted in figure A.2.(ii) as a function of N.

Since this curve is only applicable to tubes having 100% internal efficiency, some means is required of deducing the effect of using a practical tube. If it may be assumed that

- a) the simplified $P(\theta)$ distribution of figure A.2.(iii) may be used;
- b) the corridor width is defined by only two tube edges; and
- c) the weighted mean corridor width $\bar{\mu}$ occurs at both levels;

then the probability of a particle traversing any portion of μ is not constant as with 100% efficient tubes, but is unity over the central portion of

ANGULAR ERROR
 σ_{ϕ} RADIANS ($\times 10^3$)

FIG A 2 (ii) COMPARISON OF
 σ_{ϕ} - VS - N FOR 100% EFFICIENT
AND PRACTICAL TUBES.

FOR 100% EFFICIENT TUBES ——— □
 FOR PRACTICAL TUBES OBTAINED-
 FROM ABOVE USING THE -
 "SMUDGE" EFFECT ——— ⊗
 FOR PRACTICAL TUBES ~
 COMPUTER RESULTS. ——— ○

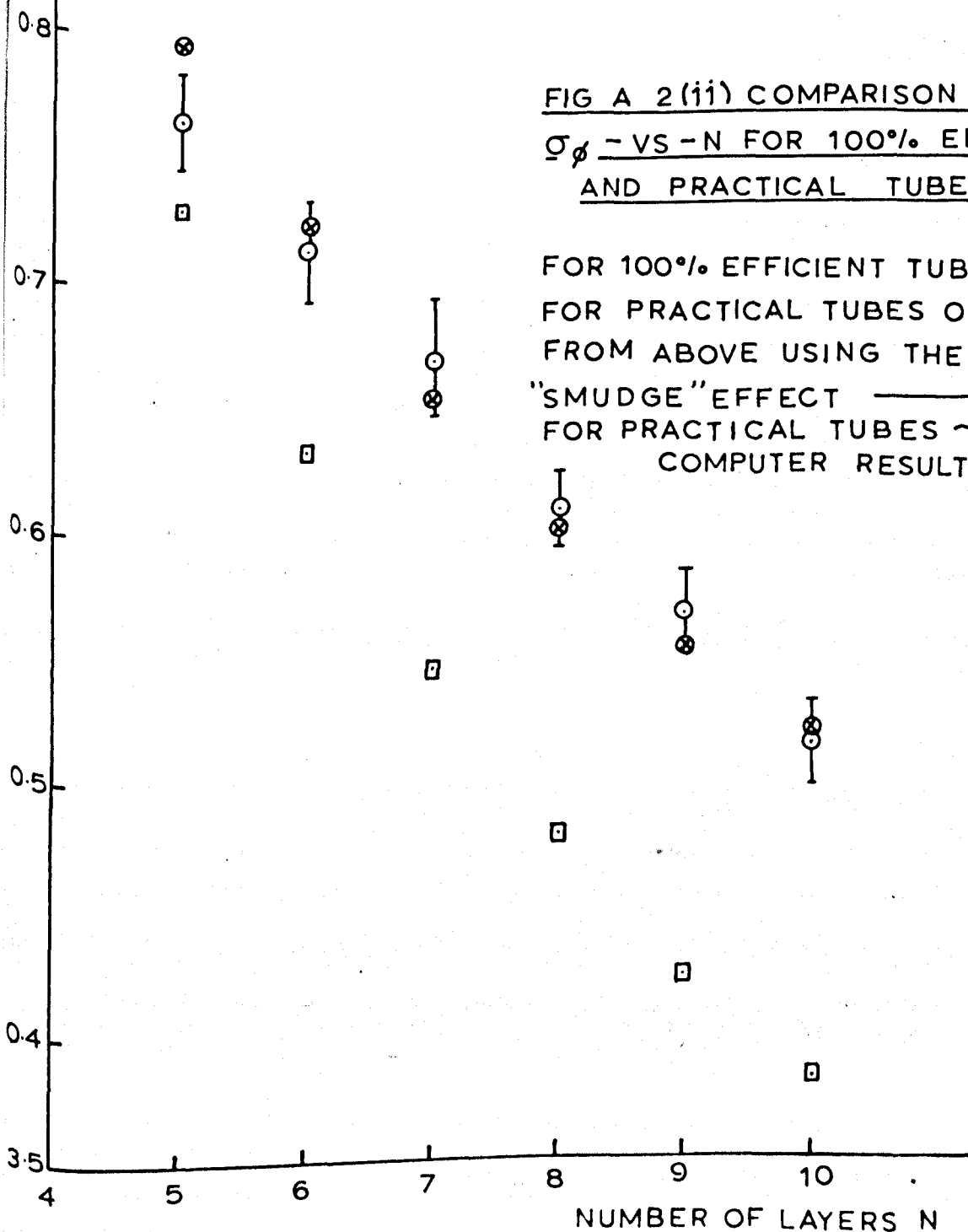
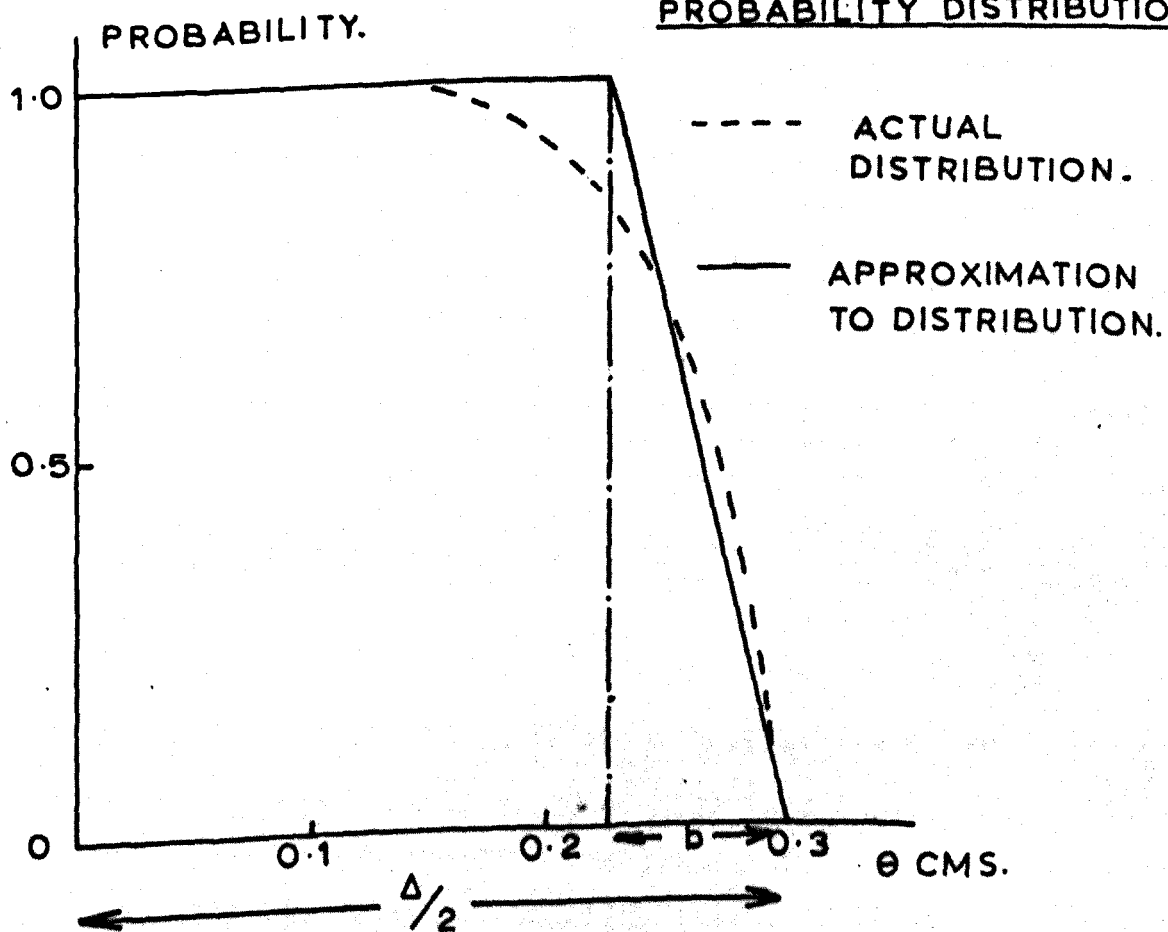


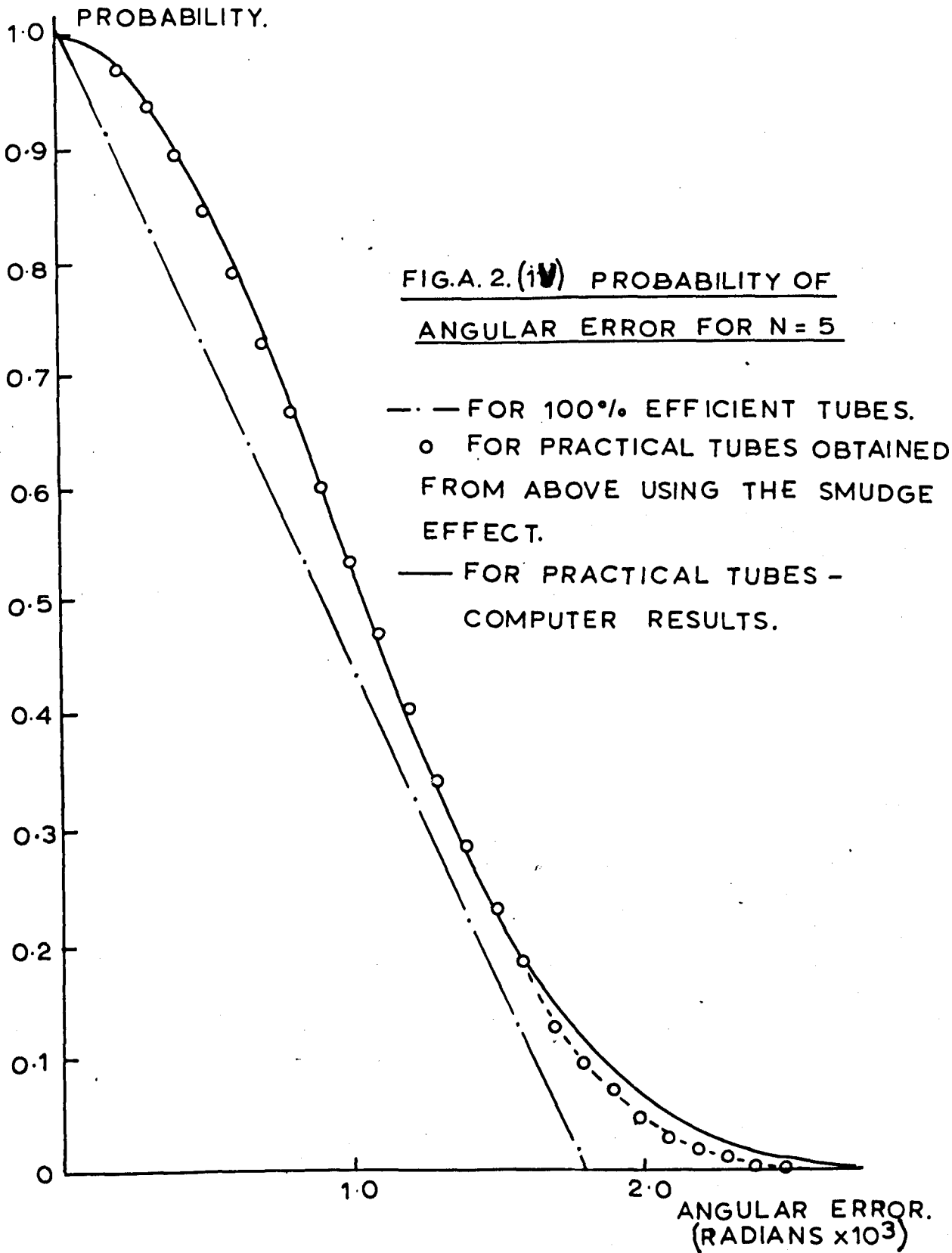
FIG A. 2. (iii)
APPROXIMATION TO THE
PROBABILITY DISTRIBUTION.



length ($\bar{\mu} - b$) and falls to zero outside the boundaries suggested by the tube edges. The consequence of using practical tubes is then to 'smudge' the clearly defined corridor boundaries of 100% efficient tubes. The effect is to modify the angular error versus probability curve from a triangle to a broadened distribution the nature of which is determined by the value of b in figure A.2.(iii). Estimates of b were made, and σ_{ϕ} deduced as a function of N for high pressure tubes and for a ten layer low pressure tube arrangement (figure A.2.(ii)).

This simplified and approximate analysis can be expected to be unreliable when $b \approx \bar{\mu}/2$; that is for high values of N , or for the large values of b encountered with low pressure tubes. In figure A.2.(iv) the expected angular error versus probability curves are compared for

- a) 100% efficient tubes (dashed line)
- b) for practical tubes using the simplified analysis (full line)
- c) for practical tubes using the computer analysis (points).



The good agreement between (b) and (c), together with that between the values of σ_ϕ for both low and high pressure tubes at various values of N, afford a convincing check on the validity of the computer results.

(5) Tube Diameter Variations, and Random Errors in Tube Location

Random errors in the location of the tubes and variations in their diameters are inevitable in practical arrays. Their effects are identical and may be investigated in three equivalent ways. Firstly, the assumed efficiency function $P(\theta)$ may be corrected for these effects, the result being an effective distribution $P'(\theta)$ which may be used in analysis in the ordinary manner. Secondly, an approximate value of b may be deduced from the function $P'(\theta)$ and the consequent increase in σ_ϕ found. Thirdly, in the analysis of an event using $P(\theta)$, the values of E_i may be changed by small random amounts δE_i which form a random sample from a normal distribution of standard deviation V cms. By comparing the m.p.t. (of angle α_V) of such an analysis with that (of angle α) using the actual E_i values, an estimate of the effect

may be made. Figure A.2.(v) shows a graph of

$$\sigma_v = \sqrt{n^{-1} \sum (\alpha_v - \alpha)^2 - [n^{-1} \sum (\alpha_v - \alpha)]^2}$$

as a function of V , (n is the number of trajectories analysed).

The dotted line is the result of the second method of analysis, and although this must necessarily be less accurate and less reliable, it provides a useful check on the results using the third method. The first method, although direct and the most reliable, is not convenient to use in practice; however, it has been used for $V = 0.045$ cms., the result being shown in the figure.

Since the effect of random variations is to broaden the distribution (that is, to increase the value of b) and since the effects of a finite b value are greater for higher values of N , it would be expected that an increased number of layers would accentuate σ_v . Whilst this is true the effect is very small and, using the second method, it is found that the σ_v against V curve for a 16 layer array does not differ appreciably from that for a 10 layer arrangement. It may be noticed that the absolute value of the corridor width is of only secondary importance in this investigation, and that

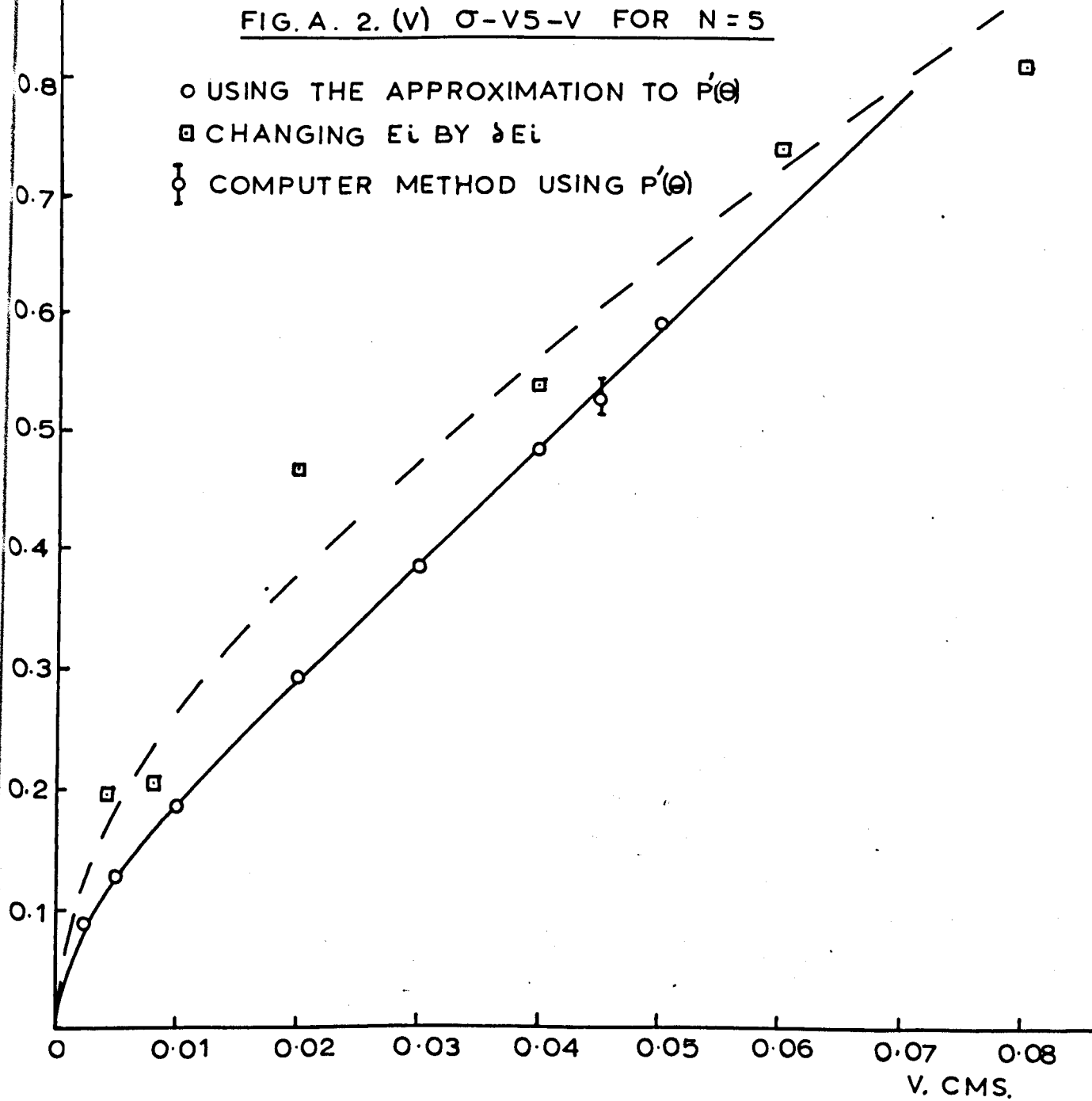
σ_V RADIANS
($\times 10^3$)

FIG. A. 2. (V) σ -V⁵-V FOR N=5

○ USING THE APPROXIMATION TO $P'(\theta)$

□ CHANGING E_i BY δE_i

⊖ COMPUTER METHOD USING $P'(\theta)$



the 'smudging' effect has the primary influence on the curve of figure A.2.(v). The agreement between the modes of analysis provides support for the approximate manner in which practical tubes have been treated using the corridor width approach.

(6) Tube Diameters

The effect of varying tube diameters is complicated by the lack of precise empirical knowledge of P(θ). However, Lloyd (1960, and private communication) has deduced tentative theoretical data which has permitted an investigation sufficient to indicate the general effect of using different tubes. This data has been used to predict an absolute efficiency (η) of 80% for tubes of 0.53 cms. diameter, compared with a measured value of 79 ± 2%.

Probability distributions were evaluated for various values of Δ between 0.4 and 0.7 cms., and estimates of b made. If Δ/r is kept constant, maintaining the same separation of the trays (D), values of σφ as a function of Δ may be obtained, and are shown in table A.2.(ii). The results indicate a definite minimum value of tube diameter below which

the natural reduction of the error because of the reduced scale is rapidly swamped by the increase in error due to the low efficiency of the small tubes.

If the number of layers in an array is not important, it is possible to obtain greater accuracy by increasing the tube diameter, and having more layers without increasing the labour of manufacture. The value of $\sigma_\phi(N=5, \Delta)$ for tubes of diameter Δ in an array with $N = 5$ may be compared with $\sigma_\phi(N, \Delta=0.6)$ for 0.6 cms. diameter tubes with a value of N such that the total number of tubes is the same in both cases. The ratio $I_\Delta = \sigma_\phi(N, \Delta=0.6) / \sigma_\phi(N=5, \Delta)$ is tabulated in table A.2.(ii). The results indicate a minimum value of σ_ϕ , roughly constant for a relatively wide range of tubes. If Δ is decreased, the low efficiency of the tubes rapidly increases the error. For large Δ , changes in diameter have little effect on $P(\theta)$, but the scaling effect is slightly greater than that due to increasing the number of layers, causing a slow increase in the error.

Δ cm	Efficiency η (%)	σ_ϕ radians ($\times 10^4$)	I_Δ
0.7	91	8.6	1.06
0.65	90	8.0	1.01
0.6	88	7.6	1
0.55	84.5	7.4	1.00
0.5	80	7.5	1.05
0.45	67	9.3	1.55
0.4	40		

Table A.2.(ii)

(7) Spacing between Tubes

An investigation of σ_ϕ as a function of Γ may be accomplished in either of two ways. Firstly, the computer analysis may be used with different values of Γ , or secondly, the effect on the mean

corridor width, $\bar{\mu}$, of varying Δ/Γ may be investigated, and the results suitably scaled. The former is much longer and has been used only as a check on the results obtained by investigating $\bar{\mu}$.

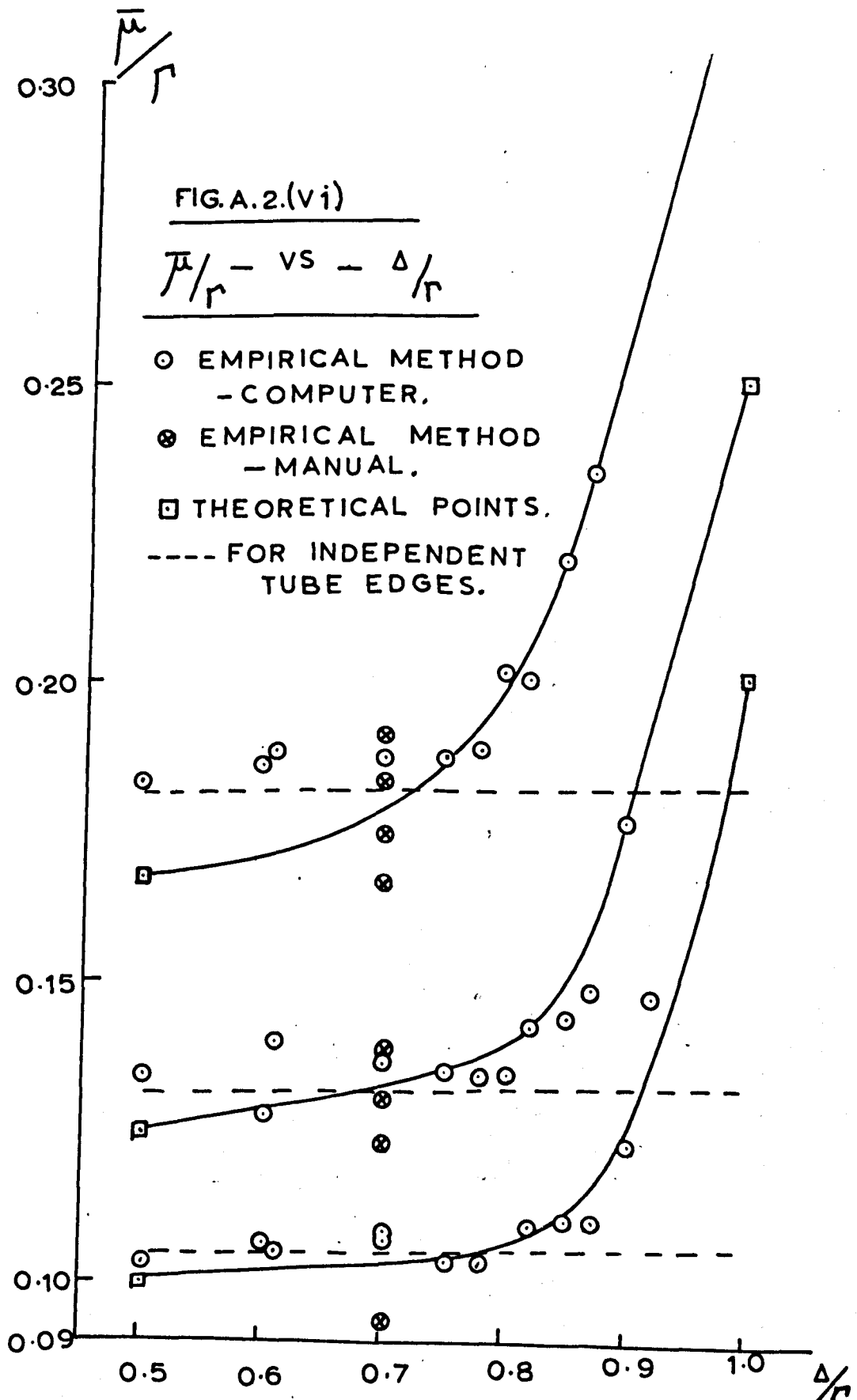
The effect of variations in Δ/Γ on $\bar{\mu}$ has been found empirically by a computer programme, and the circled points in figure A.2.(vi) were thus obtained for $N = 5, 7, \text{ and } 9$ for a fixed $\Gamma = 1$ and variable Δ *. Other points were obtained manually in a few cases (crosses). A complete theoretical analysis of the corridor width as a function of N and Γ is not available. However, points at $\Delta = \frac{1}{2}\Gamma$ and

$\Delta \rightarrow \Gamma$ are easily derived, and are marked as squares in figure A.2.(vi). Considering n tube edges randomly distributed in a length L , the probability $F(\mu)$ of a distance μ occurring between adjacent tube edges is given by

$$F(\mu) d\mu = A (\Gamma - \mu)^{n-2}$$

where A is a normalisation constant. Since the probability of a particle traversing a corridor width μ is proportional to μ , the weighted mean corridor

*The tubes are assumed to be 100% efficient at this stage of the analysis.



width $\bar{\mu}$ is given by

$$\bar{\mu} = \frac{\int_0^L \mu^2 (\Gamma - \mu)^{n-2} d\mu}{\int_0^L \mu (\Gamma - \mu)^{n-2} d\mu}$$

In the particular case of $\Delta \rightarrow \Gamma$, $n = N$;
 $L = \Gamma$, and $\bar{\mu} = 2\Gamma/N+1$. Further, if
 $\Delta = \Gamma/2$, then $L = \Gamma/2$; $n = N$, and
 $\bar{\mu} = \Gamma/N+1$. The dotted lines in
 figure A.2.(vi) are obtained assuming that all the
 tube edges are independent (i.e. $L = \Gamma$, $n = 2N$).
 Such an assumption cannot be true as $\Delta \rightarrow \Gamma$, and
 it may be expected that $\bar{\mu}$ would increase rapidly
 as the gap width approached, and became smaller than,
 $\bar{\mu}$. Such an effect is to be seen in
 figure A.2.(vi).

$\bar{\mu}(\Gamma)$ may be deduced as a function of Γ for
 constant Δ , and the corresponding values of $\sigma_\phi(\Gamma)$
 may be computed. These are shown in figure A.2.(vii)
 in the form of the ratio $\sigma_\phi(\Gamma)/\sigma_\phi(\Gamma=0.843)$
 for $N = 5$ and 9 , together with points obtained directly
 from the computer analysis for $N = 5$.

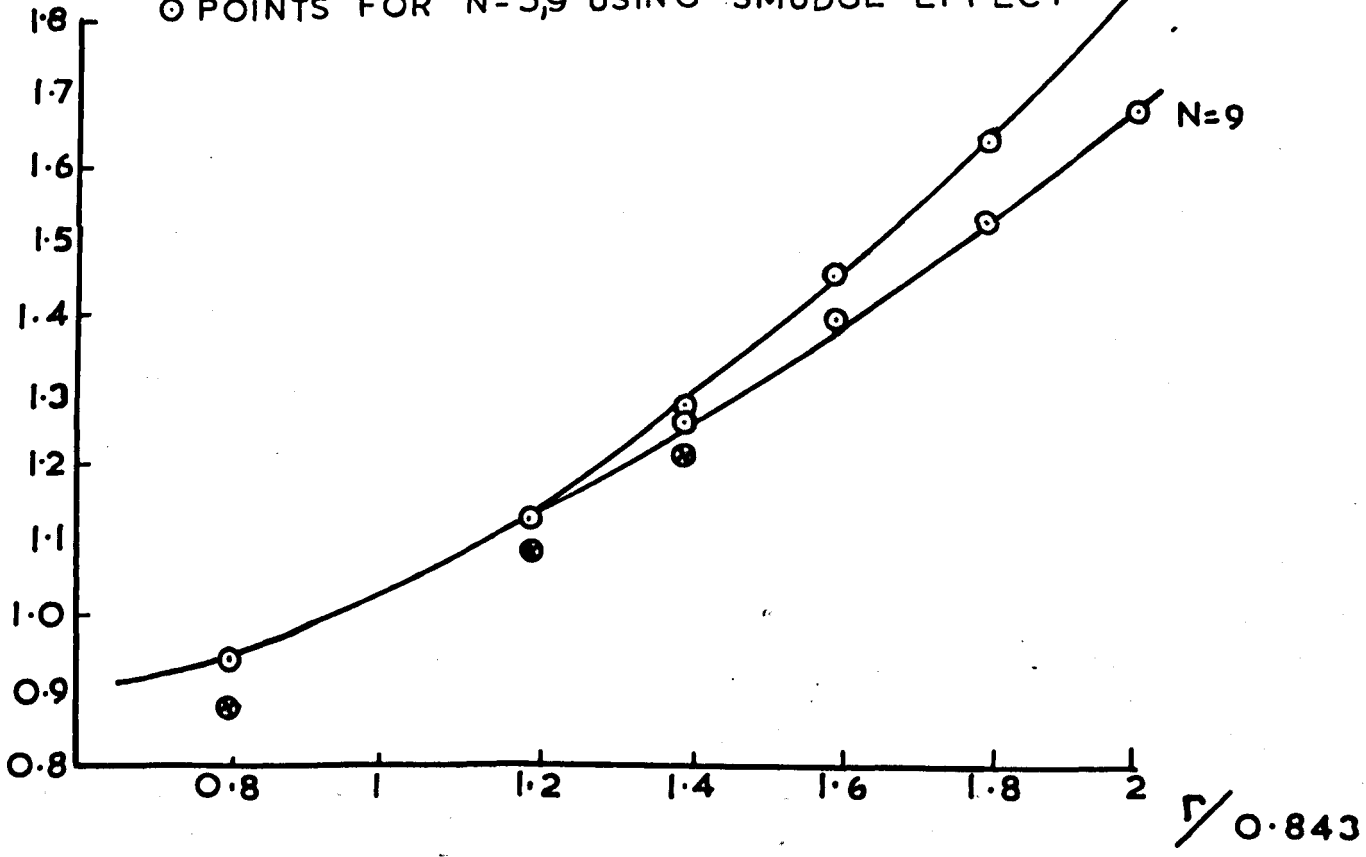
It is possible that for the same total number of
 tubes, σ_ϕ is a function of N . This condition implies
 that N/Γ is constant, and σ_ϕ has been evaluated

FIG. A. 2. (vii)

$$\frac{\sigma_{\phi_r}}{\sigma_{\phi}(r=0.843)} \text{ --- vs --- } \frac{r}{0.843}$$

$\sigma_{\phi_r}/\sigma_{\phi}(r=0.843)$ \odot COMPUTER POINTS FOR N=5. N=5

\odot POINTS FOR N=5,9 USING "SMUDGE" EFFECT

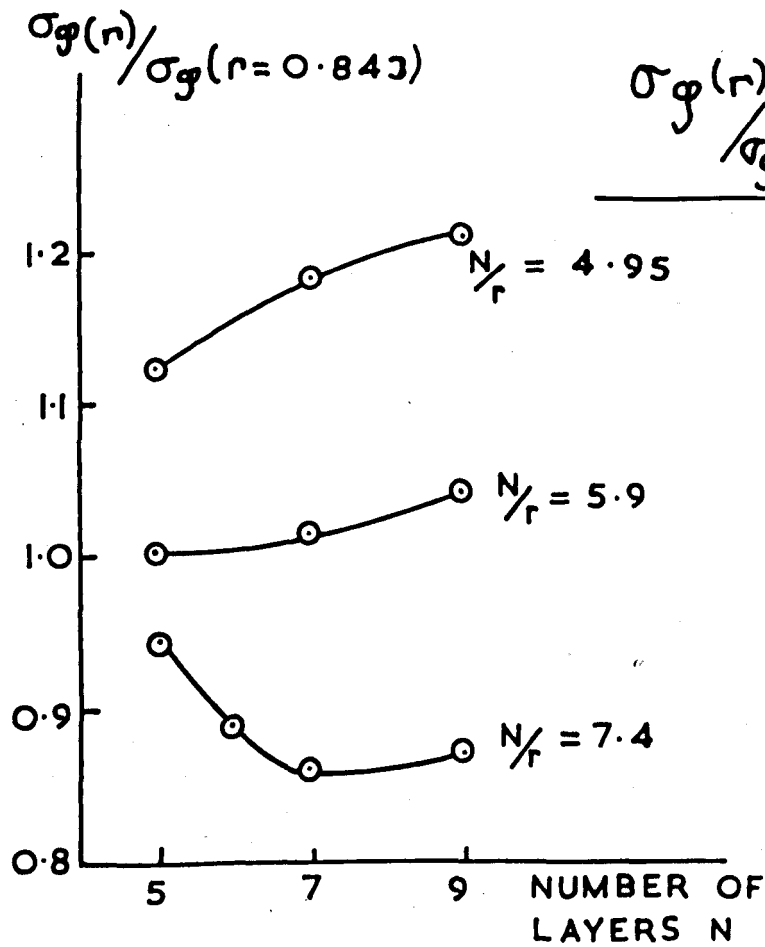


for three values of N/Γ and N . The results are shown in figure A.2.(viii) relative to $\sigma_\phi (N=5, \Gamma=0.843)$

(8) Staggering of tube layers

The value of σ_ϕ for the random arrays (table A.1.(i)) has been compared with that for the Durham, (Wolfendale, private communication) and the Nottingham array. Both of these were designed to give constant σ_ϕ as a function of angle of incidence, over a limited range of angle. The comparable average values of σ_ϕ , suitably scaled, are given in table A.2.(iii). The agreement is seen to be good. As a measure of the variation of σ_ϕ with angle, the standard deviation about the mean σ_ϕ has been compared for the random arrays and the Nottingham array. The results indicate very similar variations with angle. In table A.2.(iv) the values of σ_γ for the Nottingham spectrograph are given as a function of angle of incidence. The variations are small, indicating that fluctuations in σ_γ are smoothed out by the use of two arrays.

FIG. A.2.(v iii)



$\frac{\sigma_g(n)}{\sigma_g(r=0.843)}$ vs N

	σ_{ϕ} (radians $\times 10^4$)	
Random arrays	7.64 ± 0.15	6.05 ± 0.16
	Nottingham	Durham
	7.95 ± 0.17	6.14 ± 0.22

Table A.2.(iii)

Angle of Incidence (rads.)	0 - 0.02	0.02- 0.03	0.03- 0.05	0.05- 0.07	0.07- 0.08	0.08- 0.09
σ_{ϕ} (radians $\times 10^3$)	1.13	1.14	1.14	1.15	1.17	1.24

Table A.2.(iv)

The conclusions to be drawn are limited. The criterion for tubes of small dimensions or low pressure is more likely to be that there shall be a high probability that at least one tube should flash for particles incident at any angle. This is not

necessarily compatible with a constant σ_ϕ as a function of angle. Also it may not be possible to design an array for constant σ_ϕ over a wide range of incident angle. In view of the smoothing effect described above, one may tentatively conclude that there is no significant difference between random and designed arrays.

(9) Errors in $P(\theta)$

An effect of errors in $P(\theta)$ is to produce an error in the estimate of σ_ϕ . The magnitude of this error has been estimated using the smudge effect, described in section (4). Assuming a tube of diameter 0.59 cms. for which $b = 0.1$ cm., the percentage errors in occurring if various values of b are used are summarised in table A.2.(v), as a function of N .

$\begin{array}{l} N \\ b \\ \text{cm.} \end{array}$	5	7	9
.04	- 6%	- 15%	- 19%
.06	- 5%	- 12%	- 15%
.08	- 3%	- 6%	- 9%
.12	+ 4%	+ 8.5%	+ 11%
.14	+ 8.5%	+ 15%	
.16	+ 17%		
.19*	+ 22%		

Table A.2.(v)

* $b = 0.19$ cm. for low pressure tubes

A.3 Conclusions

The conclusions may be summarised as follows:-

- 1) For a random array of more than five layers the decrease in the error of angular measurement, σ_ϕ , obtained by using high pressure (2.4 atm.) tubes rather than low pressure (1 atm.) tubes of 0.59 cm. diameter, is 25%.
- 2) Using high pressure tubes, σ_ϕ does not decrease with increasing N as rapidly as would be expected for 100% efficient tubes.
- 3) No advantage can be obtained by increasing the vertical separation between the layers in a tray.
- 4) For the Nottingham Spectrograph, the contribution to σ_ϕ made by the random errors in tube diameter, and errors in location (0.045 cm.) is only 12%.
- 5) For a given number of tubes, there is a wide range of tube diameters giving a nearly constant value of σ_ϕ , providing the other parameters are correctly chosen, as indicated in table A.2.(ii).

6) For a fixed number of tubes of given diameter, the parameters are best chosen to work where the ratio of the mean corridor width to tube separation (\bar{r}/r) is not increasing rapidly with the ratio of tube diameter to separation (Δ/r) .

7) For a 5 layer array, σ_{ϕ} , assuming 100% efficient tubes is 10% lower than for practical tubes. For an 8 layer on the other hand, the change is 33%. The result of this is that previous workers who have assumed 100% efficient tubes have overestimated the m.d.m. of their spectrographs. For example, the Durham instrument (Ashton 1960, and Wolfendale, private communication) whose m.d.m. assuming perfect tubes is 709 ± 30 Gev/c (in agreement with the figure of 680 ± 140 Gev/c estimated by Ashton et al.), has an m.d.m. of 460 ± 16 Gev/c assuming perfectly located practical tubes of known constant diameter. Using an r.m.s. error in tube location and tube diameter of 0.02 cm. (which is a lower limit), the m.d.m. is 410 Gev/c.